

futurities

The Simulation Based Engineering & Sciences Magazine

Year 19
01
Spring
2022



SPOTLIGHT ●
Origami Engineering



um
2022

ESTECO
USERS' MEETING
29 - 30 JUNE

Meet **VOLTA** and
modeFRONTIER
users and experts

**From speakers' corners to
immersive workshops.**

**From on-demand presentations
to live Q&A with speakers.**

Join the online ESTECO International
Users' Meeting 2022 for the best
virtual experience possible.
Discover all the sessions and register
for **free**.

um22.esteco.com



KEYNOTE SPEAKERS



LIVE Q&A



SPEAKERS' CORNER



INTERACTIVE WORKSHOPS



INDUSTRY TRACKS



GET TO KNOW US

VOLTA

modeFRONTIER



- Editor's Note

Welcome to the first edition of **Futurities** – the revamped, revisited, and renewed version of the *EnginSoft Newsletter!* The word “futuraity”, as defined by the Oxford English Dictionary means “the time that will come after the present and what will happen then”. As the world, hopefully, begins emerging from the pandemic, yet teeters precariously on the brink of another major world conflict, the only certainty we have is that change will be ever more present, faster and both more predictable and unpredictable than ever before. As business leaders and technologists, we need to embrace this fact and harness our know-how and ability to capitalize on the opportunities this presents, and mitigate the threats to our businesses, our products, our safety, and our environment.

The new version of the magazine is intended to encapsulate all of this intention and focus it into a forward-looking instructive tool for knowledge transfer, seasoned with food for thought and reflection – in a nutshell to present the future of engineering simulation in all its facets and what will happen then. We have reorganized the content into several focused areas including **Technology Transfer**, that will feature technical or mathematical analyses of different engineering problems, as well as academic papers, **Know-How**, that will present industrial use cases describing the engineering challenge faced, the approach taken, and methodology used in resolving it, **Research & Innovation**, that will offer updates and insights from research projects, as well as providing a showcase for interesting innovative applications, **Product Peeks**, that will provide an overview of some of the latest software products on the market, and still more sections to come.

The main novelty is the **Spotlight** that will focus on an aspect of simulation, presenting leading edge approaches, techniques and technology developments. In this first issue of **Futurities** our **Spotlight** falls on the emerging

area of Origami Engineering, which holds great promise to help resolve some of the most pressing current and future engineering problems. While not yet fully harnessed, we are seeing increased global interest in the topic across the world, with some of the brightest minds being brought to focus on how the ancient Japanese art of paper folding can be applied to innovative materials to provide light-weight, secure, compact and expandable solutions to widely disparate areas and scales, from the nano to the massive.

Also under our **Spotlight** in this issue, is a design thinking approach to the application of Finite Element Method to traffic accident kinematics in order to assess risk and damage in the insurance industry, with the triple objective of satisfying customer requirements for satisfactory compensation, while containing costs for insurers, and increasing trust in the insurance industry.

Other interesting articles in this issue include a look at one of the new frontiers in simulation for microsystems using deep learning-based reduced order models, the challenges of testing and simulating lattice structures, how the Johnson Cook plasticity model can be used in high strain rate regime applications and the use of moving particle simulation method to optimize the spray cooling of e-drives.

I invite you to send us your feedback on the evolution of the magazine and to make suggestions for areas you believe should fall under our spotlight or any other section – it is here to share knowledge and inspiration.

Stefano Odorizzi

Editor in chief



“

Futurities is intended to [be] ... a forward-looking instructive tool for knowledge transfer, seasoned with food for thought and reflection



Futurities

Year 19 n°1 - Spring 2022

To receive a free copy of the next magazine, please contact our Marketing office at: marketing@enginsoft.com

All pictures are protected by copyright. Any reproduction of these pictures in any media and by any means is forbidden unless written authorization by EnginSoft has been obtained beforehand. ©Copyright EnginSoft.

EnginSoft S.p.A.

24126 BERGAMO c/o Parco Scientifico Tecnologico
Kilometro Rosso - Edificio A1, Via Stezzano 87 • Tel. +39 035 368711
50127 FIRENZE Via Panciatici, 40 • Tel. +39 055 4376113
35129 PADOVA Via Giambellino, 7 • Tel. +39 049 7705311
72023 MESAGNE (BRINDISI) Via A. Murri, 2 - Z.I. • Tel. +39 0831 730194
38123 TRENTO fraz. Mattarello - Via della Stazione, 27 • Tel. +39 0461 915391
10133 TORINO Corso Marconi, 20 • Tel. +39 011 6525211

www.enginsoft.com

e-mail: info@enginsoft.com

Futurities is a quarterly magazine published by EnginSoft SpA

COMPANY INTERESTS

EnginSoft GmbH - Germany
EnginSoft UK - United Kingdom
EnginSoft Turkey - Turkey
www.enginsoft.com

CONSORZIO TCN www.consorziotcn.it • www.improve.it
M3E Mathematical Methods and Models for Engineering www.m3eweb.it
AnteMotion antemotion.com

ASSOCIATION INTERESTS

NAFEMS International www.nafems.it • www.nafems.org
TechNet Alliance www.technet-alliance.com

ADVERTISING

For advertising opportunities, please contact our Marketing office at: marketing@enginsoft.com

RESPONSIBLE DIRECTOR

Stefano Odorizzi

PRINTING

Grafiche Dalpiaz - Trento

Autorizzazione del Tribunale di Trento
n° 1353 RS di data 2/4/2008

The Futurities editions contain references to the following products which are trademarks or registered trademarks of their respective owners:

Ansys, Ansys Workbench, AUTODYN, CFX, Fluent, FORTE, SpaceClaim and any and all Ansys, Inc. brand, product, service and feature names, logos and slogans are registered trademarks or trademarks of Ansys, Inc. or its subsidiaries in the United States or other countries. [ICEM CFD is a trademark used by Ansys, Inc. under license] (www.ansys.com) - modeFRONTIER is a trademark of ESTECO Spa (www.esteco.com) - Flownex is a registered trademark of M-Tech Industrial - South Africa (www.flownex.com) - MAGMASOFT is a trademark of MAGMA GmbH (www.magma-soft.de) - FORGE, COLDFORM and FORGE Nxt are trademarks of Transvalor S.A. (www.transvalor.com) - LS-DYNA is a trademark of LSTC (www.lstc.com) - Cetol 6σ is a trademark of Sigmatrix L.L.C. (www.sigmatrix.com) - RecurDyn™ and MBD for Ansys is a registered trademark of FunctionBay, Inc. (www.functionbay.org) - Maplesoft are trademarks of Maplesoft™, a subsidiary of Cybernet Systems Co. Ltd. in Japan (www.maplesoft.com) - Particleworks is a trademark of Prometech Software, Inc. (www.prometechsoftware.com). Multiscale.Sim is an add-in tool developed by CYBERNET SYSTEMS CO.,LTD., Japan for the Ansys Workbench environment - Masta is a trademark of SMT - Smart Manufacturing Technology Ltd. (www.smartmt.com) - Rocky is a trademark of ESSS (www.esss.co) - industrialPhysics is a trademark of Machineering GmbH (www.machineering.com) - SIMUL8 is a trademark of SIMUL8 Corporation (www.simul8.com) - ViveLab Ergo is a trademark of ViveLab Ergo Ltd. (www.vivelab.cloud) - True-Load is a trademark of Wolf Star Technologies (www.wolfstartech.com)

Contents

TECHNOLOGY TRANSFER



- 23 Optimizing the spray cooling of e-drives with moving particle simulation
by EMOTORS



- 28 Calibration of the Johnson-Cook plasticity for high strain rate regime applications
by MBDA



- 31 Aerodynamic analysis of the new generation Korea Train eXpress (KTX) pantograph
by TSNE

KNOW-HOW



- 34 ESTECO sponsors UniTS Racing team to optimize design of Formula SAE electric car
by UniTS Racing Team

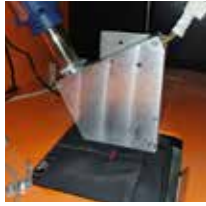


- 36 Characterization of lattice structures: testing and simulation challenges
by EikoSim

RESEARCH & INNOVATION



40 Simulation of impact testing on a protected and unprotected human hand
by West Virginia University



44 Optimization of an explosive trace detector using CFD simulation
by EXA



49 Deep learning-based reduced order models: the new frontier in numerical simulation for microsystems
by Politecnico di Milano

PRODUCT PEEKS



52 Overview of the latest developments in Multiscale.Sim, a virtual material testing tool to accelerate materials design
by CYBERNET SYSTEMS CO.

56 Ansys 2022 R1: CFD release highlights
by EnginSoft

SPOTLIGHT



6 **Origami Engineering**
Focus on Origami-based designs, crash simulation and packaging

7 Origami Engineering: inspired by Japanese folding culture
by Meiji University

13 Comparison of homogeneous and micromechanical modelling approaches for paper honeycomb materials
by Bosch Thermotechnology

16 Creating new services based on reconstruction of accident kinematics with FEM prototypes and a design thinking approach
by DCA Consulting

15 SEMINARIO ONLINE
giugno
ore 9:30 - 13:00

Le sfide dell'elettrificazione con le migliori metodologie di simulazione numerica

RELATORI:
A. Serra, S. Carrino, E. D'Alessandro, G. Lombardi, M. Lucchesi, M. Merelli

 **ENGINSOFT**





SPOTLIGHT

Origami Engineering

Focus on Origami-based designs, crash simulation and packaging

Origami engineering is an emerging area that is receiving increasing attention across the globe. It has already been successfully applied in medicine, space, packaging, robotics, construction and the automotive industry and other sectors. It is the object of all this interest due to its various features: the ability to compress large structures into small spaces and then expand them again, or vice versa; the ability to add greater stability or resiliency to items including packaging; the ability to create highly complex items from a single sheet, saving on manufacturing, transport and warehousing costs; the ability to generate curved elements by folding; the ability to create self-assembling objects from new innovative materials that change their structure based on changes in substance around them.

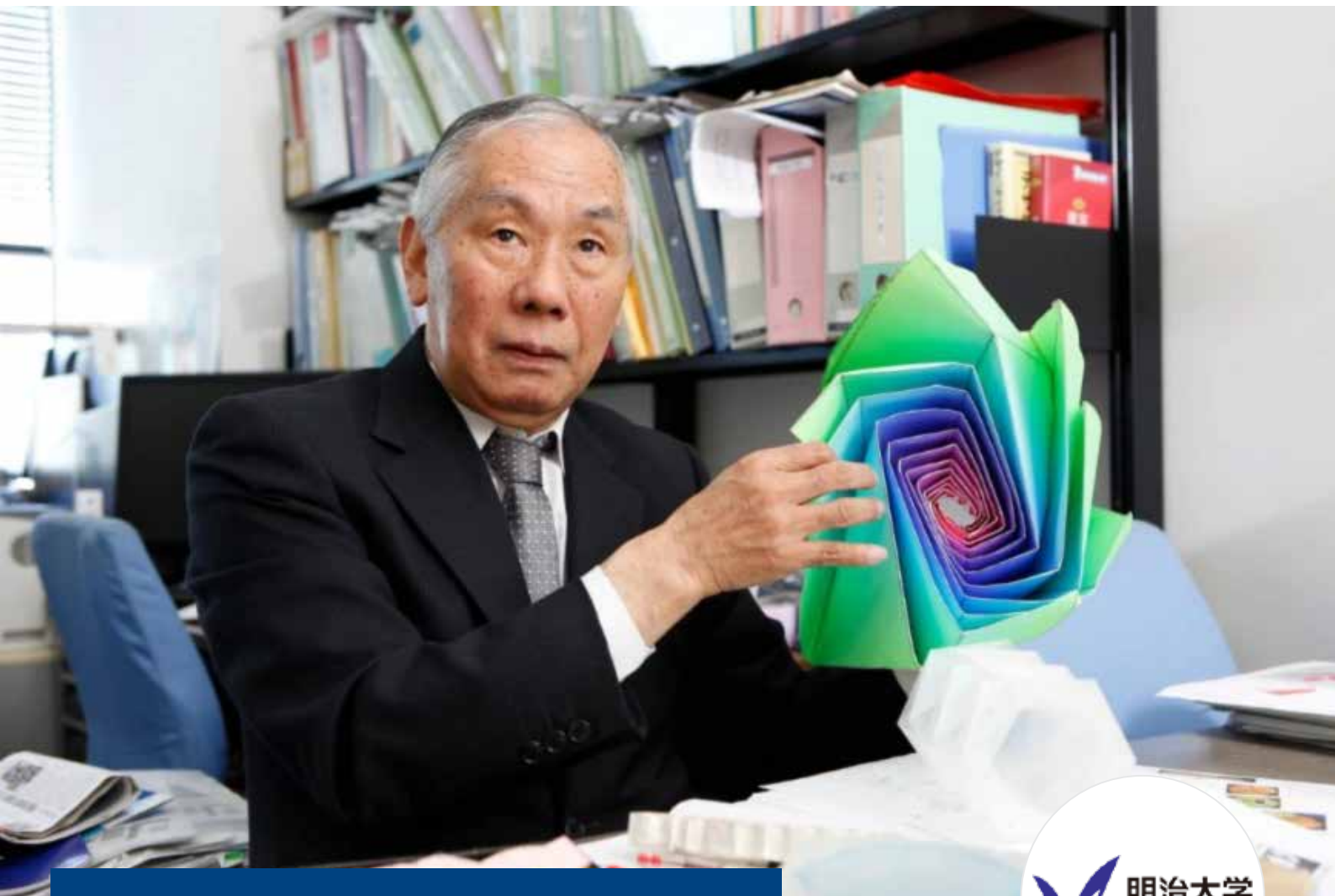
Kirigami, another traditional Japanese art form, which involves the application of strategically placed cuts to a flat material to generate an adaptable 3D object is also attracting a lot of attention.

Our first Spotlight article is written by Professor Ichiro Hagiwara of Meiji University and discusses various examples of origami that are being studied for their potential industrial

applications. Our Spotlight also includes a study of the mechanical behaviour of honeycomb packaging materials, which have their origin in paper folding techniques.

For a detailed look at the various successful applications over the past 15 years, as well as the existing challenges still to be addressed, interested readers are directed to the following research article: *Meloni, M., Cai, J., Zhang, Q., Sang-Hoon Lee, D., Li, M., Ma, R., & Parashkevov, T. et al. (2021). Engineering Origami: A Comprehensive Review of Recent Applications, Design Methods, and Tools. Advanced Science, 8/13: 2000636. DOI: 10.1002/adv.20200636 available online at onlinelibrary.wiley.com/doi/full/10.1002/adv.20200636*

Our other Spotlight article focuses on the use of the emerging field of design thinking to resolve a challenge in the traffic insurance industry by means of the application of fixed element analysis to replicate the kinematics of a traffic accident in order to evaluate the physical and material damage claims to ensure fairness in client compensation and enhance trust in the insurance industry while also containing large claim costs for the insurer.



Origami Engineering: inspired by Japanese folding culture

Kirigami and fan folds represent new opportunities

by **Ichiro Hagiwara¹** and **Akiko Kondoh²**

1. Distinguished Professor Emeritus, The Strategic Coordination of Research and Intellectual Properties, Advanced Study of Mathematical Sciences, Meiji University

2. Prometech Software, Inc.

Origami, the Japanese art of transforming a single sheet of paper into various shapes, is a traditional cultural activity and form of play that children all over the world are familiar with. More recently, it has been adopted by international educational institutions as an tool to enhance thinking skills and concentration.

The artistic aspect of origami also attracts adults, and origami exhibitions are held in many countries around the world. More recently, the application of origami-inspired approaches to engineering have been attracting attention, since the structural characteristics of origami can be applied to industrial products and daily necessities.

However, while many people know about origami, few people have heard about origami engineering.

The history and industrialization of origami

Papyrus, the origin of the word paper, began to be used for paper in Egypt around 2500 BC. Since Egyptian and Western writing instruments were designed to scratch, the papyrus-based paper of the time had to be thicker and could not be folded. In Japan and China, on the other hand, brushes were used as writing tools, so the thinner the paper, the better.

Such paper for brushes was first invented in China, and these paper-and ink-making methods were introduced to Japan in AD 610. Later, other paper-making techniques developed independently in Japan, and the Japanese created the world's first foldable paper using tenacious elm. Subsequently, it was discovered that washi became more rigid and produced a beautiful lustre when folded.

During the Edo period (1603-1868), when Japan adopted a policy of national seclusion, paper became more popular, and a more playful form of origami to create animals such as cranes and turtles was developed. It was also during this period that the world's oldest book on origami was produced. Later, during World War II, a British engineer evolved and developed a method to mass-produce honeycomb origami, inspired by the Japanese Tanabata festival decorations. This was the beginning of the industrialization of origami. Industrial honeycomb, which has the highest axial rigidity for its weight, is now used in rockets and bullet trains and has become a multi-trillion-yen industry.

The birth of origami engineering and application of honeycomb

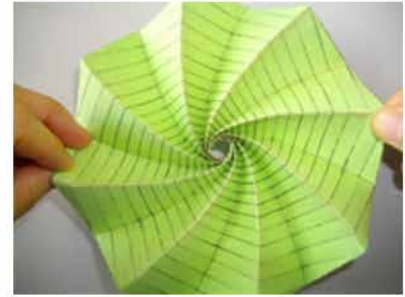
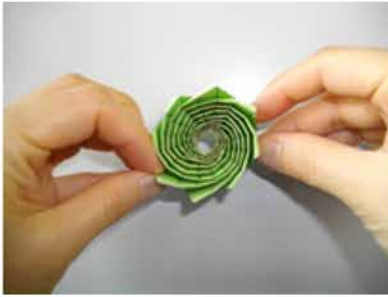
In Japan, where origami is a part of traditional culture, Dr. Taketoshi Nojima of Kyoto University proposed the concept of origami engineering to further apply its advantages to industrial applications. Currently, research on origami engineering is mainly promoted by the Origami Engineering Research Group of the Japanese Society for Applied Mathematics, which was established by Prof. Hagiwara.

One of these research undertakings is to improve the honeycomb structure. Conventional manufacturing methods were unable to produce curved-surface honeycombs. However, by applying traditional Japanese paper-cutting techniques (kirigami), three-dimensional curved honeycomb has been successfully manufactured. Furthermore, changes to the pattern of cuts and polygonal lines used, enables the creation of wing- and eave-shaped honeycombs.

Automobile interior parts generally have complex shapes. Conventional technology is rarely able to reproduce these complex components and, when it is possible, it is not easy to produce them as a continuum. However, by applying the kirigami honeycomb technology approach, it was found that the parts could be reproduced entirely in one piece. We have also succeeded in creating arbitrarily shaped structures with a single honeycomb using a state-of-the-art robot. We expect these discoveries to revolutionize design. This curved-surface honeycomb technology based on kirigami has had such a significant impact on industry that kirigami has also become an international term, alongside origami.



Courtesy of Kazuya Saito of Kyushu University



Courtesy of Meiji University

Industrial engineering aspects of origami engineering

There are three core aspects of origami engineering for industrial engineering, namely:

- the design and manufacture of origami structures that can expand and shrink;
- an effort to create an origami design for anything; and
- the design and manufacture of origami structures that are lightweight yet rigid.

Below, we explain these three approaches and provide examples.

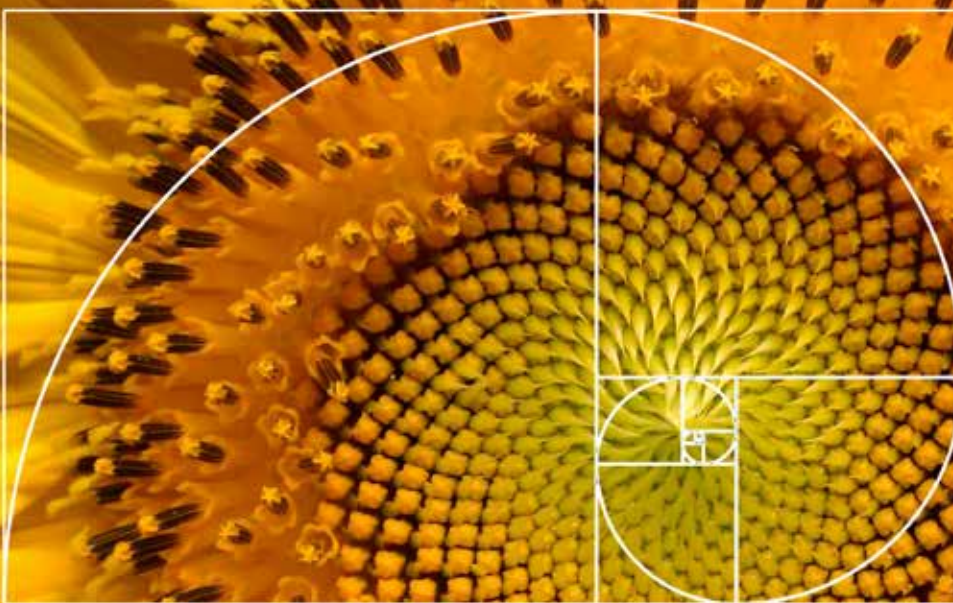
1) The design and manufacture of origami structures that expand and shrink (biomimetics origami)

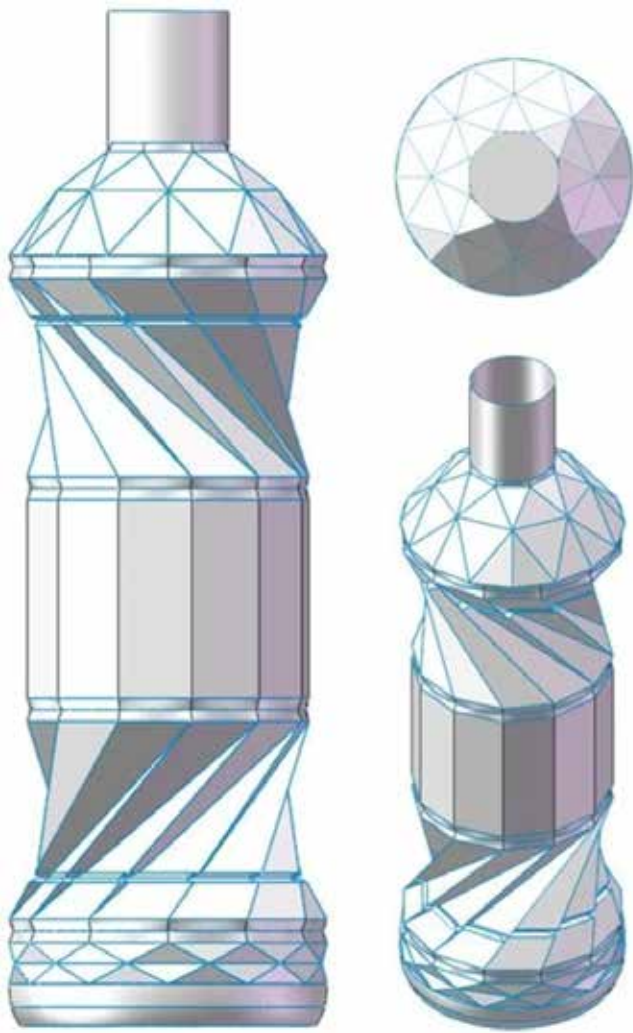
Dr. Nojima, who first proposed origami engineering as mentioned earlier, also succeeded in making insects out of origami, thus creating a new field known as biomimetics origami. As indicated, biomimetics origami is inspired by the natural world. For instance, various insects are able to fold their wings very compactly, and these complex folding patterns can be drawn using elementary geometric rules and then reproduced using origami.

The origin of biomimetic origami began with the study of plants: many plants grow new parts at specific angles, thus creating a spiral pattern that consists of right- and left-handed equal-angle spirals. An example is the arrangement of the seeds of a sunflower. The number of loops in the spiral follows the Fibonacci sequence (where every number is the sum of the previous two numbers, i.e. 1,1,2,3,5,8, etc.).

The ratio of the adjacent numbers in the Fibonacci sequence gradually approach the golden ratio, which is the point at which the balance between the length and width of a rectangle form is most stable and aesthetically pleasing. Found abundantly in nature, the Fibonacci sequence has also been applied in historical buildings and works of art. This spiral arrangement can also be expressed in origami, an example of which, based on the arrangement of sunflower seeds, can be seen below.

Biomimetics origami also has industrial applications. Its structure has been used in the energy-absorbing materials for cars because of its excellent ability to absorb impact energy as gently as a cushion. When a conventional rectangular type of absorber is used, the initial





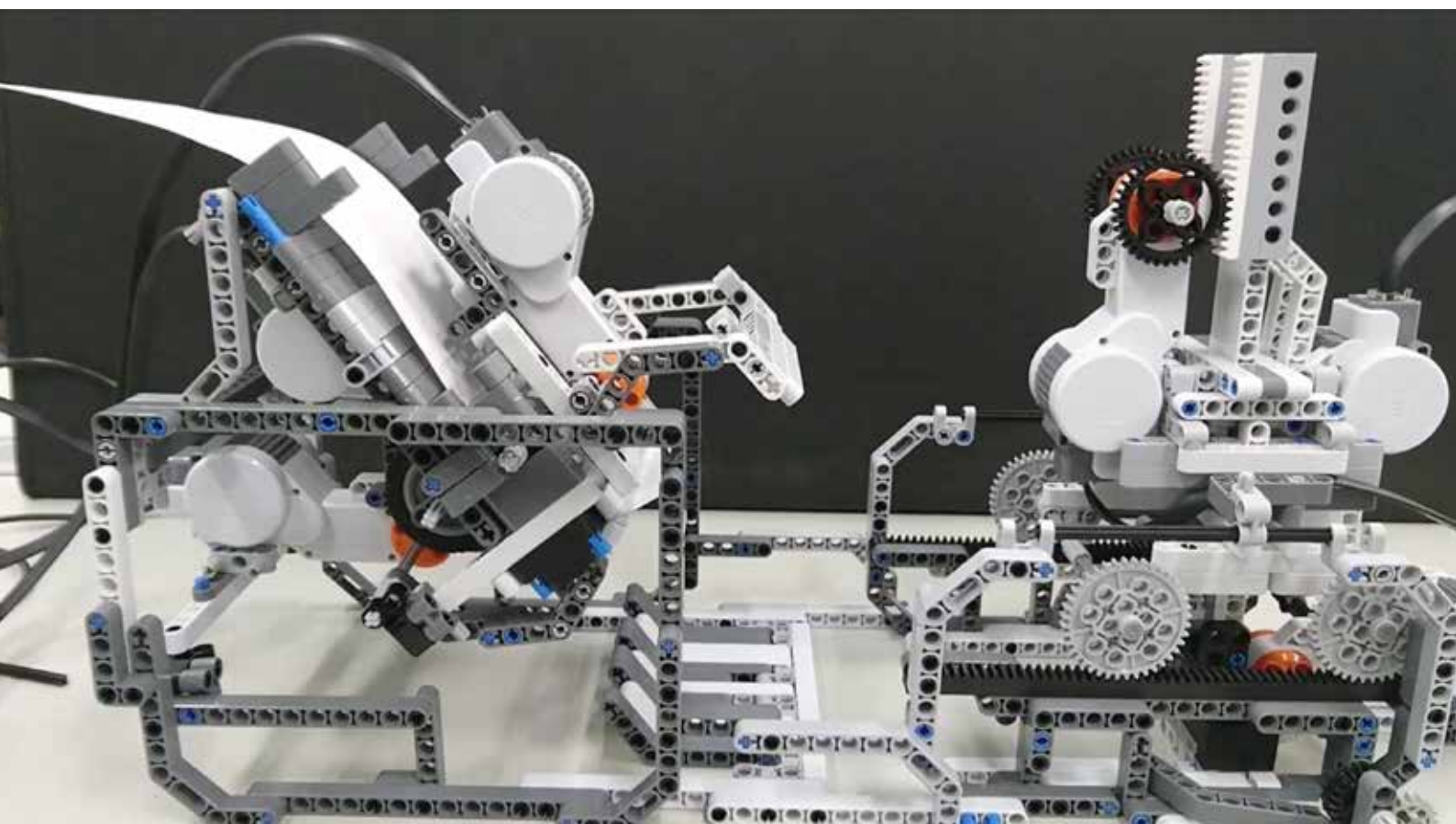
peak load is high, which can sometimes harm the occupants. With this type of absorber, the amount of deformation is only about 70% of its length. On the other hand, when an inverted spiral origami structure is used as an energy-absorbing material, the load value remains almost constant without changing with the deformation, while the amount of deformation reaches 90% of its length due to the characteristics of the origami folding. Consequently, research is now being conducted on the use of the new origami structure for absorbing materials that are able to absorb high impact energy, reduce the impact load, and that can be manufactured at a lower cost than the current structures. Another application is plastic bottles. Today's PET bottles are designed to be foldable and small enough to be easily recycled, but it originally took ten years to achieve the commercialization of this product. At first, the foldable feature of the origami structures was able to be incorporated into the design, but then the unfolding feature, or spring-back, would occur, with the result that the bottle did not maintain its folded state and would return to its original height. The addition of grooves to accommodate the folded parts finally enabled us to create a PET bottle that can be folded easily and neatly and does not return to its original height.

The expandable and shrinkable characteristics of this origami structure are now also being researched and developed for use in other sectors, such as in space for solar panels for satellites and telescopes, and in the medical field, for stents to expand blood vessels from the inside, and for stomach-cleaning robots.

2) Creating an origami design for anything

Next, let's look at origami design, which attempts to make anything out of origami. It is a particular challenge to fold a complex polyhedral shape from a single sheet of paper without any gaps. To begin with we used reverse engineering, mainly used in manufacturing, to build a system that uses a photo of the product to create a development

Fig. 2 - 3D origami robot printers. Courtesy of Meiji University



drawing with a glue allowance, and origami mountain and valley lines. Reverse engineering means working backwards in the design and manufacturing process to investigate the specifications and original manufacturing methods, operating principles, and blueprints. In practice, for instance, a point cloud is generated from the data of an actual vehicle or clay model; STL data is generated for conversion to CAD; and then a CAD or finite element method (FEM) model is generated for simulation to verify the part.

An Origami Geometry Calculation System is used to support reverse engineering. A real stuffed toy (seen here on the right of the picture) was formed into a laminated structure using a 3D printer, while the item on the left was made from paper using this Origami Geometry Calculation System and a 3D origami robot printer (see Fig. 2 below). This type of origami printer is currently being used in many sectors, including medicine, education, and urban development, for design support systems, daily necessities, and hobbies.

3) Design and manufacture of origami structures that are lightweight yet rigid

Origami structures can also be rigid in spite of their light weight. Inspired by the origami honeycomb, we created a space-filling model using tetrahedra and octahedra. The octahedral and tetrahedral halves create a spatial emphasis and, when they interlock, make a structure very strong.

These interlocking origami structures have been used commercially for solar cell panels and solar heliostats. Panels made by multi-stage press forming are 6~7 times stiffer than a conventional panel of the same weight and do not require additional reinforcement to maintain this flatness even for wide surfaces which tend to have weak rigidity. As the height of the cores is limited when constructing multiple cores from a single panel, the concept of the Assembly Core Truss Panel (ACTP), in which the cores are built and assembled one by one, was



Courtesy of Meiji University

considered. For example, a paper core made of 24 hollow octahedral and 25 hollow tetrahedral interlocking halves can support a person weighing 60 kg.

The properties of these ACTPs can be applied to pentagonal and cubic octahedral semi-shapes, for example to create effective packaging materials for transporting foods such as strawberries and eggs, which are prone to breakage during transport, as well as for pluripotent stem cells or blood, which degrade easily during transport.

Origami is customarily made from paper; when using cardboard, plastic, or metal, however, one has to confront many issues, such as a lack of stability after folding and unfolding, difficulty in reproducing complex folds, and the challenge of manufacturing inexpensive objects while maintaining their original functions. Fortunately, modelling and numerical simulation techniques are now helping to solve these problems.

Digital reproduction of a fan

Finally, we should mention the folding fan, unique to Japan. Fans were used to repel insects and to start fires, and were created almost simultaneously around the world. At that time, fans were still made to be flat fans. However, the Japanese applied their folding culture to fans, too, allowing them to be folded. The three-dimensional folding fan, made of Japanese paper and bamboo sticks or “bones”, originated in Japan during the Heian period (AD 794-1185) and subsequently spread all over the world.

In the Edo period (1603-1868), fans were painted by famous painters such as Sotatsu Tawaraya, Hokusai Katsushika, Korin Ogata. Their paintings were compositions that integrated the bamboo bones into a three-dimensional shape that was most effective when made into a fan.

Here, we present a case study of a digital fan that reveals this fact mathematically. The surface of the fan is distorted in various ways. The rate of contraction above and below the arc are due to the length of the fan bones that hold the arc in place. The fan model was created by approximating the distorted surface as a plane.



Courtesy of Meiji University

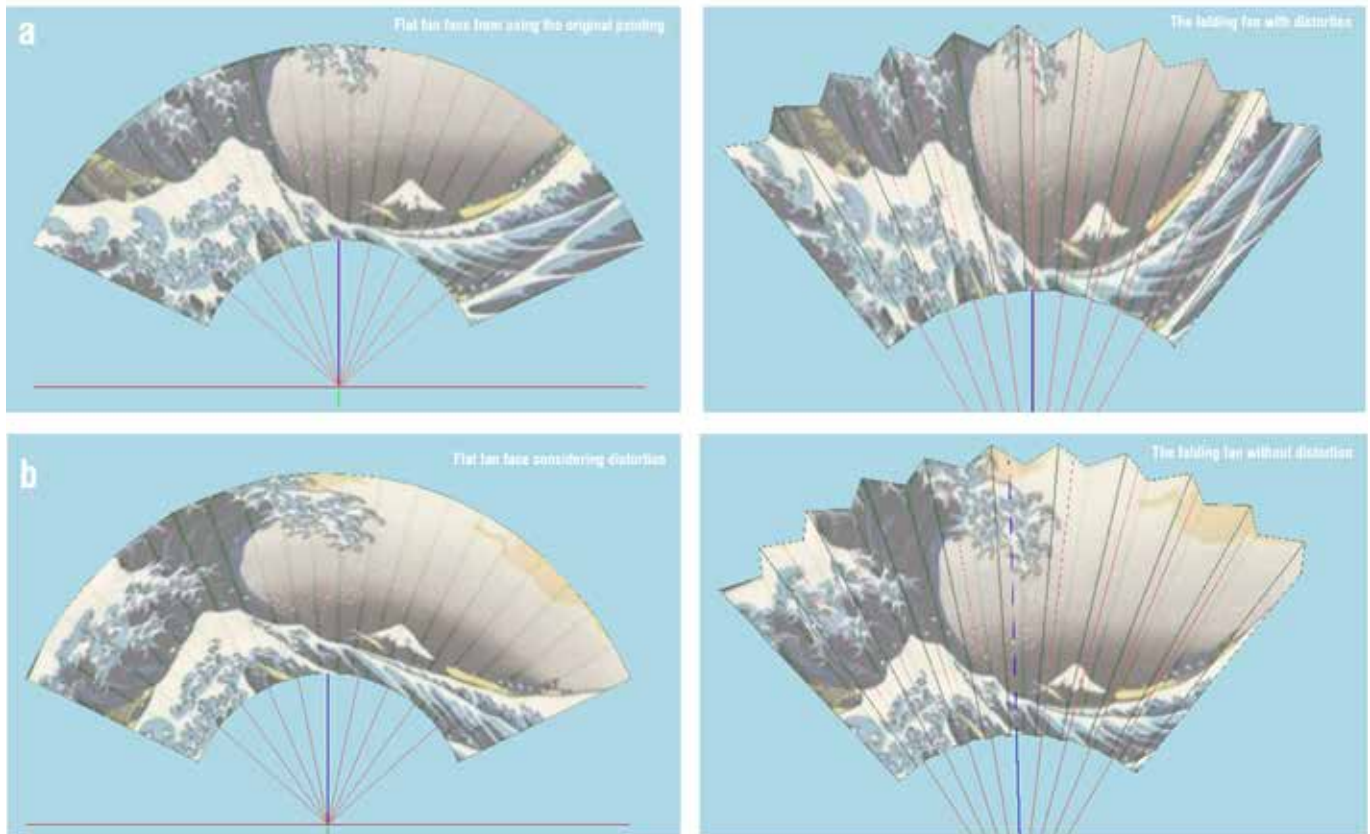


Fig. 3 - a) The original drawing is cut out as it is and is made into a fan; b) the original drawing is adapted for the finished fan using the digital fan program. Courtesy of Meiji University

We then applied ourselves to the challenge of rendering one of Hokusai Katsushika’s Ukiyo-e “36 Views of Mount Fuji” (The Great Wave off Kanagawa) as a fan painting using the digital fan. Firstly, we cut out a part of this Ukiyo-e to make a fan shape. As shown in Fig. 3a, the distortion of the image is more pronounced, especially in the case of a long-boned fan. In the case of a short-boned fan, the distortion was less pronounced and it looked pleasant, but not good enough for an artistic work. Therefore, we used the digital fan program mentioned earlier to mathematically illustrate what is overlooked in a general sense.

We applied a fan template with the fan bones extended, in which the surface image was noticeably distorted when tailored to the Ukiyo-e. The program reverse-engineered the image to obtain the original fan image. In this case, when viewed as a plane, Mt. Fuji has “fallen sideways” and the wave shapes have been stretched horizontally, creating a completely different impression to the original painting (Fig. 3b, left). However, when folded to the planned size, the original Ukiyo-e appears on the surface of the three-dimensional fan. The difference can be clearly seen when comparing it with the distorted fan made earlier.

The motivation for the mathematical description of these digital fans is the tendency for Japanese folding fans of historical value to be preserved in flat form, with their bones removed, in wall paintings and hanging scrolls. This detracts from the value of the skilful drawing of the Edo-period painters and the three-dimensional artistic expression created from them. We wish to emphasize, therefore, the importance of

maintaining and complementing the original three-dimensional form of these Japanese fans on display all over the world. This will reveal their value as a three-dimensional art form, which has been overlooked so far and will lead to the succession and development of traditional art forms.

Conclusion

It is now 20 years since the advent of origami engineering. Thanks to its light weight and high rigidity, as well as its ability to expand and shrink, there has been a great deal of interest in applying the results of origami engineering research to products. The wide range of applications that have already been realized suggests that origami engineering will grow as an essential technology in industry. Just as 3D additive printing has influenced design and manufacturing, origami engineering has the potential to revolutionize the way we design. At the same time, the mathematical thinking of origami engineering can help to preserve and pass on long-established cultural traditions.

References

- [1] I. Hagiwara, invited lecture presented at the Prometech Simulation Conference, Tokyo, Japan, Nov. 2021
- [2] I. Hagiwara, inspirational presentation presented at the International CAE Conference and Exhibition, Vicenza, Italy, Nov. 2021
- [3] Saito, K., Nomura, S., Yamamoto, S., Niiyama, R., & Okabe, Y. (2017). Investigation of hindwing folding in ladybird beetles by artificial elytron transplantation and microcomputed tomography. *Proceedings of the National Academy of Sciences*, 114(22), 5624-5628.
- [4] Kazuya Saito, Tachi Tomohiro, Fujikawa Taro, Niiyama Ryuma, Yoshihiro Kawahara, Deployable Structures Inspired by Insect Wing Folding, in *Origami 7: Proceedings from the seventh meeting of Origami, Science, Mathematics and Education*, Vol.3, 747 - 762, 2018.9

Comparison of homogeneous and micromechanical modelling approaches for paper honeycomb materials

by Berkay Türkcan İmrağ¹, Yiğit Gürler¹, Taylan Güçkiran¹, İbrahim Şimşek¹, and Prof. Alper Taşdemirci²

1. Bosch Thermotechnology Manisa R&D Department

2. Department of Mechanical Engineering, Izmir Institute of Technology



Paper honeycomb sandwich structures have a wide range of uses across the packaging and furniture industries due to their low weight, high strength, easy recyclability, low cost, and high customizability. They are also widely used in logistics as an environmentally friendly cushioning material alternative to traditional expanded polystyrene (EPS) material to protect products from damage caused by shocks and vibration.

Properties such as core thickness, cell diameter, and paper type are important for the energy absorption capacity of paper honeycomb sandwich structures.

Therefore, the influence of these parameters should be considered when designing packaging concepts that uses them.

Numerous mechanical tests are required to determine the influence of each parameter on energy absorption capacity. This makes it difficult, in terms of cost and time, to determine the optimum paper honeycomb structure for a packaging application.

The use of numerical modelling approaches in these studies significantly reduces the number of tests and the time required to determine the effect of the parameters. In this way, the studies become cost- and time-efficient. The main aim of this study is to create numerical models using micromechanical and homogeneous modelling approaches validated by compression test results. The study therefore investigated the advantages and disadvantages of these approaches.

Today, companies are increasingly striving to limit their reliance on single-use plastics due to legal regulations announced by governments to enforce carbon footprint reduction in the near future.



Fig. 1 - Paper honeycomb samples.

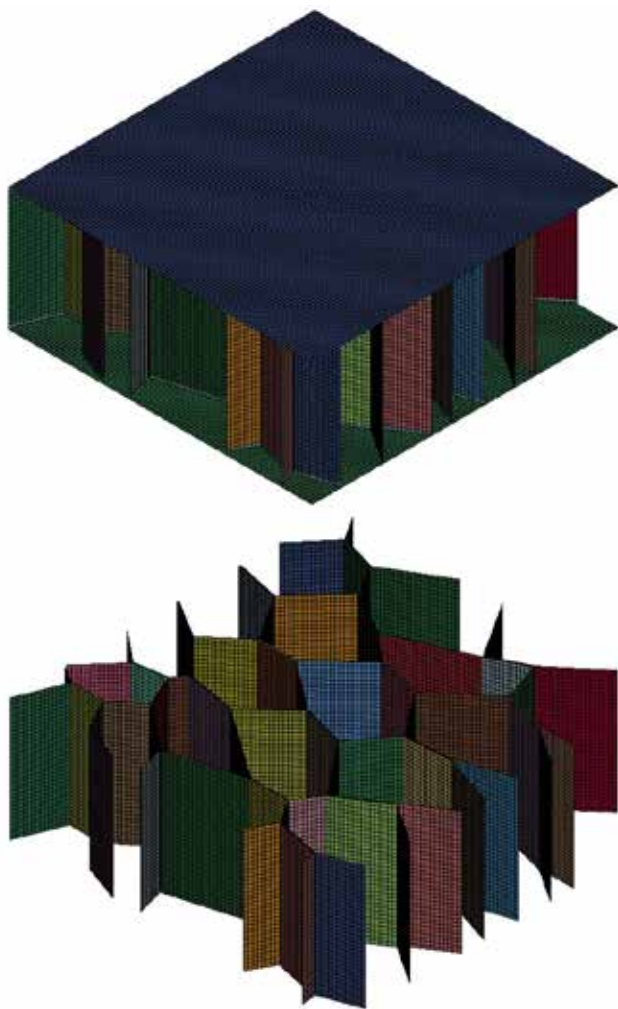


Fig. 2 - Micromechanical modelling.

For this reason, many researchers are investigating environmentally friendly alternative materials to replace the widely used EPS material. However, these candidate alternative packaging materials must satisfy the acceptance criteria at least as well as the EPS material. Considering their mechanical properties and advantages, paper honeycomb sandwich structures are become an interesting alternative for environmentally friendly packaging material. This study investigated the strength of a paper honeycomb structure using a compression test and two different numerical modelling approaches. The validation study was conducted by comparing the results of the numerical model with the results of the compression test. The numerical modelling studies were conducted in LS-Dyna, which was selected because it offers special material cards and various contact algorithms for honeycomb sandwich structures.

Testing procedure and sample preparation

Mechanical tests for the modelling and validation studies were conducted in accordance with the following ASTM standards:

- ASTM C365 / C365M - 16 - standard test method for flatwise compressive properties of sandwich cores;
- ASTM C364 / C364M - 16 - standard test method for edgewise compressive strength of sandwich constructions;
- ASTM C273 / C273M - 20 - standard test method for shear properties of sandwich core materials;
- ASTM D828-16 - standard test method for tensile properties of paper and paperboard using constant-rate-of-elongation apparatus.

Paper honeycomb samples with dimensions of 50x50mm and 20mm thickness were used in the tests (Fig. 1). All honeycomb samples have the same cell diameter and wall thickness. The input parameters for the micromechanical and homogeneous material models were obtained using the results of experimental tests.

Numerical modelling micromechanical approach

In this approach, the cell walls and faces are modelled with 2D shell elements (ELFORM=10). The paper material is characterized with *MAT_24 (PIECEWISE_LINEAR_PLASTICITY) using input parameters from the tensile test (anisotropy of paper is neglected). With this approach, all geometric details of the paper honeycomb structure are modelled. The folding mechanism of the cell walls can be observed under compression load. This modelling approach allows the modelling of the honeycomb sandwich structure with the desired geometric parameters for any paper material whose mechanical properties are known. Therefore, it is a suitable modelling approach for optimization studies.

Numerical modelling homogeneous approach

In this approach, the honeycomb sandwich structure is modelled with 3D solid elements (ELFORM=1). This structure is characterized with *MAT_126 (MODIFIED_HONEYCOMB) and fed input parameters and curves from the compression and shear tests. In this approach, 3D solid elements are modelled to complete the outer dimensions of the paper

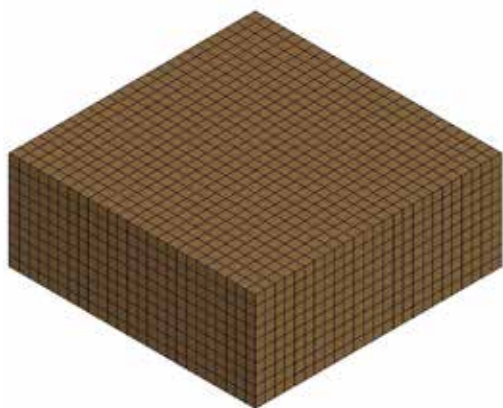


Fig. 3 - Homogeneous modelling.

honeycomb sandwich structure. Although visibly crushed like a box, its cushioning behaviour is characteristic of honeycomb. Since this modelling approach uses input parameters obtained from the tests on the structure, the geometric parameters of the core cannot be changed. The mechanical tests must be repeated for each new type of core.

Results and discussion

Fig. 4 compares the results of the compression test and the two numerical models. As can be seen, while the micromechanical model provides better results for the peak stress value, the homogeneous model offers more accurate results for the plateau region.

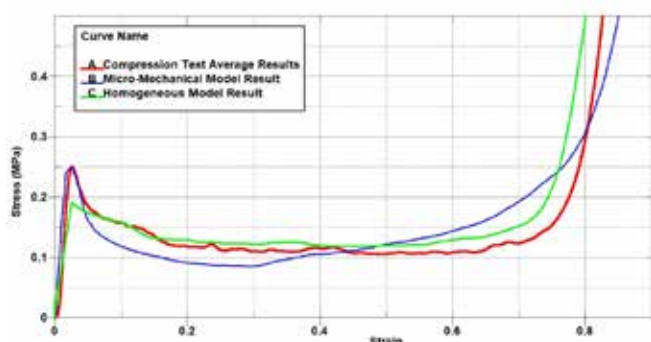


Fig. 4 - Comparison of result curves.

Curve Name	Peak Stress (MPa)	Stress at $\epsilon = 10\%$	Densification Strain
Compression Test	0.251	0.159	0.74
Micromechanical Model	0.248	0.12	0.68
Homogeneous Model	0.191	0.159	0.71

Table 1 - Data from stress-strain curve

It was concluded that the main reason for this difference with the micromechanical model is the change in the folding mechanism based on the element size of the cell walls. The values obtained from the points on the curves are shown in Table 1.

Conclusion

When the model results were investigated, it was observed that both approaches produced a similar result to the result of the experimental test. In this study, it was seen that the micromechanical modelling approach produced better results for the peak stress value, while the homogeneous model was more accurate for the plateau region. The micromechanical modelling approach allows local deformation levels to be observed. However, the element size needs to be reduced to better observe the local deformation levels and to improve the folding mechanism. As the element size decreases, the value of the timestep decreases significantly. In the homogeneous modelling approach, the value of the time step is larger than in the micromechanical modelling approach. This indicates that the homogeneous modelling approach will be more time efficient for setup and calculation in system level analyses such as drop tests.

Acknowledgement

This publication was supported by Bosch Thermotechnology GmbH. Its contents are solely the responsibility of the authors and do not necessarily represent the official views of the Bosch Thermotechnology GmbH. Special thanks to the Bosch Thermotechnology Manisa R&D Department for their valuable contribution.

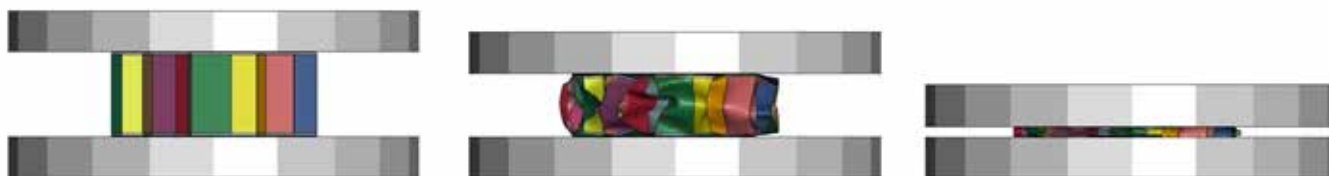


Fig. 5 - Deformation of micromechanical model at different stages.



Fig. 6 - Deformation of homogeneous model at different stages.



Creating new services based on reconstruction of accident kinematics with FEM prototypes and a design thinking approach

by Fabio Ardente¹, Alfonso Ortalda² and Claudio Martin²

1. DCA Consulting - 2. EnginSoft

One of the first tasks that most teams and projects undertake is the exploration of an idea or solution in greater depth to boost critical thinking. The second priority is to use engineering solutions to harness critical business thinking. Design Thinking is an approach that looks at value and change from a people perspective, combining three factors:

- technology, how things are made, and their performance increased;
- people and the ways in which made things are valuable to customers;
- business and how organizations can profit from offering people these made things.

Design Thinking starts from a people perspective and tries to generate value for them by creating great, meaningful things, after which it seeks a profitable business model to convert this people value into business value. The assumption, therefore, is to first

find people value (users and makers), and later, of course, do business. Design Thinking is key in our technology transformed world because it can harness this abundance of technology and data to create real value for customers; however engaging people in the digital transformation process is vital for every organization. Design Thinking focuses primarily on understanding whether something is meaningful for people and starts with this change of perspective which brings with it a complete redesign in terms of mindset, processes, and tools. Profit is a consequence of creating things that are meaningful to people.

The Design Thinking paradigm can take on different forms and interpretations depending on the nature of the purpose and the companies involved, and can be classified into four different clusters:

- Creative Problem Solving: solving difficult problems with analytical and intuitive thinking;

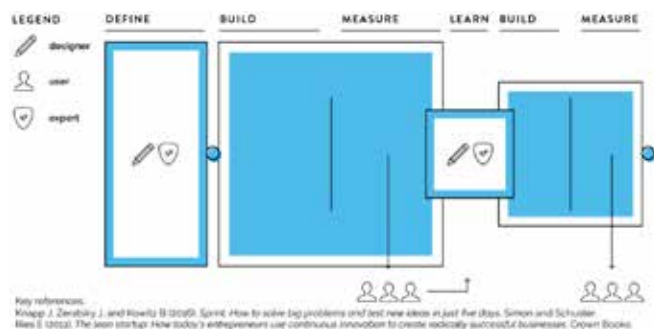


Fig. 1 - An example of an iterative Sprint Execution map

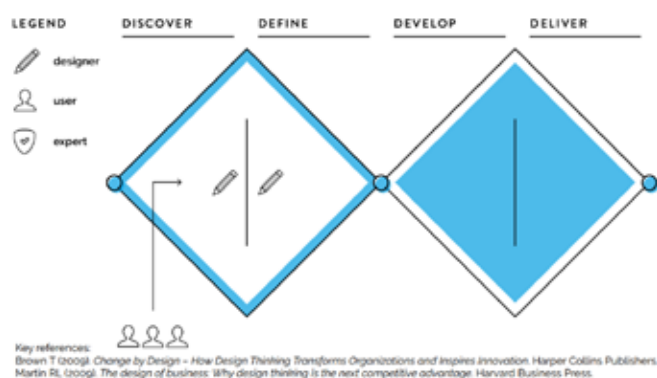


Fig. 2 - An example of an iterative Creative Problem-Solving map

- Sprint Execution: delivering and testing viable products to learn from customers and improve the solution;
- Creative Confidence: engaging people to make them more confident with creative processes.
- Innovation of Meaning: envisioning new directions that aim at people-meaningful experiences (DT4B, 2019).

The multifaceted nature of Design Thinking has been divided into three key areas:

- Design Thinking SETUP explores the composition of the team and the goals of the Design Thinking project.
- Design Thinking PRACTICES aim at exploring the delivered project phases, the capabilities collected in the team and the attitudes embedded in the project activities.
- Design Thinking VALUE encompasses the value generated by the use of Design Thinking from two different perspectives: consultancy and client (DT4B, 2019).

For the purposes of our study we will consider two forms of Design Thinking, Creative Problem Solving and Sprint Execution, where the prototype takes on two types of meaning: in creative problem solving it expresses the genesis of incremental innovation that aligns customer needs with business objectives, while in the sprint execution, in the form of the minimum viable product (MVP), it forms the basis for developing the best product that generates the greatest possible value for the customer.

To enable a better understanding of this design philosophy, we will briefly describe the themes of each approach:

Sprint Execution is characterized by a strong focus on delivering products or services that are ready for use in the market or in real-world contexts where they align with user needs. The product is the primary driver of capturing value and learning from market and user responses, and technology is used to accelerate delivery while constantly reviewing the settings in line with the initial design. The approach is from the inside out: the consulting team expert designs the product/service and then refines it through the user experience, based on user/customer feedback and reactions. In other words, a product with the basic characteristics necessary to quickly satisfy the customer requirements is generated, accurately identifying the prototype as a **minimum viable product (MVP)**.

Another approach is Creative Problems Solving. Creative Problem Solving assumes that users have a need or a problem and the best possible solution must be sought.

The innovation team must intercept these user needs by analysing the product. The assumption of the research path is that the more ideas that are analysed as the best solution to the problem, the greater the chances of actually finding the right solution to the problem. Idea generation is about sharing detailed information with the team, interpreting big data, and identifying design opportunities.

The Creative Problem-Solving approach moves from the outside in. It starts by observing how users interact with the product in the real world and then interprets those observations by empathizing with users to create original solutions. The prototype, which has to interact with the user, has to be developed from a combination of lateral thinking and new perspectives, rational thinking and strong imagination, seeking inspiration everywhere and in all contexts, with alternating convergent and divergent phases of solution creation until the most promising solutions are identified.

The Double Diamond created by the Design Council represents the design process: while the first diamond focuses on designing the right thing, the second focuses on designing things right. It can be organized into four clear phases:

- Discover: Discover insights into the user and business requirements through a range of research methods (interviews, focus groups, etc.);
- Define: By using the insights gathered, and interpreting and aligning user needs and business goals, the teams identify and converge on project objectives and define the scope for feasible, achievable, and desirable outcomes;
- Develop: To find the best solution, teams use questions such as "How could we...?" to establish hypotheses and test them internally. A proof of concept is created through rapid prototyping and iteration processes. To ensure that teams are on the right track, they need to test and validate the proof of concept externally with end users. Through this validation, they make abstract concepts more concrete;
- Deliver: In the fourth phase, the resulting project (product, service, or system) is refined and launched (DT4B, 2019)

After this necessary introduction, we contend that the use of the finite element method (FEM), with appropriate adaptations, is ideally suited to the creation of products/services due to its ability to generate a large number of prototypes in a very short time after the appropriate simulations which allow the right solution to be identified. FEM prototyping takes on two meanings at once in this particular field of application: the first is in the context of the Kinematic Reconstruction Report, which through many simulations provides an excellent historical scenario of the facts and thus part of the physical-mathematical result sought; the second is more closely related to improving the **userism** of the Kinematic Report (intended as a prototyping phase of Design Thinking - Creative Problem Solving and Sprint Execution), for example by deciding which and how many curve graphs to use, how many and which videos are more representative to support the intended uses.

In the case studied, an “ex post” reconstruction of the kinematics related to traffic accidents and injuries is possible thanks to the combined use of FEM calculations and Design Thinking to produce a final report tailored to different applications: settlements, civil, and criminal court cases.

FEM analysis case study

In the automotive industry, numerical simulation has been widely used for decades because increasingly stringent safety requirements pose engineering challenges to find the best compromise between crashworthiness performance, structural weight, design and production costs. In this case study, impact scenarios are defined by regulation, and simulation allows biomechanical parameters to be determined on dummies without building expensive prototypes. The logical flow is completely different for the presented application and the method can be roughly divided into three macro phases:

1. By collecting and interpreting data from the field (road measurements, vehicle damage, medical reports, witnesses, and other evidence), experts define a possible impact scenario with a certain margin of uncertainty.
2. A numerical simulation of the event finds the initial conditions compatible with the impact dynamics and the final state in terms of overall kinematics and damage. Therefore, when conditions are not fully known (e.g. passenger wearing a seatbelt or

not) or some of the data collected is not entirely reliable, simulation permits the definition of those hypotheses that are compatible with the reliable data (Step 1).

3. Once the numerical model has described the event, a what-if analysis can be performed to study whether the evolution of the accident might have been different if the initial conditions had been modified.

LS-DYNA, the most common software tool for crashworthiness analysis has been used for this activity.

Scenario description

The scenario has been reproduced by analogy with other accidents but does not reflect any real case, for obvious reasons. Nevertheless, the case study presented is representative of a general approach to the problem. In general, there are three types of data available:

- Reliable data known with accuracy (e.g. vehicle damage);
- Reliable data which is not known with accuracy (e.g. angle of impact);
- Data to be verified (e.g. witness testimonies).

Data of type 1 and type 2 forms the basis for the reconstruction of the crash dynamics. In the presented case, the data corresponding to the categories is classified as follows:

- Type 1: Vehicle type, scooter type, damage to the vehicle, damage to the scooter, police report and measurements, medical report;
- Type 2: Speed and position (GPS) of the vehicle and scooter;
- Type 3: Witnesses.

With this information it was possible to define the following impact conditions:

- Vehicle speed between 5 and 15 kph
- Scooter speed between 30 and 40 kph
- Angle of impact between 25 and 35 degrees

The exact values of the mentioned quantities and other conditions are defined on the basis of the correlation between the simulation results and the data available from the field.

Therefore, when there are too many variables and combinations to be managed “by hand”, the results need to be processed in a statistically advanced manner. It is possible to consider using a multidisciplinary, multi-objective optimizer to manage the workflow automatically. This approach will not be presented in this paper.

Model description

The FEM model consists of a pick-up truck, a scooter and two dummies. With regard to the pick-up truck involved (specific libraries could be implemented as a service), the starting point is a model of the same class with similar external characteristics so as to have an

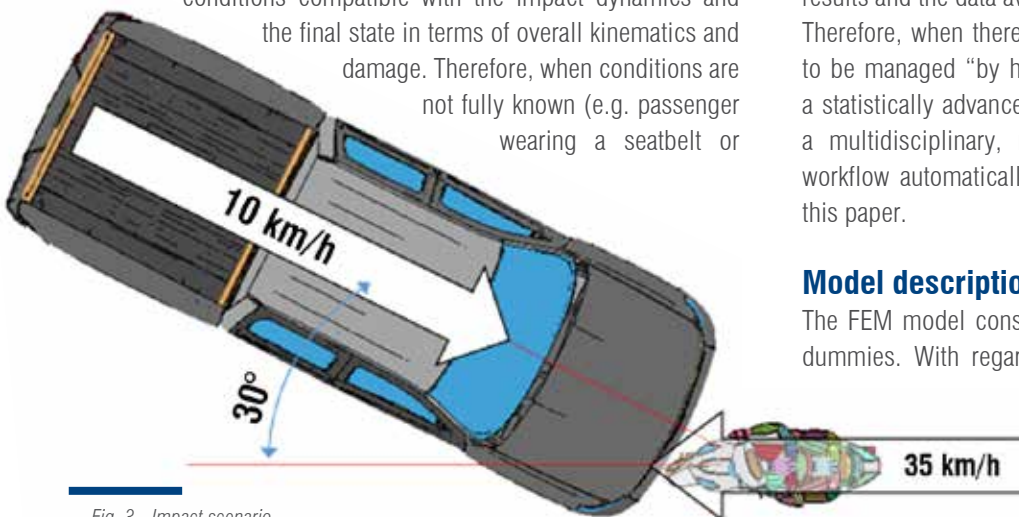


Fig. 3 - Impact scenario



Fig. 6 - Frame at the time of head impact.

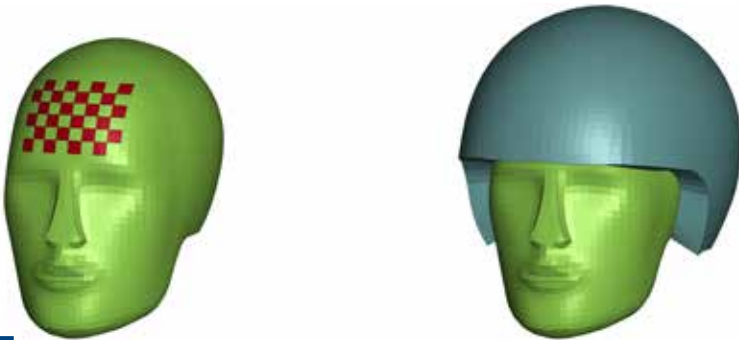


Fig. 7 - LSTC Head and Helmet models.

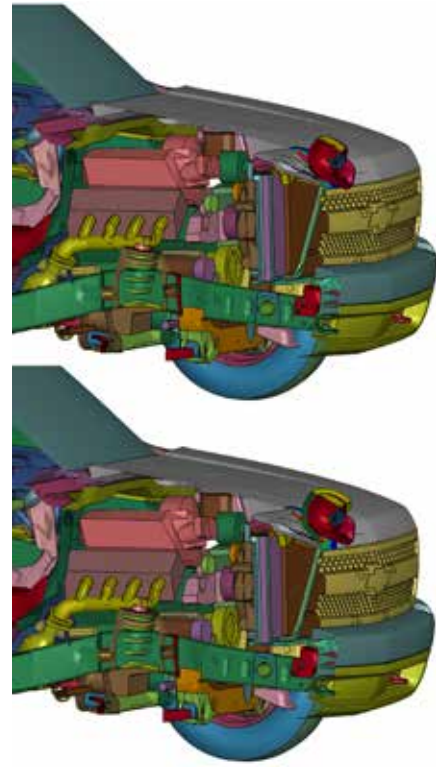


Fig. 8 - Section at time of head impact (without and with helmet).

Due to the fact that embedded models are not compiled until the simulation is run, correctly positioning the occupants in a model can be a tedious, trial-and-error effort. Stand-alone models are easier to position but are more CPU intensive. For the purposes of this accident reconstruction simulation, the built-in *COMPONENT_GEBOD model was selected for integration and evaluation.

Specifically, the user must create a file named gebod.dummyID that has to reside in the directory with the LS-DYNA input file. The positioning file consists of 40 lines of code relating to the angular measurements of the body segments.

Sub model description and initialization

In the case history presented the objective was to evaluate the head injuries with and without a helmet in order to define whether, in the real accident, the rider was wearing a helmet correctly or not.

As described before, thanks to the dynamic reconstruction with “fast” dummies, the impact conditions responsible for the main injuries are now available.

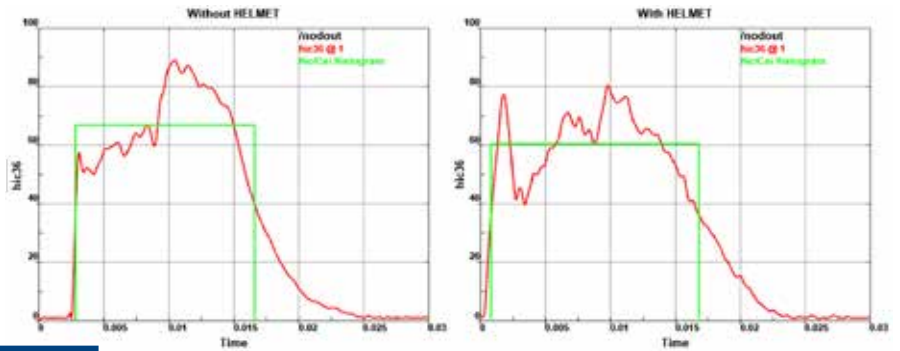


Fig. 9 - Head acceleration diagrams.

These conditions are the “initial conditions” for a submodel in which the simplified headform is replaced with a new model capable of assessing injury risks. The LSTC Free Motion Headform, a Hybrid III-type dummy head used to assess head injuries inside a vehicle and equipped with accelerometers to measure head acceleration during impact in order to calculate head injury criteria, was used.

The helmet is made of an expanded polystyrene (EPS) foam with a polycarbonate shell.

Results and discussion

Using the model discussed above it is possible to extract the amount of injury to

the instrumented head for the two cases (with and without the helmet).

The result with the helmet shows a decrease in the acceleration peak and a smoother curve due to the absorption of the charged energy by the protective foam of the helmet.

The most commonly used criterion for assessing head injuries in the automotive industry is called HIC (head injury criterion), and measures the risk of injury in terms of prolonged linear acceleration for durations of between 15 and 36 milliseconds. This criterion attributes brain damage measuring translational acceleration.

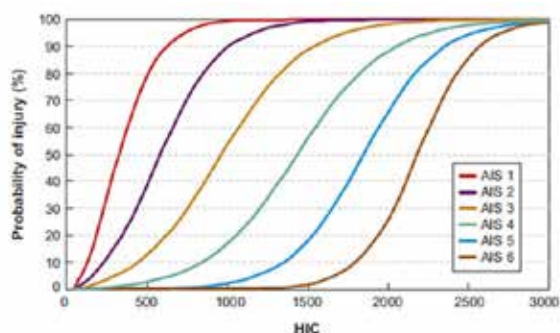


Fig. 10 - AIS-HIC diagram.

AIS	Severity	Type of injury
0	None	None
1	Minor	Superficial
2	Moderate	Reversible injuries; medical attention required
3	Serious	Reversible injuries; hospitalization required
4	Severe	Life threatening; not fully recoverable without care
5	Critical	Non-reversible injury; not fully recoverable even with medical care
6	Virtually unsurvivable	Fatal

Alongside the HIC, for some specific brain injuries, other measuring instruments also analyze the rotational effects, known to be important for causing the deformation of the brain cut. Some of these are combinations of linear and rotational acceleration, and some are entirely based on head rotation, namely the Brain Damage Criterion (BrIC), the Rotational Damage Criterion (RIC), and the Power Rotational Head Injury Criterion (PRHIC). The presented work, however, focused on the relationship between HIC and human trauma. Biomechanics experts agree that an HIC score of 1000 represents the “safe” limit for human tolerance, above which the risk of a severe head injury is nonzero.

In the scenarios analysed for the case study, the presence of the helmet reduced the HICd (dummy head injury criterion) value from 550 to 500, showing that the helmet clearly mitigates the consequences of the accident to the rider. As mentioned, the potential for head injury can be quantified using the Head Injury Criterion (HIC), which is calculated as a function of the magnitude and time duration of head acceleration. In the context of road traffic and accident insurance reconstructions, the required output is not a score, however, but rather an assessment of the trauma suffered. For this purpose, the HIC values were correlated with the Abbreviated Injury Scale (AIS), which codifies the severity of injuries to all regions of the body.

The AIS incorporates current medical terminology, providing an internationally accepted tool for ranking injury severity. It is an anatomically based global severity scoring system that classifies an individual injury by body region according to its relative severity on a 6-point scale (1=minor and 6=maximum) and is the basis for the calculation of the Injury Severity Score (ISS) of the patient with multiple injuries.

Conclusion

One of the main objectives of the work presented here was to demonstrate that the use of numerical simulation is a fundamental tool in the reconstruction of road traffic and accident insurance reports.

The work focuses on the use of the finite element method (FEM) to analyse the outcome of an accident, and whether input parameters can modify the scenario. In addition, the work focuses on the assessment of the level of head trauma using the Head Injury Criterion and links it to the AIS scale.

The behaviour of pick-up trucks, scooters and dummies is assessed using full three-dimensional models of complete vehicles, a helmet, dummies, and heads. The results are presented and discussed in terms of HIC values and the probability of acceleration-induced trauma to assess the relevance of the helmet in terms of injury to the rider.

From the results obtained in the scenario analysed, it can be seen that the presence of the helmet reduced the HICd value from 550 to 500, leading to a reduction of serious injuries.

As the use of FEM in the field of the kinematic reconstruction of car accidents impressively demonstrates, the relative compatibility of the respective property damage between several vehicles enables economic value to be calculated, both as a decision support tool in the insurance case, by analysing the compatibility of physical injuries to pedestrians or passengers through methods derived from design thinking that have a direct impact on the insurance company’s profit and loss account, and as value creation for the consumer, improving the customer experience by fairly quantifying compensation, leading to greater brand loyalty and advocacy, which generally improves trust and credibility in the

About DCA Consulting

DCA Consulting was founded in 2001 and targets corporates in the specific areas of claims, collections management, and strategic-organizational consultancy, offering highly innovative operational solutions through digital solutions designed around customer centrality.

The company addresses a stimulating and engaging work environment specializing in the professional management of networks and digital solutions designed for business process management and people management in the insurance, banking, and automotive sectors.

The DCA Innovation division was established in 2015 to focus on the design and development of software to support innovation and digital transformation through Design Thinking.

Insurance Company	YEAR 1	YEAR 1+1	YEAR 1+2	YEAR 1+3	YEAR 1+4	YEAR 1+5
Annual growth of savings due to FEM		10%	10%	10%	10%	10%
Savings on Large Claims Payments	500	550	605	666	732	805
Operating expenditure + Capital expenditure	180	220	220	250	250	280
Ebitda	320,0	330,0	385,0	415,5	482,1	525,3
% Ebitda	64,0%	60,0%	63,6%	62,4%	65,8%	65,2%
Depreciation	50	50	50	50	50	50
Ebit	270,0	280,0	335,0	365,5	432,1	475,3
%Ebit	54%	51%	55%	55%	59%	59%
Tax rate	40%	40%	40%	40%	40%	40%
- Taxes	108,0	112,0	134,0	146,2	172,8	190,1
Net Income	162,0	168,0	201,0	219,3	259,2	285,2
% Net working capital vs saving	10%	10%	10%	10%	10%	10%
Net Working Capital (NWC)	50,0	55,0	60,5	66,6	73,2	80,5
- NWC variation		5,0	5,5	6,1	6,7	7,3
- Additional investments in FEM		30	30	40	50	50
FCFF		133,0	165,5	173,3	202,6	227,8
WACC (Example)		9,00%	9,00%	9,00%	9,00%	9,00%
Year		1	2	3	4	5
DCF = FCFFt / (1+WACC) ^ t		122,0	139,3	133,8	143,5	148,1
Σ DCF						686,7
TV = (FC09*(1+g)) / (WACC-g) =						3911,1
TV actual = TV / (1+WACC) ^ 5						2542,0
EV = ΣDCF+Tvatt						3228,6
Value €*000						

insurance market. Like any new and innovative tool, FEM must find an appropriate role to support:

- strategic planning (business model canvas, balanced scorecard, budgeting)
- management control, ex-ante evaluation of the cost-effectiveness of the project investment and of the actual cash flow generation by the prototype.

For the sake of simplicity, we will use accounting indicators to summarise and measure the performance of a company. More precisely, we can divide the indicators into three groups:

- A first set of indicators is derived from ROE, which measures the ratio of profit generated to capital employed: if this ratio is positive, profits are higher than the cost of capital.
- A second set of indicators, derived from Residual Income (RI), identified as Economic Value Added (EVA), measures economic performance as the difference between the profit generated and the cost of capital employed. When RI is greater than or equal to zero, profits are greater than the cost of capital.
- A third group of indicators called Value Based, adjusts the previous two methods and replaces profit with cash flow.

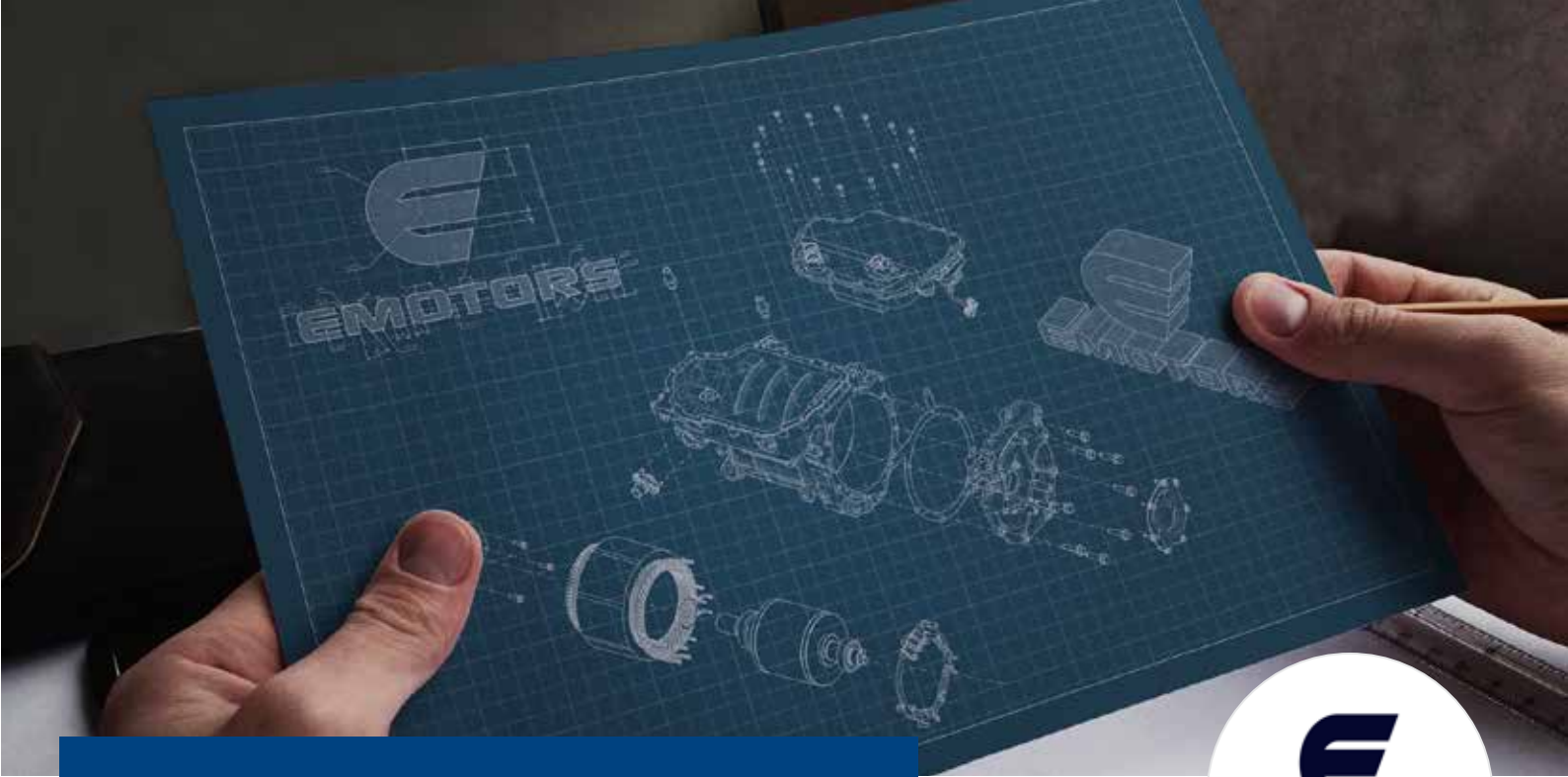
We will focus on the third group of indicators by looking at them through an expected Discounted Cash Flow (DCF) simulation. This is a valuation method that estimates the value of an investment based on its expected future cash flows. As shown in the example below, we can see how the FEM methodology brings significant profits to the company and proportionally reduces the investments associated with the new technology year after year.

Example:

- For Year 1, we set a target of saving €500,000 in large claims compensation. We also allocated a reasonable amount of €180,000 for operating costs and capital expenditure.
- Assuming a 10% annual growth in large claims savings, we can realistically calculate a total DCF of around €690,000.
- Assuming a cost of capital (WACC) of 9%, the Enterprise Value (EV) of the investment reaches €3.2 million.

For more information:

Fabio Ardente – DCA Consulting
fabio.ardente@dcaconsulting.it



Optimizing the spray cooling of e-drives with moving particle simulation

by Ioan Deac¹, Juan Wang¹ and Michele Merelli²
 1. EMOTORS - 2. EnginSoft

Moving particle simulation (MPS)

The advances in simulation methods and computing power have resulted in new simulation methods becoming available over the last three to five years. One of the most interesting for powertrain applications is MPS, a meshless CFD approach.

The MPS method is a deterministic Lagrangian particle method for calculating incompressible free-surface flows and non-Newtonian liquids. MPS was proposed by Koshizuka and Oka in 1996 [1]. While its core concept is similar to smooth particle hydrodynamics (SPH), MPS has evolved from a semi-implicit predictor-corrected formulation to fully explicit formulations that are more efficient for large-scale models, reducing simulating time and computing effort.

The use of MPS has grown in popularity within the automotive sector and it is now a well-established approach to free-surface flow and liquid flow analyses. Applications include oil splash and sloshing in gearboxes and transmissions, forced lubrication by oil jet, piston cooling, crankcase sloshing, and jet or spray cooling of wet electric motors.

The simulation process of e-motor cooling

The simulation of oil-cooled e-motors is difficult mainly due to the geometrical complexity of the system (culminating in the winding region), the multiphase nature of the flow dynamics, and the rotational speeds up to 20,000 rpm.

Traditional, Eulerian mesh-based fluid dynamics solvers are unable to produce models with affordable setup times and computing requirements. These are critical functions to efficiently integrate CFD codes into the industrial R&D workflow.

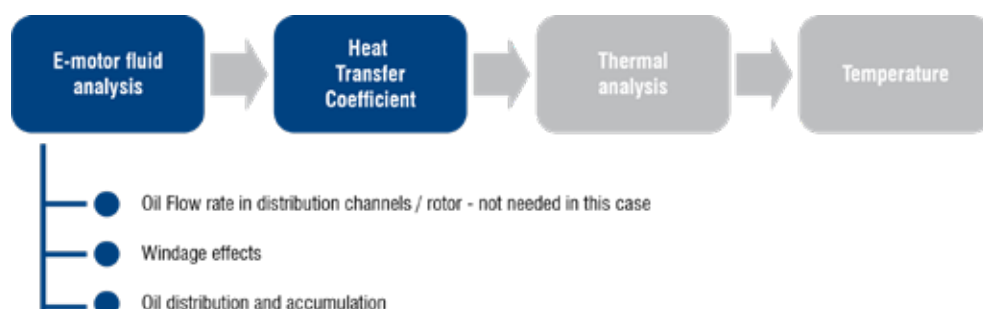


Fig. 1 - Schematic of the simulation methodology for e-motor cooling. The CFD related topics analysed with the MPS method are shown in blue.



Engineers from EMOTORS and EnginSoft have developed virtual e-motor prototypes based on different simulation requirements, rarely considering the subsystems of the unit for further analysis.

However, the main objective of e-motor cooling simulations is to evaluate and improve oil distribution for different cooling branches and to maximize heat transfer between the oil and the e-motor components. The process can be summarized into the following steps (Fig. 1):

1. Evaluation of the oil flow distribution in the rotor shaft channels and at the nozzle outlets;
2. Calculation of the windage effects (aerodynamic drag);
3. Visualization of the oil jets and flow in the e-motor, from nozzle outlet to motor outlet;
4. Mapping the heat transfer coefficient and heat fluxes over the critical geometrical element;
5. Transferring the cooling effects to a thermal model for temperature prediction.

More specifically, given the above-mentioned steps, the entire simulation process (from CAD preparation to the configuration of the different simulations and including the hardware simulation times) takes about two weeks.

As for the numerical parameters and the particle size (a concept comparable to the minimum mesh size of traditional Eulerian methods), these may vary from one sub-simulation to another. In general, MPS simulation times are mainly influenced by:

- Volume of fluid/air to initialize
- Total number of resulting particles (calculation nodes)
- Initial delta time (DT) of the simulation and the Courant-Friedrichs-Lewy condition (usually the Courant Number for MPS is 0.2)
- The type of pressure solver (if implicit or explicit)
- The activation of an additional physics model (turbulence, thermal equation, conjugate heat transfer, etc.)

As shown in Fig. 1, the first step in the simulation process is to analyse the flow distribution inside the e-motor circuit. Fig. 2 summarizes the flow pattern with flow distributed in the rotor, winding and stator regions. It is important to study the distribution of the flow across all sub-circuits and to verify it with respect to different conditions of speed and viscosity to avoid unbalanced configurations. In this step, the pressure distribution of the fluid within the channels can be measured and verified against the design requirements or manufacturing specifications.

Considering that the rotor speed can be up to 20,000 rpm, windage and air drag effects have to be taken into account. For this purpose, an additional simulation is usually included in the presented methodology. In this step, only the air is simulated, with a discretization size capable of providing results within a few hours of simulation. As a result, the same MPS model can be used to extract the internal air flow without creating any additional numerical model and without mesh/geometry cleaning.

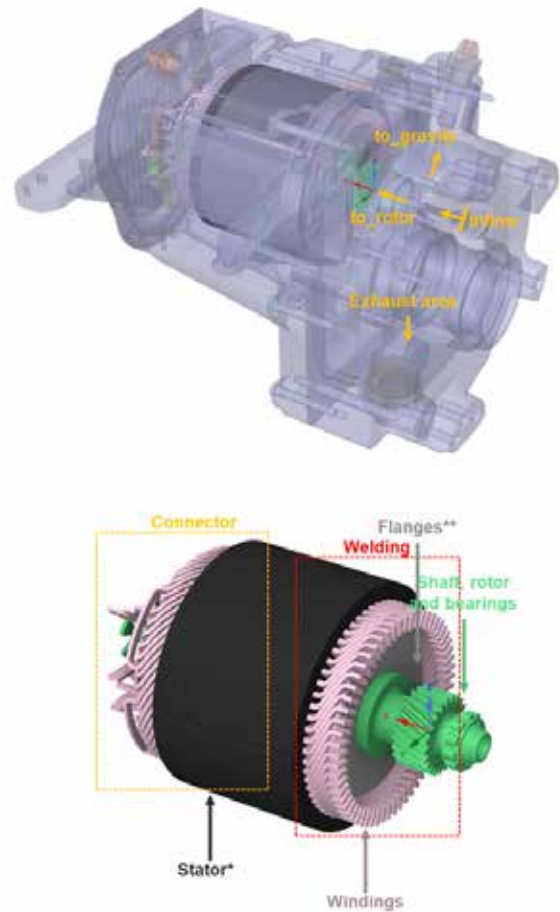


Fig. 2 - Isometric view of the e-motor presented. On the left, the names of the cooling sub-channels. On the right, the names of the most important parts of the e-motor.

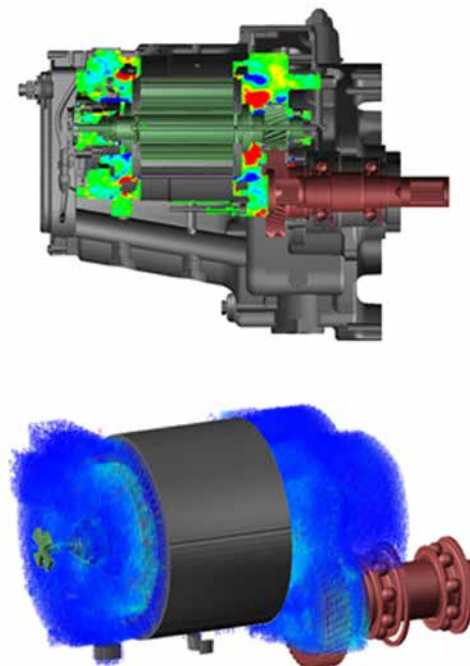


Fig. 3 - Overview of the airfield as calculated by the MPS method (top) and the same airflow as imported into the oil-only simulation (bottom).

Next, the main simulation is performed, focusing on the extraction of the heat transfer coefficient (HTC) maps which are then used to calculate the temperatures inside the e-motor components. The precalculated airfield is transferred to the oil-only simulation, with a one-way coupling (air influencing oil with a specific drag coefficient). The numerical parameters (particle size, simulation time step, thermal modelling) are adjusted to better capture the jet spray effect and for a more correct thermal assessment.

The convergence of the CFD model is checked by monitoring the oil distribution with control volumes in different areas (end-windings, stator, brackets). Subsequently, HTC maps, usually averaged over the last 0.5-1 s of steady-state operation (see Fig. 4) are extracted. In this way, maps as shown in Fig. 4 are obtained for each wetted element inside the e-motor. These maps are also exported as .csv files by the software, ready to be transferred to the finite element analysis (FEA) model for predicting the temperature distribution. For the temperature distribution prediction, the MPS methodology introduced was previously validated by experimental tests [2].

Cooling circuit and validation of the methodology

In the design stage of the prototype, EMOTORS conducted several simulations focusing on different aspects of the e-motor design. The cooling circuit diagram of the analysed prototype is shown in Fig. 5.

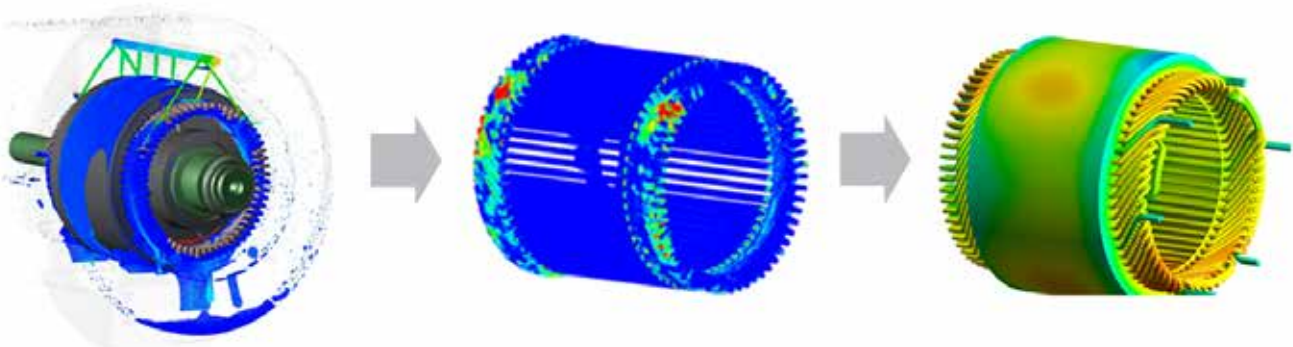


Fig. 4 - From oil distribution to temperature distribution. On the left, the oil can be inspected and, once stabilized, an HTC map is extracted. The maps are transferred to the FEA model to obtain the temperature prediction.

The housing contains two oil cooling circuits: one static (gravity cooling) and one rotating inside the shaft and rotor (rotor cooling).

As shown in Fig. 4, the oil enters the housing from a lateral main circuit which then splits and part of the oil passes into the middle channels of the shaft (rotor cooling) while the remaining oil is directed to an additional upper layer above the windings and stator (gravity cooling). The rotor cooling circuit is designed to cool the inner surfaces of the windings, while gravity cooling sprays the outer surface of the end windings and the outer surface of the stator plate. Volume flow rates are measured by probes placed near the inlet and at the inlet of the rotor cooling and gravity cooling passages.

The simulation of this first step and approaching the problem using the RANS VOF (Reynolds-Averaged Navier-Stokes Volume of Fluid)

method, proved to be troublesome at first. The challenge of modelling this internal flow is mainly related to the multiphase nature of the flow and the high rotational speed. The MPS method has proven to be more reliable for this purpose. In order to validate this first step of the MPS model we used a dedicated prototype designed to test multiple flow configurations and parameters. Different circuit configurations of the prototype were obtained using nozzles and plugs to limit the internal diameter or even to close off certain portions of the circuit. We also had control over other parameters: oil temperature, inlet flow rate and rotation speed. In addition, we measured the pressures at the inlet and at some intermediate points of the circuit and the flow rate for an outlet branch of the circuit. In addition, we opted for a Design of Experiment (DOE) approach to testing in order to prepare the results for statistical post-processing. The purpose of statistical post-processing of the results is to help us assess the physics and reliability of the measurements and to remove noise from the readings.

We also decided to verify the statistical model we developed with an out-of-sample control configuration that was not used in the post-processing. As can be seen in Fig. 5, the statistical model correctly predicts the flow rate distribution of the out-of-sample dataset. Fig. 6 compares the results between the experimental data and the MPS calculations, for a single flow operating condition (8 l/min).

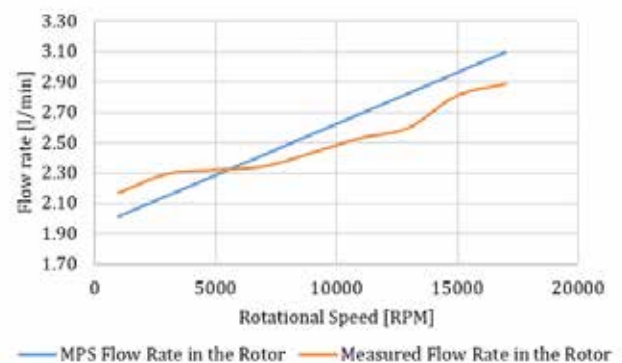


Fig. 5 - Flow rate through the rotor cooling circuit of the out-of-sample dataset (orange) and the predicted trend of the statistical model constructed using the DOE (blue).

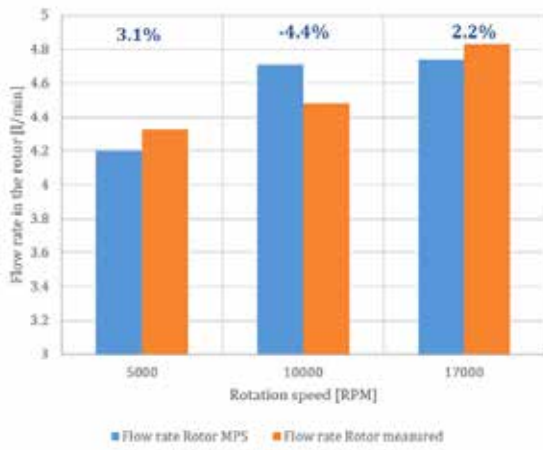


Fig. 6 - Flow rate to the rotor cooling system (rotor circuit) for three rotor speeds. The MPS predictions (blue) are compared to the experimental results (orange).

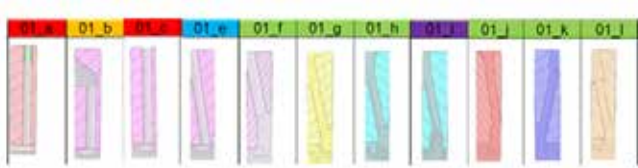


Fig. 7 - Cross sections of the flanges considered in the single jet HTC analysis.

areaAve(Wall External Heat Transfer Coefficient)@Complete Connector

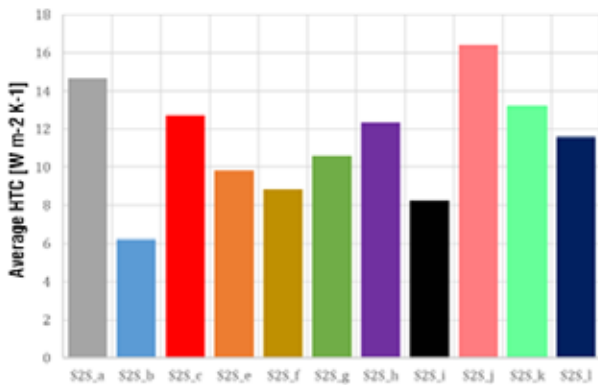


Fig. 8 - Area weighted average HTC across the windings for different flanges (contribution of a single oil jet).

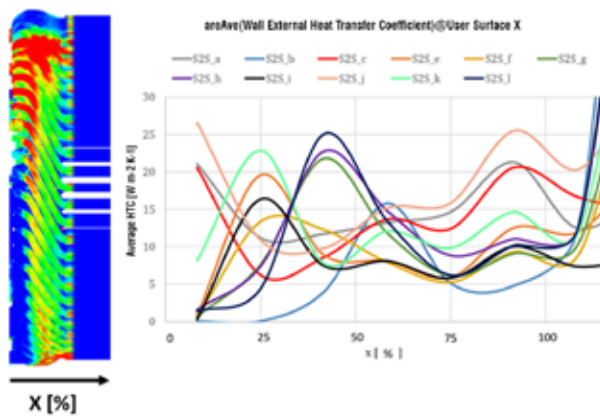


Fig. 9 - AreaAveHTC for different x-slices of the windings. This analysis allows the HTC values to be mapped spatially in a quantitative way.

The flow through the rotor cooling system is reported for three different rotor speeds. We obtained an error of ±5% between the simulation results and the post-processed experimental data.

Design improvements: flanges and brackets

After validating the MPS methodology for internal flow analysis, an important element to analyze in the early design phase are the flanges at each side of the rotor laminations. The size of the oil passage in the flange can change the balance of the oil flow between the rotor and the stator. The shape of the passage was found to have a critical influence on the trajectory of the oil particles and on the size of oil jet before it hits the windings.

To reduce calculation time, only the rear of the windings (the side corresponding to the phase connector element) is simulated. Also, only part of the channel (one of the four jets) is modelled to further reduce the quantity of oil simulated.

Several geometrical modifications to the rotor flanges were considered to improve the cooling efficiency of the e-motor. These geometrical details are shown in Fig. 7.

In order to compare the configurations, we computed the area weighted average of the HTC values (AreaAveHTC) across the exposed windings. The following formula averages the n-th HTC value calculated on the n-th triangular surface of the .stl file, weighted for its surface area:

$$AreaAveHTC = \frac{\sum HTC_n \cdot A_n}{\sum A_n} \text{ (Equation 1)}$$

The results for the designs discussed are shown in the chart below (Fig. 8). As can be seen, careful design and direction of the flow in specific areas of the windings can result in a two- to three-fold improvement in the cooling efficiency, compared to the poorest configuration.

In order to evaluate the flow distribution on the windings in more detail, the average HTC was evaluated for different slices (in the axial direction). The results are shown in Fig. 9. The AreaAveHTC for each slice x is reported against the x % (0 % end of the windings, 100% inner side of windings, rotor side).

It can be observed that:

- Flanges O1_a, c, and j have the best HTC near the 0 and 100% mark of the length of the end winding;
- Flanges O1_g, h, and I have the higher HTC near the 50% mark of the length of the end winding;
- Flange O1_e has a better HTC near the 25% mark of the length of the end winding;
- A small nozzle (O1_k) has the effect of focusing the oil near the 25% mark of the length of the end winding (closer to the stator lamination) compared to O1_g and O1_l.

The stator brackets also help to improve heat transfer inside the e-motor. They are situated between the inner surface of the housing



and the outer surface of the windings. Without the stator bracket, the oil jet from the rotor will mainly spray the inner surface of the housing. The stator bracket's purpose is to redirect the oil from the rotor injection towards the windings. We decided to test the possibility of improving the performance of the baseline bracket design. The geometrical features of the two variations (labelled as Small and Axial) are shown in Fig. 10 below.

One way to monitor the efficiency of a specific design is to measure the amount of oil in the region of the windings by means of a control volume. Fig. 11 shows the oil accumulation trend for the first two seconds. A clear difference can be seen between the proposed designs and the baseline. To examine the efficiency of the system more closely, we focused on the AreaAveHTC on the windings, comparing the two bracket designs with the baseline. The AreaAveHTC result trends follow the oil accumulation, with the baseline design showing better cooling performance.

These simulations enabled us to test and exclude two proposed bracket designs that proved to be less efficient at keeping more oil in the area of the windings.

Conclusions

This paper described the simulation of e-motor cooling using MPS, a mesh-less approach well-suited to impinging jet and free-surface flow analyses. We reported the methodology of the MPS e-motor simulation, the internal flow rate split, the windage effects, the HTC distribution, and the temperature distribution.

At the internal flow distribution step, we validated the MPS methodology using a dedicated prototype and a statistical technique. This validation also demonstrated the range of reliability and confidence of the simulation results, significantly reducing the number of prototypes necessary to move from the initial design to the final product.

Moreover, we showed how MPS simulation can provide insightful design indications for key components of the e-motor, like the rotor flanges and the stator brackets. The EMOTOR engineers were thus able to propose further improvements to the cooling of their e-motors, achieving competitive power densities for the motor while reducing the use of materials and increasing the reliability of key components.

References

- [1] S. Koshizuka and Y. Oka (1996). *Moving particle semi-implicit method for fragmentation of incompressible fluid*: Nuclear Science and Engineering, Vol 123, pp. 421-434.
- [2] M. Brada (2020). *Thermal Simulation of an Oil-Cooled E-Motor*: 36th International CAE Conference and Exhibition.

For more information:
 Michele Merelli, EnginSoft
 m.merelli@enginsoft.com

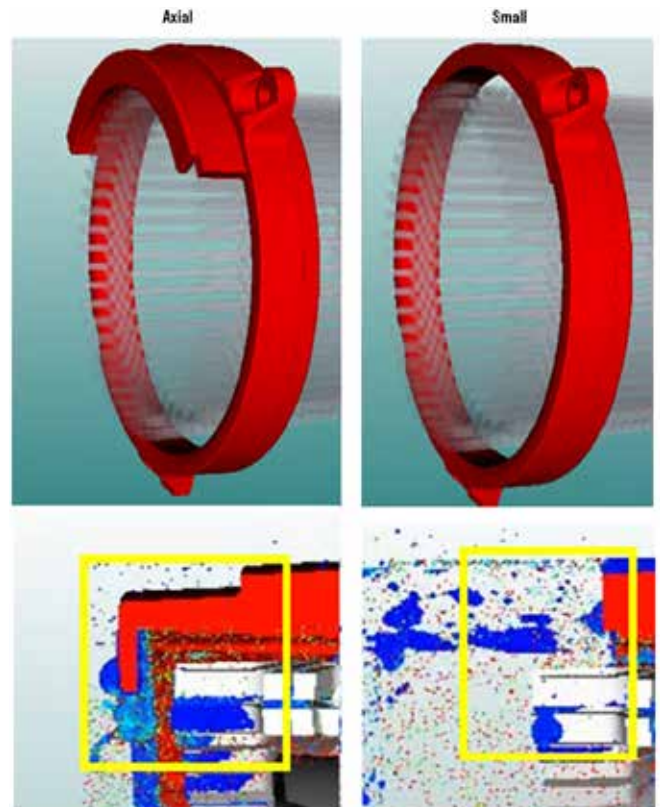


Fig. 10 - Overview of the bracket design (top, isometric view) and detail of the modification near the windings (bottom). As can be seen, the Axial bracket design collects the oil (blue) so it does not splash onto the external housing as seen on the bottom right.

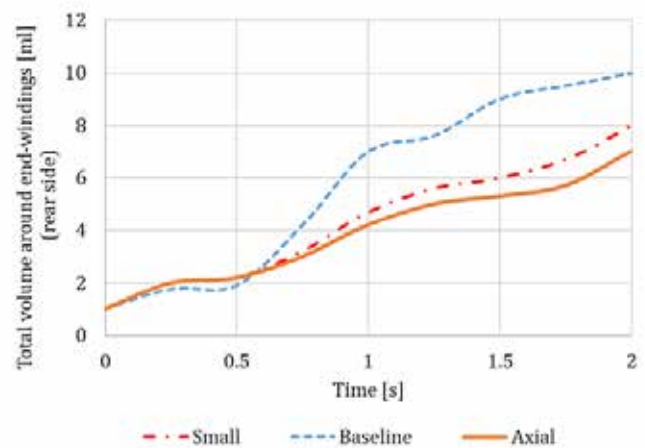


Fig. 11 - Total amount of oil in millilitres around the windings (at the rear of the e-motor). Two proposed bracket designs (Small, Axial) are considered as possible improvements of the baseline.

	Area Weighted Average HTC
Small	68
Baseline	84
Axial	63

Fig. 12 - AreaAveHTC for the two proposed brackets (Small, Axial) compared to the baseline design.

Calibration of the Johnson-Cook plasticity for high strain rate regime applications

by Simone Dichiario and Fabrizio Marcelli
MBDA



Numerical simulation based on finite element method (FEM) technology generally accommodates the thermomechanical behaviour of metallic materials, with the advantage of greatly reducing the experimental effort required for testing and validation of components and parts. In order to obtain reliable numerical results, the calibration of material model parameters is of paramount importance, especially for high strain rate applications.

The characterization of material behaviour can be very challenging, especially if the number of parameters that govern the constitutive equations is significant. In most cases, sophisticated formulations consist of multiple parameters that require dedicated calibration from different sets of experimentally measured data. Among the phenomenology-based models, the Johnson-Cook formulation [1] is one of most widely used constitutive relations for metals subject to large strain, high strain rate, and high temperature.

In order to calibrate the material model parameters, it is necessary to evaluate each isolated contribution of the formulation and associate dedicated experimental tests to each, ranging from the classical tensile test to the less common Split-Hopkinson tensile test. Once the test data is available, a common approach to calibrating the material parameters is the numerical reverse engineering of the experimental test through the finite element method (FEM), matching the experimental curve to the numerical one.

This paper deals with the mechanical characterization of a metallic material at high strain rates. The methodology is based on the synergy of numerical tests and FE simulations, enhanced by optimization based on genetic algorithms

Experimental tests

The experimental campaign was structured as follows:

- Quasi-static tensile tests at room temperature;
- Quasi-static tensile tests at high temperatures;
- Hopkinson bar dynamic tests.

Quasi-static tensile tests were performed on a universal testing machine (see picture above), using a clip gauge and digital image correlation (DIC) to measure the specimen's elongation. Since temperature strongly influences the mechanical

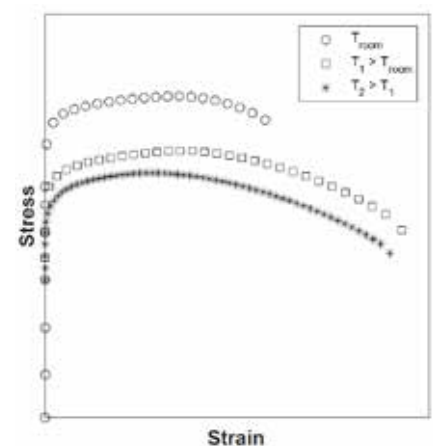


Fig. 1 - Stress-strain tensile curves at room and high temperature.

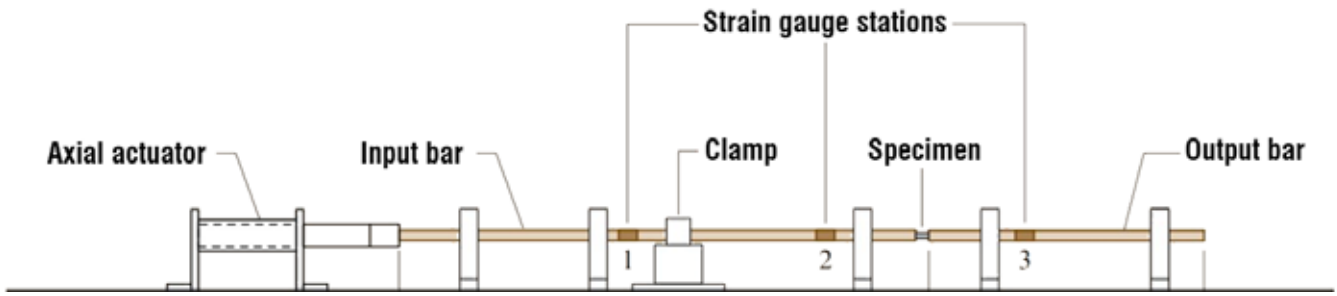


Fig. 2 - Hopkinson bar with direct-tension split.

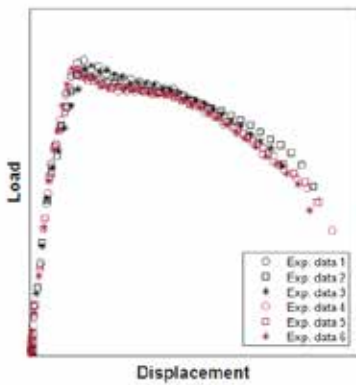


Fig. 3 - Load-displacement curves from split Hopkinson bar tests

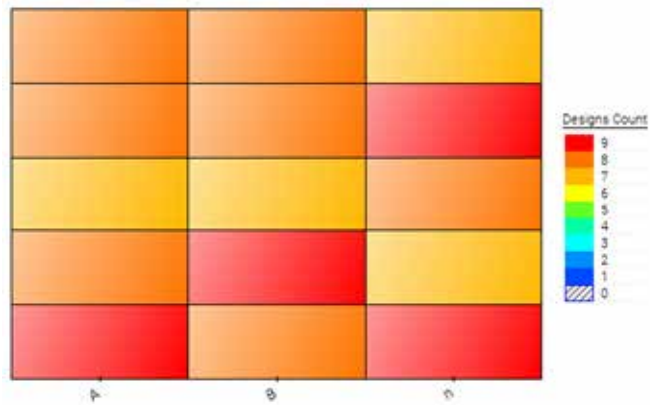


Fig. 5 - Design distribution on DOE.

behaviour of metallic materials, high temperature tensile tests were carried out to study its effect using the climatic chamber, with a thermocouple to control the temperature levels.

The engineering stress-strain curve obtained from the room temperature and high temperature tests is shown in Fig. 1.

Hopkinson bar tests allow the material behaviour to be studied in the high strain rate regime. The sample is placed between two long, thin bars (the incident and the transmitted bar). Depending on the type of impulse generated in the incident bar, it is possible to obtain tension, compression, torsion (or a combination of these) conditions. The incident and transmitted bars are designed to operate in the elastic region for the entire duration of the test. In

this study, a Hopkinson bar with a direct-tension split was used, as shown in Fig. 2 [2]. The load-displacement curves obtained from the test under a high strain rate regime are shown in Fig. 3.

Material model

The material constitutive law selected for this activity is the Johnson-Cook model [1] [3] because it allows the effects of strain hardening, strain rate and temperature to be taken into account within a single formulation. According to this formulation, the equivalent stress is expressed as:

$$\sigma = (A + B\varepsilon^n)(1 + c \ln \dot{\varepsilon}^*) (1 - T^{*m})$$

where ε is the equivalent plastic strain, $\dot{\varepsilon}^* = \dot{\varepsilon} / \dot{\varepsilon}_0$ is the plastic strain rate $\dot{\varepsilon}$ with respect to the reference value $\dot{\varepsilon}_0$ and $T^* = (T - T_{room}) / (T_{melt} - T_{room})$ is the

homologous temperature considering the room temperature T_{room} and the melting temperature T_{melt} . In this formulation, the calibration concerns the parameter set A, B, n, c and m.

Numerical calibration procedure

At this point, the numerical simulation of the experimental test (Fig. 4) is performed for both the quasi-static and the high strain rate test.

The former evaluates the subset of parameters A, B and n. The latter enables us to find the refinement of the first values c and m obtained by analysing the experimental curves. All the simulations were performed using the LS-DYNA FE code, its implicit solver, and the formulation of 2D axisymmetric elements.



Fig. 4 - 2D axisymmetric FE model for Hopkinson samples.

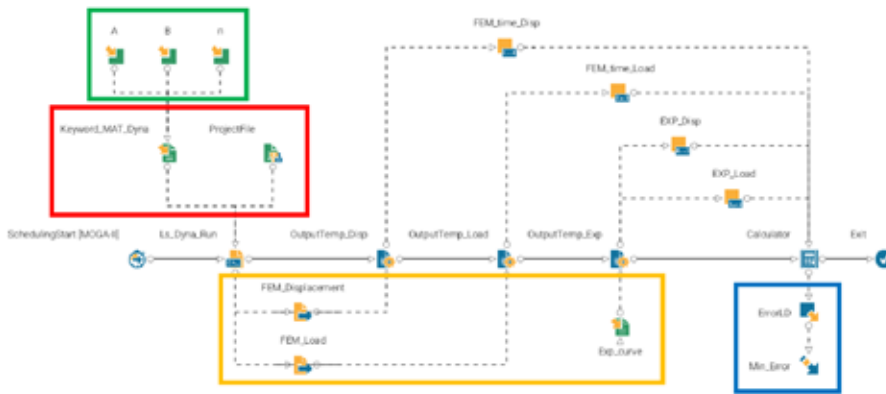


Fig. 6 - Calibration diagram for integrating LS-DYNA into modeFRONTIER.

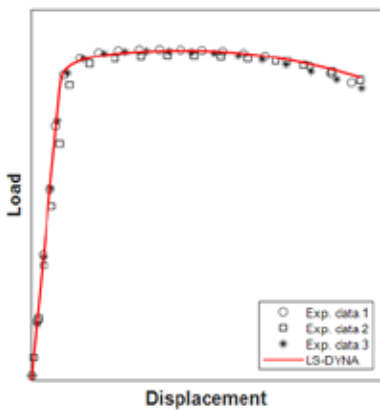


Fig. 7 - Comparison of experimental data and numerical curves for quasi-static tensile tests.

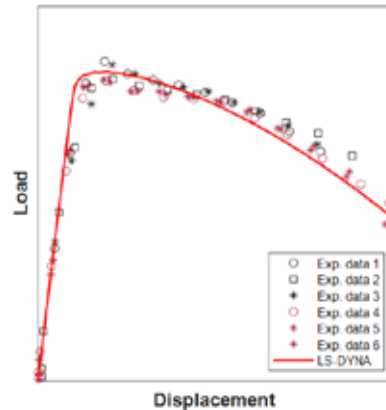


Fig. 8 - Comparison of experimental data and numerical curves for high strain rate Hopkinson bar tests.

These simulations were integrated into a fully automated procedure using modeFRONTIER optimization software. In order to minimize the correlation between parameters and maximize the distance between the generated designs, the uniform Latin hypercube (ULH) was used to create the initial design of experiment (DOE). Then, the incremental space filler (ISF) algorithm added new points to uniformly populate the input space (Fig. 5).

From the initial DOE, the generation of a new set of parameters was guided by the multi-objective genetic algorithm (MOGA) II, with the aim of minimizing the error between the experimental and numerical curves. (Fig. 6). The new set of parameters (green box) is edited within the LS-DYNA material keyword file (red box). The numerical and the experimental curves (orange box) are vectorized and compared. The difference is then minimized (blue box).

Results

From the quasi-static optimization cycle, a suitable set for A, B and n allows the tensile test to be reproduced with great accuracy in the low strain rate regime, as shown in Fig. 7. By fixing this set of values, a second calibration scheme leads to a refinement of the values for c and m obtained from the analysis of the experimental data. With the complete set of parameters, the material behaviour is fully reproduced in the high strain rate regime for the Hopkinson tests (Fig. 8).

Conclusions

This work presents the calibration of the parameters for a metallic material model, capable of reproducing plastic flows under high and low strain rates. Results from experimental tensile and Hopkinson bar tests served as the starting point for feeding the optimization scheme.

The tests, reverse-engineered using FEM and LS-DYNA's implicit solver, were incorporated into modeFRONTIER, and an optimization based on genetic algorithms produced a set of parameters on the Pareto frontier. The corresponding numerical curve were compared to the experimental data, obtaining good agreement for both the tensile and Hopkinson tests.

For more information:

Vito Primavera - EnginSoft
v.primavera@enginsoft.com

References

- [1] G.Johnson, W.Cook, "A constitutive model and data for metals subjected to large strain, high strain rates and high temperatures," Proceeding of the 7th International Symposium on Ballistics, 1983
- [2] W.N.Sharpe, "Springer Handbook of Experimental Solid Mechanics", Springer Science & Business Media, 2008
- [3] Livermore Software Technology Corporation, LS-DYNA Keyword User's Manual, Material Models, vol. II

About MBDA

MBDA is the only European defence group capable of designing and manufacturing missiles and missile systems to satisfy the full range of current and future operational requirements of the three armed forces (land, sea and air).

With a significant presence in five European countries (France, Germany, Italy, UK, Spain) and in the USA, the group offers a range of 45 missile and countermeasure systems that are already in operation with over 90 customers and more than 15 others projects are under development. MBDA is jointly owned by Airbus (37.5%), BAE Systems (37.5%) and Leonardo (25%).



Aerodynamic analysis of the new generation Korea Train eXpress (KTX) pantograph

by **Jinwook Kim**
TSNE

A train's pantograph is primarily used to collect and supply electrical energy by connecting the train to the catenary line. Since it is located on the roof of the train, the pantograph is an aerodynamically unfriendly buff structure that affects both the train's aerodynamic drag and lift, as well as the aero-acoustic noise of the train, when travelling at high speeds. When determining the total variations in contact force, aerodynamic uplift is one of the primary dynamic components with mechanically preloaded spring force. In this study, Ansys Fluent was used to perform a computational fluid dynamics (CFD) simulation to analyse the aerodynamic performance of the cantilevered or single-arm pantograph of the new generation Korea Train eXpress (KTX) in both closed- and open-knee positions.

Rail has long been the most representative means of ground transportation with huge transport capacity and speed. With the development of railway technology, the speed of trains is becoming faster and faster and a number of eco-friendly regulations are being issued. Basically, a railway is powered by electricity from a catenary supply, so most railway systems make use of a pantograph mechanism. Optimal contact force between the pantograph and the catenary wire should always be maintained to avoid serious engineering problems such as excessive friction, driving resistance due to excess uplift, or

loss of contact due to negative lift. Consequently, pantograph design aims to achieve a stable and desirable contact force at high speeds and for various driving conditions.

The high velocity airflow caused by the operation of the train generates strong aerodynamic drag and uplift forces on the pantograph, which are the main causes of contact force variations between the pantograph and the catenary wire. In particular, at high speeds in excess of 300 kph, extreme uplift can cause excessive friction on the contact shoe to prevent loss of contact from negative lift. Both these undesirable phenomena can also accelerate occurrences of serious electrical and mechanical damage. Therefore, the analysis of aerodynamic performance is essential to identify the optimal lift contact force and design the most appropriate geometrical shapes.



Fig. 1 - The pantograph of a high-speed train.



Regulations

The optimal total contact force between a pantograph and a catenary wire due to preloaded mechanical forces and aerodynamic lift is defined by several standards and regulations. In Europe, EN50119 Railway Applications established by CENELEC (the European Committee for Electrotechnical Standardization) states that the difference between the mean contact force and three times the standard deviation must be statistically greater than 0 N and the maximum contact force should be less than 350 N. If the mechanical contact force cannot be measured, the contact loss ratio can be used as an evaluation criterion for this standard. For safety reasons, the International Union of Railways' UIC 799 limits the maximum permissible lift to 120 mm. UIC 794-O limits the average contact force to less than 120 N, to 200 N for speeds over 300 kph, to 0 N for discrepancies between the average contact force and three times the standard deviation, and to 40 N or more in Spain and France.

Modelling

In this study, a cantilevered or single-arm pantograph was studied primarily to understand its aerodynamic performance. Single-arm pantographs are better suited for high-speed trains because they can be adapted to a wide range of catenary heights and are comparatively lightweight with robust structural integrity.

Pantographs inherently have complex geometries and since each part has a different section, such as a square or circular cylinder, it creates complex flow phenomena in the downstream wake. To simulate this type of aerodynamically unfriendly bluff structure, higher fidelity modelling and mesh refinement are necessary.

Ansys Fluent 2021R2 was used for this study. The computational domain corresponding to the wind tunnel was constructed with about 13L extensions in both the up- and downstream directions, which avoids the necessity of regenerating the volume mesh according to the driving direction. A volume mesh was applied using Poly-Hexcore Fluent Meshing and was gradually refined by octree-based far-field body adaptation. The total number of volume cells was around 55 million, and the grid height of the first layer was configured with a Y+ value of less than 10 to capture the boundary layer separation of the near-wall surface and of the ground of the tunnel on the pantograph body.

The pantograph design is not symmetrical with respect to its longitudinal direction, thus creating different aerodynamic properties depending on the direction of travel. Consequently, simulations were performed for both up- and downstream wind directions at wind speeds of 250, 270, 300, 330, 460 and 400 kph, respectively. The numerical techniques applied included the SST k-w model for turbulence closure, a velocity-pressure coupling algorithm, and double precision to minimize rounding errors.

Results

Figs. 2 and 3 show the distribution of speed and pressure at travelling speeds of 250, 330, and 400 kph. The simulation results showed airflow recirculation at the contact shoe, in the junction between the upper and lower arms, and in the connection area to the roof of the train. In front of the lower arm, the airflow stagnates in the area around the lower base

support of the pantograph creating a complex airflow around that region. In contrast, in the case of the closed-knee position a different airflow pattern is generated because the airflow is directed through the lower arm and strut rod before reaching the base support.

Furthermore, Fig. 4 describes a 3D iso-surface that extracts the zero value of the total pressure coefficient defined in equation (1) below. The iso-surface corresponding to this region can be considered as a bubble zone for airflow separation. Since there is a larger separation bubble around the base supports, it is concluded that the primary contributor to drag in the present model may be this base support.

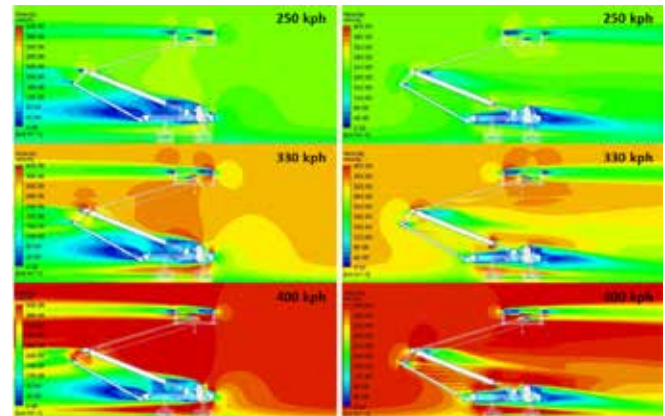


Fig. 2 - Velocity contour.

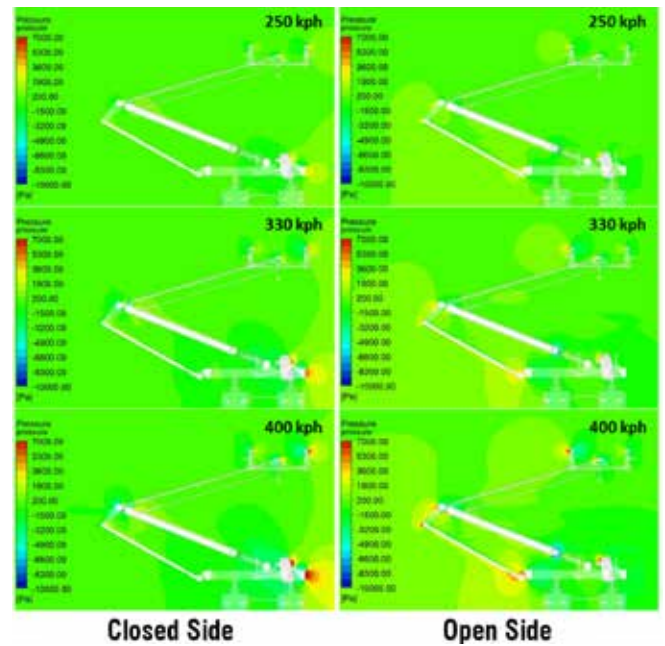


Fig. 3 - Velocity contour.

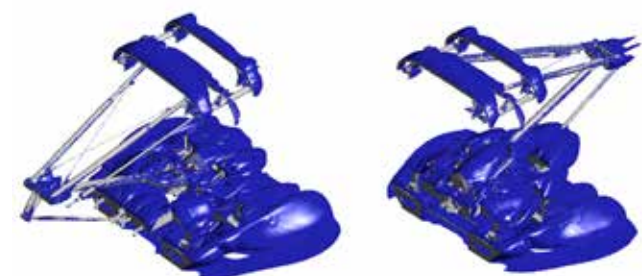


Fig. 4 - Total pressure coefficient distribution at 400 kph.

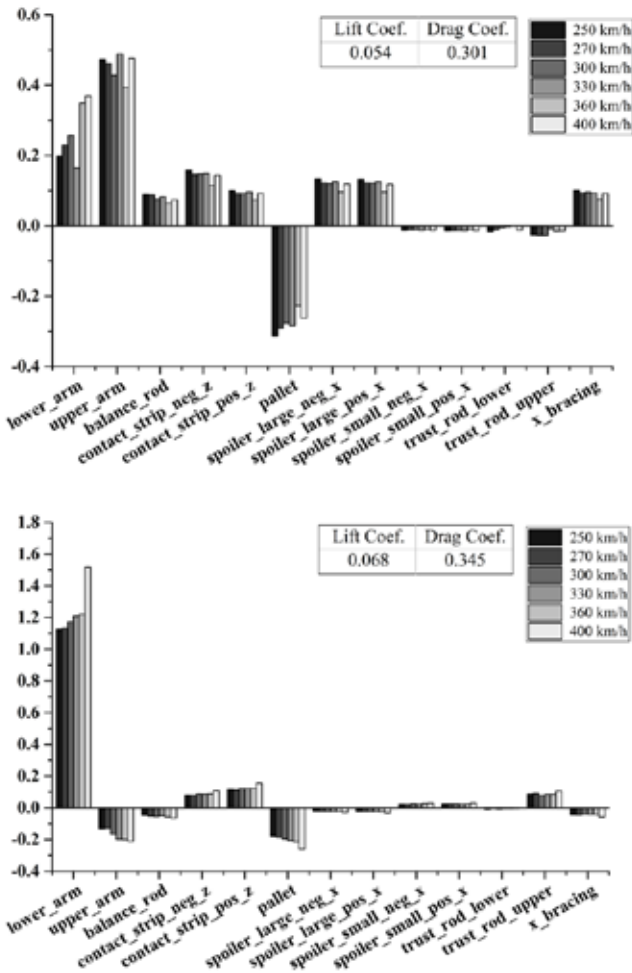


Fig. 5 - Contribution of each part to the lift force in the open-knee position (top), and in the closed position (bottom).

Fig. 5 shows the contribution of each part to the total lift force. A positive value indicates uplift while a negative value indicates negative lift. In the open-knee position, most parts contribute to uplift, but the pallet part contributes significantly to negative lift. By contrast, in the closed-knee position, the lower arm is the main contributor to uplift force, while the upper arm contributes to negative lift.

The dimensionless coefficient of lift for all speeds has averaged values of 0.054 and 0.068 for the open- and closed-knee positions, respectively. This means that the uplift force of the pantograph is greater in the closed-knee position than in the open position, so we can conclude that the contact force between the pantograph and the catenary wire will also increase proportionally. In addition, as for the drag coefficient, the closed-knee position has a greater value than the open position, so the drive resistance will require increased power consumption.

Fig. 6 shows the uplift force for both the closed-knee and open-knee positions. It increases in line with speed and the uplift force is greater in the closed-knee than in the open-knee position. At a maximum speed of 400 kph, the uplift forces generated in the open-knee and closed-knee positions were 323.6 N and 333.4 N respectively. This complies with Euro standard EN50119 which requires the maximum contact force to be below 350 N at speeds above 200 kph.

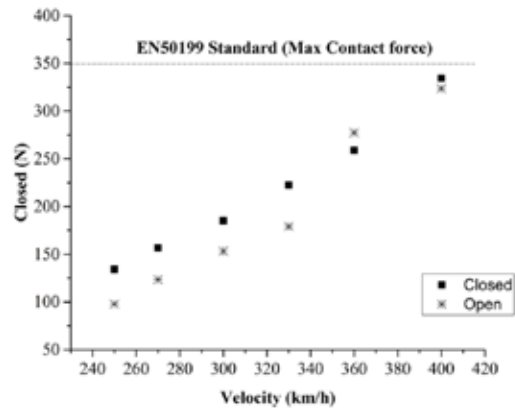


Fig. 6 - Speed-lift graph.

Conclusion

In this study, CFD simulations were conducted with Ansys Fluent to analyse the aerodynamic performance of the single-arm pantograph of the next generation KTX in both the open- and closed-knee positions at various driving speeds. The conclusions of the simulation results are summarized as follows:

1. Drag and lift performance is worse in the closed-knee position than in the open-knee position.
2. Each part's contribution to uplift force is dependent on the direction of travel because each part has a different aerodynamic incidence with respect to the wind direction.
3. The primary parts and design factors to be optimized can be identified.
4. The pantograph of the new generation KTX is believed to satisfy the Euro EN50119 standard in both the open and closed-knee positions for all driving speeds.

For more information:

Jinwook Kim - TSNE
 jw.kim@tsne.co.kr

About TSNE

Since its establishment in 1988, TSNE has specialized in CAE, providing engineering programs and services to Korean customers. Tae Sung S&E (TSNE) aims to be the "One Stop Total CAE Solution Provider" (OSTS) both in domestic and global markets. The company leverages its large base of business capabilities and its team of CAE experts to provide services to customers in various industries (aerospace, automotive, civil engineering, biomedical, shipbuilding, electrical and electronics, energy, defense, chemical industries, etc.) and is expanding its business scope to research innovative technologies and apply them in the field.

It strives to become a global engineering company and increase its potential as a sustainable engineering company. Tae Sung S&E is partner to all engineers who endeavour to solve challenges. Tae Sung S&E will work with you to achieve "NO PROBLEM, BE HAPPY".



ESTECO sponsors UniTS Racing team to optimize design of Formula SAE electric car

modeFRONTIER helped improve aerodynamic performance of the car's front wing

by UniTS Racing Team | Università degli Studi di Trieste

The UniTS (University of Trieste) Racing Team has begun participating in the international Formula ATA competition, the Italian division of Formula SAE, in which universities from all over the world compete to design and build a racing prototype. For the development of the first prototype, the URT-B01, UniTS initially used modeFRONTIER to solve a relatively simple problem concerning the front wing.

Challenge

The e-car's aerodynamic package includes a front and a rear wing. The team planned to introduce a floor with underbody channels and a diffuser to maximize the car's performance. In addition, to ensure that this floor functions correctly, it must be fed with non-turbulent air. Consequently, it is essential that no aerodynamic part at the front (e.g. the central foil of the front wing) significantly disrupts the flow. While a symmetric foil would guarantee the least turbulent flow, it would also waste a large surface capable of providing significant downforce. As a result, UniTS opted for a highly efficient asymmetric profile that provides downforce with the least possible drag and turbulence. Specifically, the team selected an airfoil (the BE 153-076) that is usually used in the automotive industry as a baseline on which to improve. To do so, they had to find a way to simulate many airfoils in a short period of time.

Methodology

The methodology consisted of combining XFOIL software, for simulating the airfoil performance, with modeFRONTIER to perform a parametric optimization. The best approach would have been to pair modeFRONTIER with Ansys Workbench, but this requires a lot of computing power which was unfortunately not available. As a compromise, they opted to identify some viable candidates using XFOIL and then validate those using Ansys Fluent. In order to take advantage of some significant advantages in computing speed, the team decided to study the profiles in a lift configuration for the XFOIL portion of the research. However, since XFOIL does not support ground effect simulations, the team first compared the viable candidates in both XFOIL and in Ansys Fluent in a free stream, before moving onto conducting proper ground effect simulations with Ansys Fluent alone. In the meantime, based on the initial boundary conditions, they considered the lift values because an airfoil with a good lift configuration will have the same efficiency in a downforce configuration.

The boundary conditions imposed for the simulation were those for a typical Formula SAE scenario, at the average speed expected for the dynamic events of the competition, i.e. 15 m/s. The dimensional constraints and the placement of the wing were also considered due to the technical requirements. As a result, some fixed ratios were set to obtain a minimum thickness of 50 mm and a maximum chord length of 400 mm. A preliminary XFOIL simulation revealed that the starting profile had an efficiency of 108.10 which needed to be improved.

Development of the wing with modeFRONTIER and results obtained

Firstly, the team was looking for a four-digit NACA airfoil profile using the given boundary conditions and the simplex method available in modeFRONTIER to optimize the solution.

The best profile was a NACA 6613 with an angle of attack of 4.70 degrees and an efficiency of 131.58. In this case, the team wanted to optimize the first and second variables, and the last two digits of the NACA profile. These values were inserted into XFOIL to automatically generate the associated NACA profile. Due to this feature, the team decided to conduct the first part of the study with the airfoils in a lift configuration because changing or creating the coordinates from scratch for each relevant NACA foil in a downforce configuration would have taken more time.

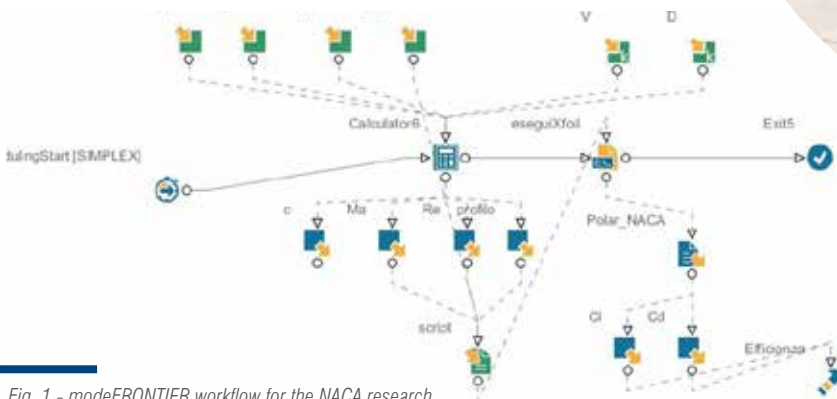


Fig. 1 - modeFRONTIER workflow for the NACA research.

Secondly, the team created an airfoil using Bézier curves. The profile was created by joining two Bézier curves to create half of the airfoil, which was then mirrored to obtain the complete, symmetric foil. Another Bézier curve was then added to augment the profile's curvature. This was done with both 4- and 5-degree curves and, given these restrictions, the entire profile could be parametrized.

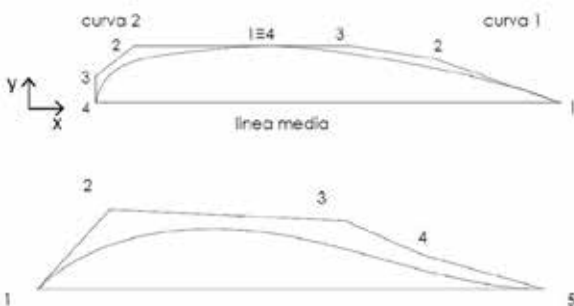


Fig. 2 - Bézier profile.

The optimization results generated a profile with an efficiency of 134.55 when at an angle of 4.76 degrees, a higher value than the NACA profile.

The graph in Fig. 3 confirms the quality of the modeFRONTIER profiles obtained, particularly for the Bézier curves.

Conclusions

The UniTS Racing Team decided to use modeFRONTIER for optimization challenges in the Formula SAE project to enable its students to apply this software, taught in a university course at the basic level, to practical

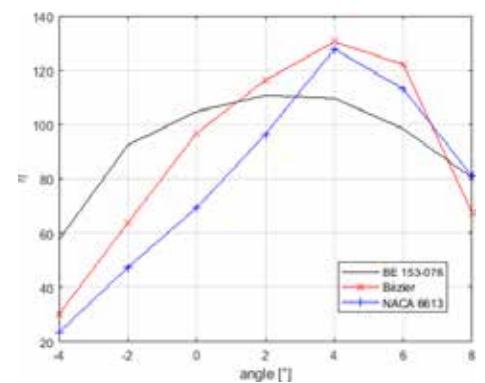


Fig. 3 - XFOIL comparison of profiles: BE 153-076 (baseline), Bézier and NACA 6613.

challenges, allowing them to develop the skills necessary to approach more complex applications in future. modeFRONTIER helped them the team to scan many profiles and select the best one, while also allowing them to design the profile from scratch using Bézier curves. The results obtained were really promising since the study generated custom airfoils with industrial performance values; without modeFRONTIER, this type of research would have been almost impossible. A standard workflow would most likely have neglected some valid candidate designs, even if double or triple the time were invested.

UniTS will continue using modeFRONTIER to further this research, for instance, combining it with more advanced computational fluid dynamics (CFD) software to design fit-for-purpose parts while also considering more complex boundary conditions, such as ground effect. From these future studies they expect to design custom airfoils with even better performance than the current ones.

For more information:
info@esteco.com



Characterization of lattice structures: testing and simulation challenges

by Florent Mathieu
EikoSim

Lattice structures (or “lattices”) are of increasing interest for the development of aeronautical and space parts in particular. In addition to the significant weight savings they offer, one can also optimize their behaviour according to the patterns that compose them. The strong growth in metal additive manufacturing technologies makes it possible to manufacture parts composed of lattice structures with materials recognized for their mechanical performance, such as nickel-based alloys, titanium alloys, or new generations of aluminium alloys. These promising architectural materials are still not widely used in the design of structural parts as they require new development methods on an industrial

scale (simulation, characterization, manufacturing). In this context, the Institut de Recherche Technologique (IRT) Saint Exupéry, drawing on the experience of the SIMaP laboratory in the field of engineered materials, is conducting a 24-month research and development project, called LASER (Lattice Structures for Engines and Launchers), bringing together major aeronautics and space manufacturers with the aim of providing them with understanding and design tools for design offices. EikoSim, a company specialized in the link between tests and simulations, provides its expertise and its field measurement software by digital image correlation to the LASER project.

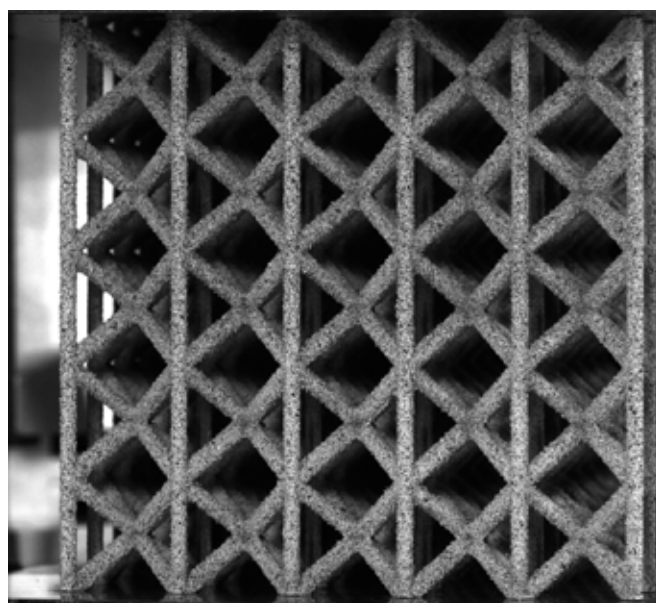
The LASER project's tests on lattice structures aim to highlight the deformation modes in compression or shear configurations with different boundary conditions and scale effects by playing with the number of elementary meshes constituting the specimens. The diversity of these configurations should allow the development and validation of a numerical modelling approach. At this stage, the study is limited to quasi-static solicitations at room temperature as a starting point for determining the methods. The structures tested consist of microbeams of up to 1 mm in diameter, organized according to BCC (cubic centred) or BCCZ (cubic centred with vertical beams) type meshes.

One cannot use a traditional measurement method to capture the complex kinematics of such lattice structures under mechanical stress. Strain gauges, for example, are very difficult to use at the micro-beam scale and only provide very partial information on the structural response. Extensometers measure the global displacement while an indispensable load cell captures the applied force. Under these conditions, the correlation between experimental results and modelling remains weak, and it appears to be very difficult to develop predictive modelling, which would allow the design of more complex structures with a high level of confidence.

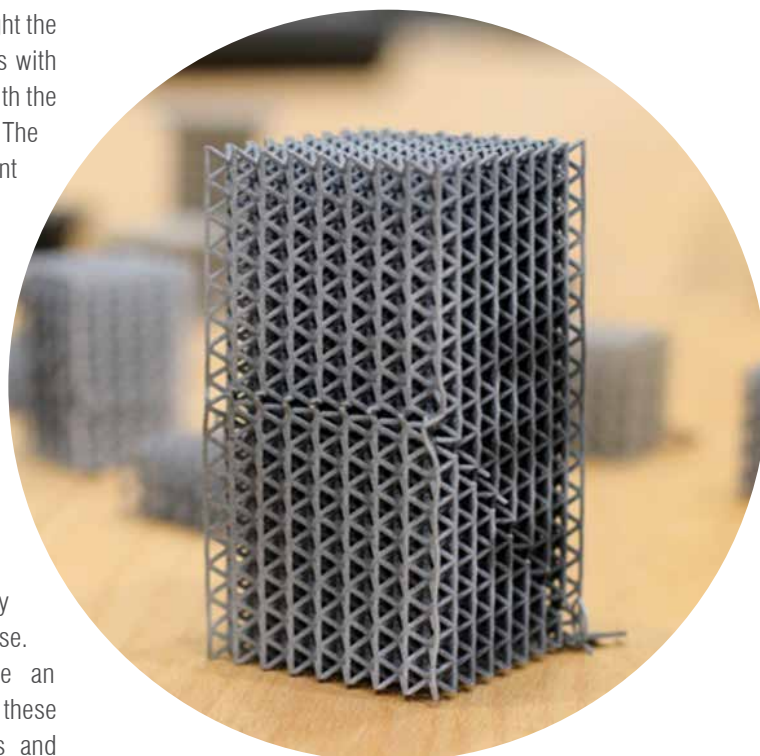
The use of more efficient measurement methods is one way to address the challenges posed by these new geometries. Field measurement, particularly by digital image correlation, is a natural candidate for capturing the heterogeneity of the deformation and the local instability phenomena that occur.

Compression test followed by image correlation

Implementing image correlation involves applying a speckle (contrast pattern) to the part, adapted to the scale and



A black speckle on a white background applied to a lattice structure.



Lattice structure with BCCZ pattern after compression test, showing a characteristic shear band.

resolution of the cameras. On lattice structures, this is applied using an airbrush to obtain spot sizes of a few tens of microns.

During the test, two sides of the sample are observed with two sets of high-resolution cameras. These enable the characteristic deformation mode of the shear band and all the complexity of the kinematics. However, from a measurement perspective, this can make processing complex. With a finite element meshing approach, as proposed in the EikoTwin DIC software, the measurement result is directly mapped to a point in the 3D space



Monitoring by 4 cameras of two faces of a lattice structure during a compression test.

of the model part. There is no theoretical limit to the number of cameras, each of which contributes to the measurement of the displacement of the points in its respective field of view. Digital image correlation is a technique that allows the displacement of points on a structure to be tracked by assuming that these points maintain the same level of greyness in the image. The lighting conditions must therefore be controlled to limit measurement uncertainty and to ensure the ability to also track large displacements.

Modelling and simulation

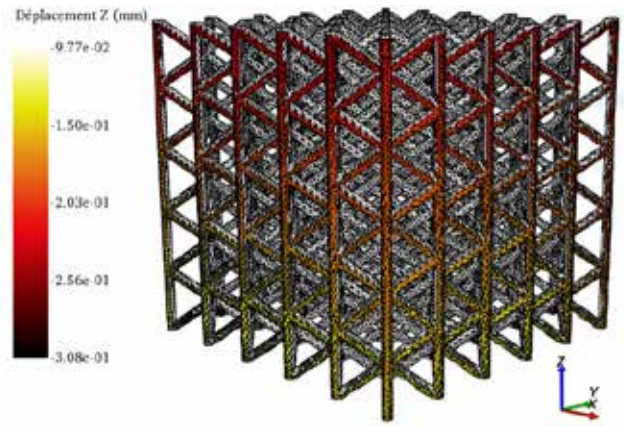
Several approaches can be considered to model the mechanical behaviour of lattice structures. The most accurate in terms of geometrical representation describes each microbeam in volume. Discretization by volume finite elements enables one to stay as close as possible to the design geometry. From a physical point of view, given the level of deformation expected during compression tests, it is important to describe the elasto-plastic behaviour of the structure's components. One difficulty at this stage is to describe the local mechanical behaviour by a suitable law. Several approaches are possible in the design office:

As a first approach, one can consider the properties of the constituent material obtained from standard tests. In this case, it is recommended that these standard tests be conducted on specimens machined from raw materials obtained by the same additive manufacturing process used for the lattice structures.

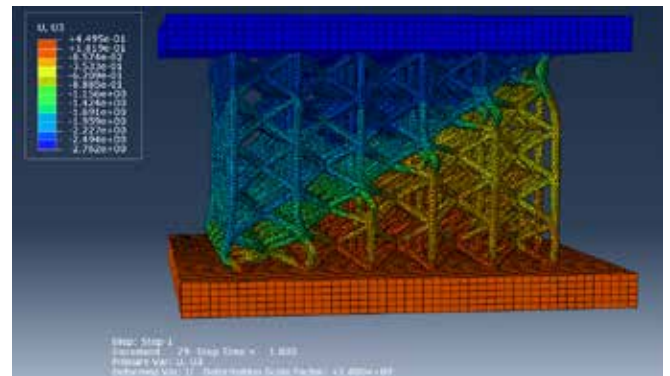
A second approach, proposed and implemented in the LASER project, consists of characterizing the constituent elements of the lattice structure, i.e. the microbeams. The geometries of the specimens were designed and built on the same platforms as the lattice structures to access the intrinsic properties of the microbeams according to their orientation (vertical, inclined). The interesting aspect of this approach is that it makes it possible to capture effects related to the fineness of the geometry, which are relatively well known in additive manufacturing: roughness, shape deviation

The application of loading and boundary conditions is an essential part of the modelling. In the same way that differences between the design geometry and the actual geometry can have a significant impact on the response, so too can differences between the "ideal" loading and the actual loading experienced by the structure. However, measurements of these deviations are rarely available to design offices. Therefore, the initial model chosen largely ignores them.

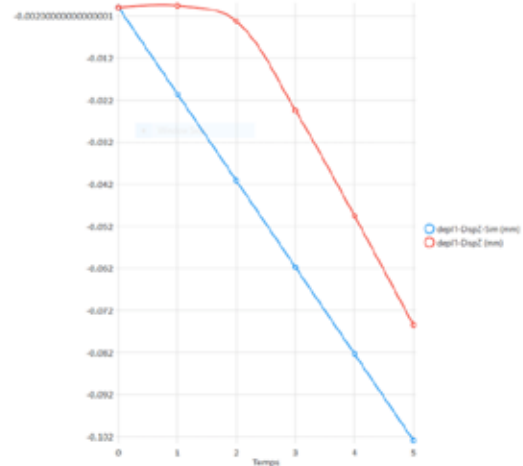
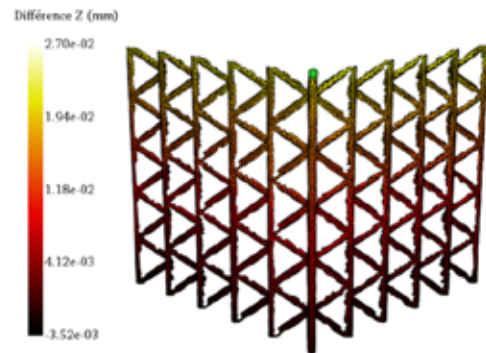
The problem of simulation time emerges quite quickly for this type of non-linear model composed of millions of elements. To address this, the LASER project is currently developing a simplified approach based on an approximation of the geometry by linear finite elements with beam kinematics, to avoid deteriorating the accuracy of the simulations.



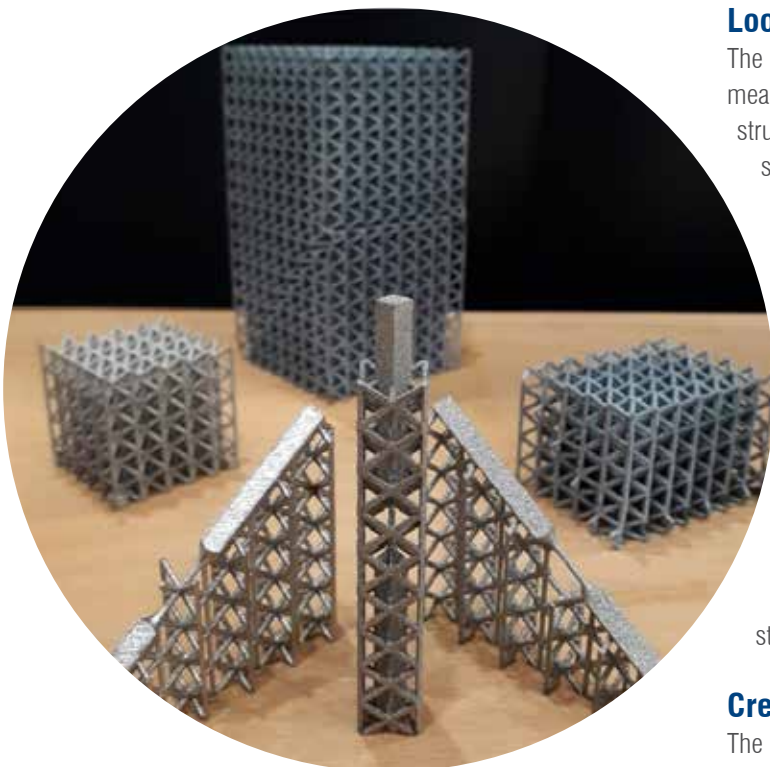
Vertical displacement field measured by image correlation on the simulation mesh, EikoTwin DIC software.



Simulation of the compression test on a 5x5x5 solid element mesh of a BCC lattice structure, Abaqus software.



Difference between the measured and simulated vertical displacement field (left), and evolution of the deviation at a mesh point as a function of time (right).



Microbeam test specimens for the characterization of the constituent elements of a lattice structure.

Test-simulation comparison

The comparison of measurements with simulation results is often a challenge in itself. The ability to measure displacements on a point cloud is interesting, but creates new problems for comparisons with simulation.

With the finite element approach implemented in the EikoTwin DIC software, the displacement field is measured directly on the numerical simulation mesh, in the same 3D reference frame.

In this way, errors arising from the projection of the measurement fields onto the mesh, or vice versa, are avoided. It also saves time for the user. For example, a difference between the ideal loading path and the one applied to the part can be visualized directly, so that the simulation model can be corrected accordingly.

About EikoSim

EikoSim is a software company that enables users to leverage validated simulation models to support design decisions. The company supports managers of engineers in charge of structural simulations. It assists its customers in explaining discrepancies between tests and models so that they can respond more quickly to program requests and reduce delivery times to the end customer. The EikoTwin software solution applies image analysis and simulation model management to improve both simulations and development cycles.

Looking ahead

The next step is to modify the initial simulations using the measurement results. These tests have taught us a lot about lattice structures, so we want to exploit these results to improve our simulations and better understand the sources of error. Firstly, the measured displacements at the edges can be used as boundary conditions for the simulation. This approach, when combined with the comparison of the experimental and simulated stress-displacement curves, will subsequently enable an inverse identification strategy to be implemented to refine the model parameters and reduce the test-simulation gap.

The EikoTwin Digital Twin software allows these two essential steps to be integrated into a single environment. It is foreseen that these methodologies will soon be able to be transferred to the design office and the potential of lattice structures for industrial applications can be developed.

Credits

The IRT Saint Exupéry (IRT) is a technological research institute accredited by the French government as part of the future investment program (PIA). It is an accelerator for science, technological research and transfer to the aeronautics, space and embedded systems industries for the development of innovative solutions that are safe, robust, certifiable and sustainable.

At its sites in Toulouse, Bordeaux, Sophia Antipolis and Montreal, the IRT Saint Exupéry offers an integrated collaborative environment composed of engineers, researchers, experts, and doctoral students from industry and academia for research projects and R&T services supported by technology platforms in four key areas: high performance multifunctional materials; more electric aircraft; intelligent systems and communications; and systems engineering and modelling.

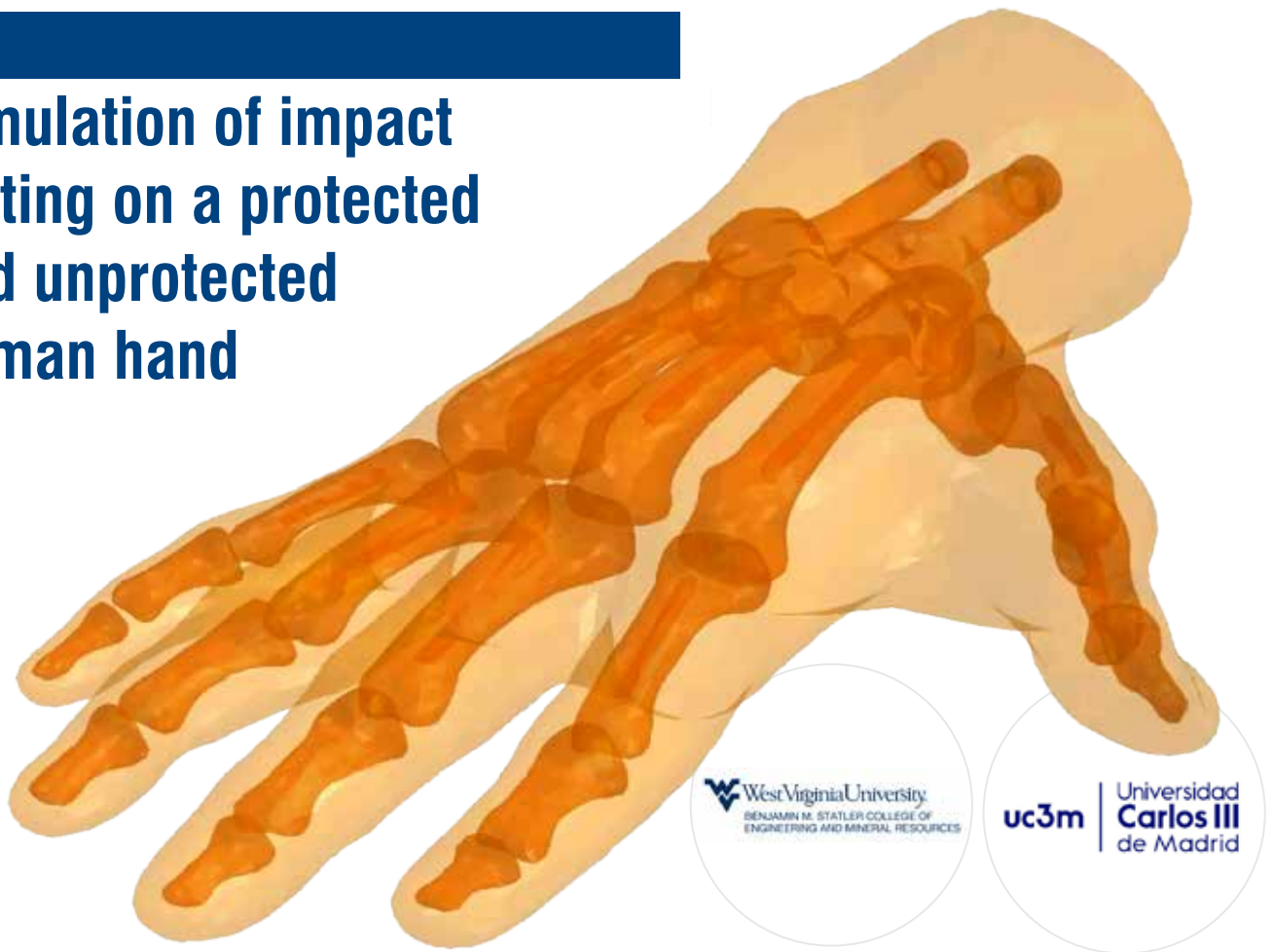
The LASER project is an IRT Saint Exupéry project funded 50% by its industrial members and 50% by the French government's Programme d'Investissement d'Avenir (PIA). It is part of the inter-IRT "LATTICES" initiative, which defines the close collaboration with the DSL (Durability of Lattice Structures) project led by IRT SystemX and the National Centre for Space Studies (CNES).

All pictures are courtesy of IRT Saint Exupéry.

For more information:
 Florent Mathieu - EikoSim
florent.mathieu@eikosim.com



Simulation of impact testing on a protected and unprotected human hand



by Eduardo M. Sosa¹, Marta M. Moure², and Álvaro García Rincón²

1. Department of Mechanical and Aerospace Engineering, West Virginia University

2. Bioengineering and Aerospace Engineering Department, Universidad Carlos III de Madrid

This paper presents an overview of the development of a finite element model (FEM) to simulate the impact of a small, low-mass object on the back of a flattened hand protected with a metacarpal glove. The FEM includes the complete bone structure, derived from high-resolution laser scanning of the bones of a human hand, surrounded by soft tissue with material properties representative of a human hand wearing a test case metacarpal glove subjected to low energy impacts. The simulations include impacts to the fingers, knuckles, and metacarpal regions of the hand. Impact reaction forces are calculated and compared to controlled impact tests performed on cadaveric hands reported in the literature. The final objective is to develop a simulation model to assess the level of protection offered by various metacarpal gloves commonly used in different industries.

Background and motivation

Hand injuries are a major problem in several manufacturing and extractive sectors. Injuries to hands are among the most common and are highly correlated with the use of machinery [1-2]. These injuries often result in functional limitation or disability and have significant financial implications. Such injuries can dramatically affect everyday activities as well as performance in the workplace and often result in hand disabilities that require work-related adjustments such as altered work responsibilities, job retraining, changing the type of employment, or even applying for disability benefits. Despite continuous advances in technology and safety procedures for production and maintenance tasks, many manual tasks with high-risk factors result in hand injuries of varying degrees of severity [3-5]. Due to the high incidence of hand injuries, workers are required to wear impact-resistant gloves (also known as metacarpal gloves) as personal protective equipment (PPE) to protect their hands from impact injuries.

Engineers, researchers, and clinicians continually seek to prevent, mitigate, and eventually heal different types of injuries that occur

in workers' hands. There is, therefore, a need to better understand how bones and tissues behave under such impacts. This understanding will enable the effectiveness of current protective measures, such as metacarpal gloves, and the development of protective devices, treatment, and recovery to be evaluated. In this regard, a recent experimental pilot study conducted at West Virginia University (WVU) measured the forces and damage associated with low-velocity impact to protected and unprotected cadaveric hands [6]. While this study provided valuable information about the magnitude of forces necessary to produce bone fractures and fracture patterns, it was limited by the number and condition of specimens that may be available for testing, and also highlights the need to develop a reliable computing model that can be used for testing of and protecting against multiple conditions.

Finite element modelling (FEM) of human parts has developed significantly over the past decades and has been used to study multiple problems. FEM has been successfully used to analyse various problems in the wrist, foot and ankle, knee, and spine [7-9]. In the field of hand surgery, FEM has been used for the wrist, extensor tendons, carpal tunnel, and for individual fingers [10-13], but so far, no cases have included the whole hand.

Based on the aforementioned considerations, this research aims to advance the development of a calibrated FE model of a whole hand that can be used to assess the level of protection offered by metacarpal gloves used in different production sectors.

Methodology

The model of the hand comprises two parts: the bone structure, and the soft tissues, represented as a whole. The hand size selected had dimensions corresponding to the 50th percentile of the population and was placed in an almost flat open position to closely resemble previous experimental results reported in the literature [6]. The bone structure was based on laser scans of an actual set of individual bones obtained for the West Virginia University's Department of Anatomy. The resulting digital bones were then scaled and assembled with Autodesk/Fusion 360 to create a digital version of the full hand's bone structure. The volume of the outer layer of the hand in the desired shape was obtained from a commercially available digital model. The digitalized bones and the hand volume were then combined using Autodesk Fusion 360 according to existing skeletal hand models [14] to ensure the correct position of the scanned bones within the hand volume (Fig. 1).

Once the geometry was defined, the resulting digital hand model was then imported into Simulia/Abaqus [15] to create the FE model of the hand. The model of the unprotected hand included two parts: the bones and soft tissues, which were discretized into solid 3D elements. The metacarpal and phalangeal bones were adjusted to include the medullary cavity. The bones were assumed to have an elastic behaviour, and the soft tissues were assumed to have a hyperplastic behaviour using material parameters obtained

from the literature. The model of the hand was placed on a flat plate and subjected to the impact produced by a vertically falling steel bar. The energy of the impact was set in the range of 5-10 Joules, which has shown to be sufficient to produce fractures in the metacarpal and phalangeal bones [6]. The interaction between the bones and soft tissues required kinematic constraints to be defined to ensure compatible displacements. Similarly, the hand, plate, and impactor assembly required contact interactions to be set to avoid spurious intersections or interpenetrations (Fig. 2).

The model of the unprotected hand was then used as the basis for the creation of a model of a metacarpal glove. There are numerous models of metacarpal gloves on the market, each of which is designed for different industries with different protection requirements. Many have localized protection elements, typically in thermoplastic rubber (TPR). The geometrical shapes and distribution of these TPR elements vary according to the model



Fig. 1 - Generation of hand geometry.

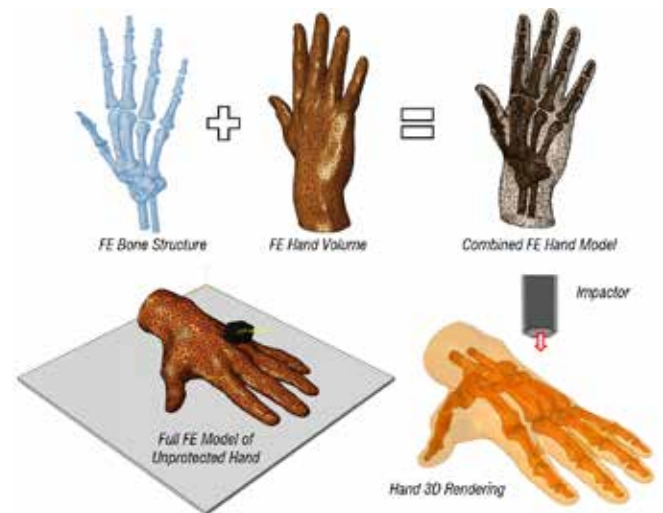


Fig. 2 - Finite element model of unprotected hand.



Fig. 3 - Finite element model of metacarpal glove.



Fig. 4 - Impact map [6] and examples of impacts to third digit of protected hand.

of the glove, while the hardness and density of the material vary between manufacturers. For this reason, a model that can be used to recreate multiple protection configurations would dramatically reduce the requirement for experimental testing with cadaveric or synthetic surrogate hands.

As a case study, a glove typically used in mining and in oil and gas extraction settings was selected to be modelled on the hand model described earlier. The selected glove has three main layers: an internal Kevlar layer, an external leather layer, and a dorsal layer of localized TPR protection elements situated over the metacarpal and finger regions of the hand (Fig. 3). These protective elements are intended to deform during an impact and function as energy dissipaters to reduce the magnitude of impact force transmitted to the bones and soft tissues beneath them.

The FE model of the glove was created as an offset element of the outer surface of the hand. This technique ensured that the glove model fitted the model of the unprotected hand “like a glove.”

Furthermore, contact and surface interactions were assigned to the inner and outer layers of the glove to ensure that all three layers behaved as a single unit during the impact loading. Boundary conditions were also applied to the wrist to account for the presence of the forearm without having to model it. Like the unprotected hand, the hand-with-glove model was subjected to a series of impacts. These impacts followed an impact map previously used to evaluate the impact forces on cadaveric hands [6] and served as a basis for comparing the experimental and numerical results (Fig. 4). The explicit solver available in Abaqus [15] was selected as a solution algorithm to capture the dynamic nature of the problem.

Simulation results

The model of the unprotected hand (without the glove) provided a baseline for comparison with models that included the protective layer provided by the metacarpal glove. The primary variable of interest for this research is the peak reaction force obtained at each point of impact. The magnitude of this force was used to assess the

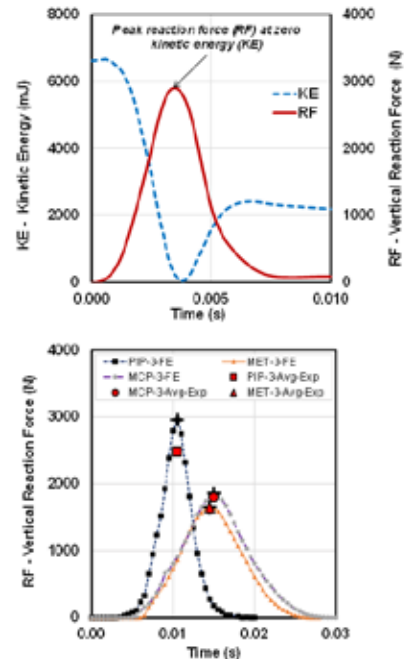


Fig. 5 - Example of peak reaction force on unprotected hand.

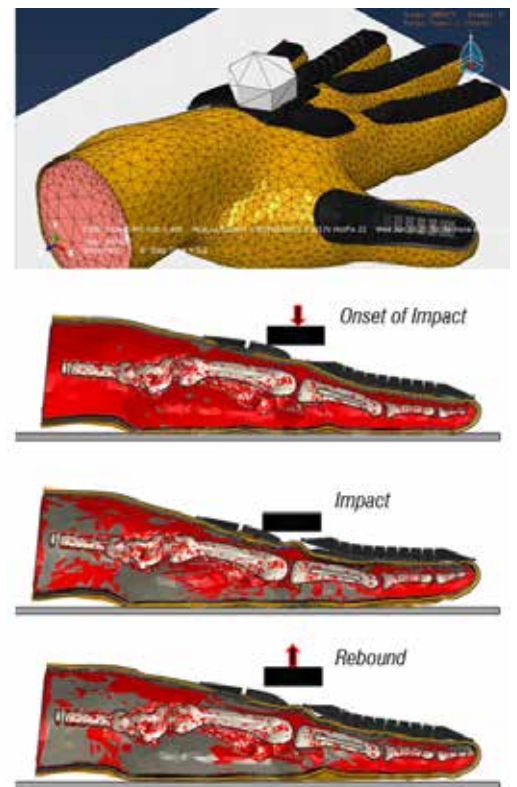


Fig. 6 - Impact evolution for a protected hand, impact on third digit, metacarpophalangeal joint, longitudinal cross-section.



occurrence of bone fractures at the impact site. The magnitude of the peak reaction force was also used to identify the level of energy dissipation at each point of impact. The peak reaction force typically occurs at the minimum level of kinetic energy, which corresponds to the instant in which the impactor reaches nearly zero velocity and then rebounds depending on the material characteristics of the TPR protection (Fig. 5). For the unprotected hand, the peak reaction forces of the FE model were in the range of the forces measured during the experimental phases with cadaveric hands. Depending on the location of the impact, the peak reaction forces can range from 1500-4000 N. Initial results showed a good correlation between the simulation results and the experimental results [6]. Fig. 5 shows an example of the simulation results compared to the experimental results for impacts to the third digit of an unprotected hand.

The simulation results of the hand with the chosen protective glove showed smaller peak reaction forces than the values obtained for the unprotected hand. The results also showed that these forces are sensitive to the properties of the material selected to represent the stiffness of the TPR shields. If the rubber material of the guard is relatively stiffer and denser, the impactor rebounds, and the peak reaction force is much lower than the experimentally observed values (Fig. 6). Conversely, if the rubber material is light and flexible, the protection deforms excessively as the soft tissues and bones of the hand absorb the reaction force of the impact. In this case, the reaction forces are close to the values corresponding to the unprotected hand, indicating that there is no protection. This behaviour was expected, and further material testing is underway to better characterize the elastic properties of the TPR protective elements.

Concluding remarks

An overview of the development of a finite element model to simulate low energy impacts on the dorsal side of protected and unprotected hands was presented.

The development of such a model provides a valuable tool to assess the forces and energies involved during an impact to the fingers and metacarpal region of the hand. It is hoped that its refinement and validation will reduce the need for experimental testing with cadaveric or surrogate hands [16].

This paper formed the basis for one of the five winning posters in the Poster Award at the 2021 International CAE Conference and Exhibition.

For more information:

Eduardo M. Sosa - West Virginia University
 eduardo.sosa@mail.wvu.edu



References

- [1] Trybus M, et al. (2006). Causes and consequences of hand injuries. *The American Journal of Surgery*, vol. 192, pp. 52–57.
- [2] Alessa FM, Nimbarte A, Sosa EM (2020). Incidences and severity of hand injuries in the US Mining Industry. *Safety Science*, 129, 104792.
- [3] Pollard J, et al. (2014). Maintenance and repair injuries in US Mining. *Journal of Quality in Maintenance Engineering*, vol. 20(1), pp. 20–31.
- [4] Chung KC, et al. (2001). The frequency and epidemiology of hand and forearm fractures in the United States. *Journal of Hand Surgery*, vol. 26(5), pp. 908–915.
- [5] Sorock GS, et al. (2004). A case-crossover study of transient risk factors for occupational acute hand injury. *Occupational and Environmental Medicine*, vol. 61(4), pp. 305–311.
- [6] Sosa, EM & Alessa, FM (2021). Experimental evaluation of protected and unprotected hands under impact loading. *Journal of Biomechanics*, vol. 118, 110326.
- [7] Popescu R, et al. (2019). Relevance of finite element in total knee arthroplasty, *Literature Review. Chirurgia*, vol. 114, pp. 437–442
- [8] Pfeiffer FM (2016). The use of finite element analysis to enhance research and clinical practice in orthopaedics. *Journal of Knee Surgery*, vol. 29(02), pp. 149–158.
- [9] Behforootan S, et al. (2017). Finite element modelling of the foot for clinical application: A systematic review. *Medical Engineering and Physics*, vol. 39, pp. 1–11.
- [10] Freutel M, et al. (2014). Finite element modeling of soft tissues: material models, tissue interaction and challenges. *Clinical Biomechanics*, vol. 29(4), pp. 363–372.
- [11] Dogadov A, et al. (2017). The biomechanical model of the long finger extensor mechanism and its parametric identification. *Journal of Biomechanics*, pp. 58(14), vol. 232–236.
- [12] Dolšak B (2016). Justification for a 2D versus 3D fingertip finite element model during static contact simulations. *Computer Methods in Biomechanics and Biomedical Engineering*, vol. 19(13), pp. 1409–1417.
- [13] Elyasi N, et al. (2017). A study of hyperelastic models for predicting the mechanical behavior of extensor apparatus. *Biomechanics and Modeling in Mechanobiology*, 16(3), 1077–1093.
- [14] White TD & Folkens PA. *The human bone manual*. Elsevier, 2005.
- [15] *Abaqus User's Manual, Documentation Collection Version 6.17*. Dassault Systemes Simulia Corp., Providence, RI, 2017.
- [16] Alessa, FM & Sosa, EM (2022). Experimental Evaluation of Impact-Resistant Gloves Using Surrogate Hands. *International Journal of Occupational Safety and Ergonomics (JOSE)*, Accepted for publication, March 2022. doi:10.1080/10803548.2022.2051865.



Optimization of an explosive trace detector using CFD simulation

by Elisabetta Pasqualotto¹, Matteo Scaramuzza¹ and Diana Magnabosco²

1. EXA - 2. EnginSoft

The VOLPE project aims to provide a solution to the growing demand for innovative security systems for early prevention and response. The aim of the project is to design, develop, and optimize a completely contactless explosive trace detector to continuously monitor dangerous and hazardous volatile compounds in the air to safeguard both citizens and critical infrastructure.

These substances are particularly difficult to monitor because they are constantly changing and improving, often being created from bare precursors, i.e. common substances that only become harmful when mixed e.g., fertilizers, fuel, and bleach. There is, therefore, a growing need for smart detection devices that can simultaneously monitor multiple chemicals and process complex correlation analyses from large raw datasets.

The project aims to develop a sensor system for the detection of volatile explosive substances, capable of continuously monitoring the air without the presence of an operator. Currently, checks for explosive substances are carried out with instruments based on buffer systems that require the presence of an operator and a sample check.

The possibility of checking all samples without the presence of an operator makes this type of technology very attractive, and it could find many other applications, such as checking postal packages, people or other sensitive venues. The final product is designed to increase the number and effectiveness of security checks within critical infrastructures, such as embassies, museums, shopping centres, post offices, etc. A pre-industrial prototype of this tool has already been successfully implemented in previous projects (SPECTRE, EXIN), and its functions have been tested in a real environment at the Marco Polo airport in Venice. The positive outcome of these experiments prompted the desire to continue with the industrialization phases of the prototype, with the aim of creating a version compatible with market requirements.

The VOLPE project was funded by the Veneto Region of Italy under the "POR FESR 2014/2020 Asse 1 Azione 1.1.4" programme and



Fig. 1 - Baggage moving on the conveyor belt under the prototype.

was developed in partnership by three companies: EXA, EnginSoft and Buson. Thanks to the shared efforts of the companies, an engineered and fully automated prototype has been created. The prototype consists of:

- an automated system capable of controlling both a conveyor belt for handling luggage and a translation system that adapts the position of the detection system to the different heights of the luggage;
- an air system capable of drawing air from the baggage and conveying the sample to the detection system;
- an optoelectronic detection system, consisting of: a reaction chamber where the air sample is conveyed; an optical sensor that varies its optical properties in the presence of the target molecules; and an optoelectronic system for signal acquisition.

This article will focus on the numerical computational fluid dynamics (CFD) simulations developed by EnginSoft to support the performance optimization and component miniaturization of the air suction system.

Case Study

The optical nanotechnology on which the sensor system is based has demonstrated the necessary performance for the detection of traces of explosives. EXA is currently the exclusive licensee of two patents (Application No. IT2016UA02589 20160414 and IT2016UA02587 20160414, owned by ARC-Centro Ricerche Applicate, EXA's partner) for the industrial production of optical devices, which are part of the sensor system in question.

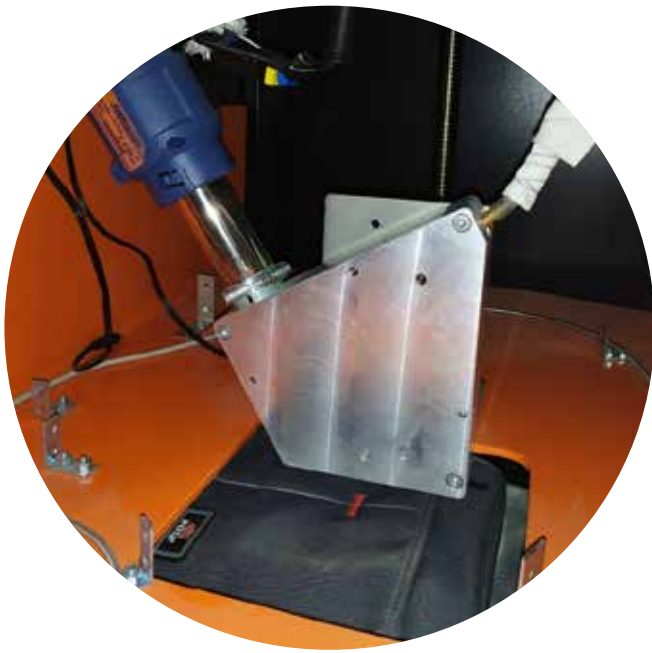


Fig. 2 - Internal part of the prototype, consisting of the heat gun on the left and the aspiration duct on the right.

The system under analysis is illustrated in Figs. 1 and 2, which show the first prototype of the detection system. The prototype is mounted on a conveyor belt, on which the suitcase can move. It includes a heat gun, which delivers 8.5 l/min of air at 450°C or 600°C to the moving luggage. There are then two aspiration ducts, one is connected to the heat gun via a nozzle, the second is connected to the measuring cell to collect molecules. The flow of 36 l/min is guaranteed by a constant flow pump.

Numerical simulations were performed in four phases. In the first step, a mathematical model was developed to reproduce the behaviour of the actual prototype, in order to calibrate the configuration of the experimental data. EXA provided a complete characterization of the functional behaviour of the prototypes, using a custom-developed test bench capable of investigating the correlations between all relevant system variables.

The second activity focused on the identification of the most relevant parameters, which led to the third step, the implementation of a parametric CFD model. Finally, these parameters were used to modify the device with a view to optimizing the design and identify an improved prototype. This last step was repeated along with experimental tests to support the numerical results and guide the optimization roadmap, so two prototypes were identified and tested consecutively.

This procedure had the following objectives:

- Optimize the fluid-dynamic characteristics of the intake air fraction
- Assess and improve baggage coverage
- Ensure the best temperature control
- Reduce cost components and energy consumption
- Minimize device size

Modelling approach

The numerical model was built using the Ansys suite to reproduce the experimental setup and then to optimize the device. The starting points were the 3D CAD geometry and the data obtained from experimental tests, which provided information on both the geometrical parameters and the operating conditions.

To simulate the aspiration system, it was not necessary to consider the complete prototype, but instead to focus on the details between the luggage, the heat gun, and the aspiration duct. Since the geometry was symmetrical, the computational domain was split in half with respect to the conveyor belt.

The fluid domain was extracted starting from the 3D CAD of the solids. De-features were used to simplify and remove details that were not relevant for fluid dynamics and could be neglected. Bodies and volumes were split to simplify the subsequent meshing procedure and to set up different physics.

The suitcase was simulated as a 2 mm thick solid, placed at a distance of 5 mm from the aspiration system, with a prescribed translational speed. The computational domain around the component (Fig. 3) was extended in three directions to consider an air plenum around the area of interest. Therefore the volume had an extension of 1 m in the direction of the belt, 0.2 m in the lateral direction and 0.2 m in the vertical direction. The air ducts, which are connected to the heat gun and the pump, were extended to stabilize the fluid flow at the boundary conditions.

To solve the CFD analysis, the geometrical model was discretized into a computational grid. The mesh was generated with an adequate cell size to evaluate local physics phenomena with good resolution. Prisms were constructed at the walls to correctly capture the boundary layer where high velocity gradients occur. Quality criteria were checked to reduce element distortion and ensure valid results. The mesh generated in Ansys Fluent Meshing

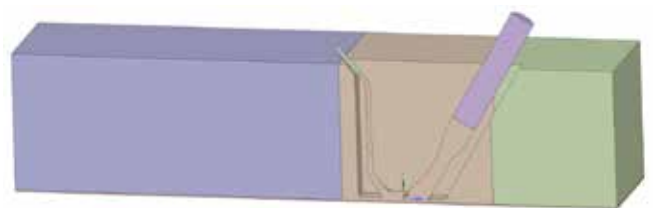


Fig. 3 - Computational domain.

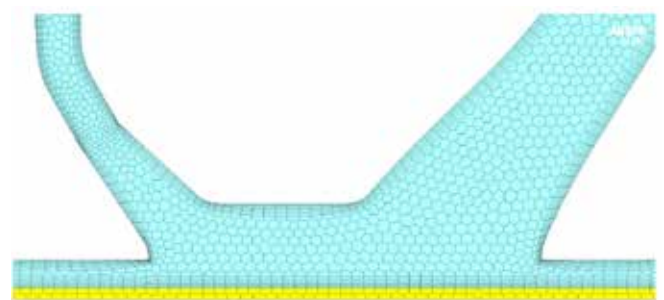


Fig. 4 - Detail of the polyhedral mesh on the symmetry plane.

Physical properties of materials	
AIR	
Density	Ideal Gas
Viscosity	1.7894E-5 [kg/ms]
Specific heat capacity	1006.43 [J/kgK]
Thermal conductivity	0.0242 [W/mK]
Molecular weight	28.966 [kg/kmol]
POLYSTYRENE	
Density	1045 [kg/m3]
Specific heat capacity	1249 [J/kgK]
Thermal conductivity	0.12961 [W/mK]

Table 1 – Material properties

REGION	BOUNDARY CONDITIONS	
HEAT GUN	Boundary type	Inlet
	Q [l/min]	8.5
	T [°C]	450 – 600
ASPIRATION PUMP	Boundary type	Outlet
	Q' [l/min]	36
CONVEYOR	Boundary type	Fluid-Solid interface
	v [cm/s]	2.31 – 4.57 – 7.60
VOLUME BORDERS	Boundary type	Opening
	p [Pa]	101325
	T [°C]	26.85

Table 2 – Summary of boundary conditions

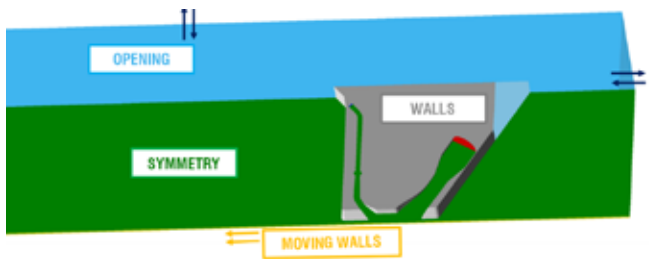


Fig. 5 - Summary of boundary conditions.

Input Parameter	Variable	Description	Range
P1	T_{gun}	Inlet temperature	450, 600°C
P2	V_{belt}	Conveyor belt velocity	2.31, 4.57, 7.6 cm/s
P3	Φ_{IN}	Diameter of the inlet duct, connected to the heat gun	2 ÷ 10 [mm]
P4	Φ_{OUT}	Diameter of the outlet duct, connected to the pump	1 ÷ 4 [mm]
P5	Q_{IN}	Inlet mass flow	0.85 ÷ 8.5 [l/min]
P6	Q_{OUT}	Outlet mass flow	3.6 ÷ 36 [l/min]
P7	α	Inclination angle of the outlet duct	15 ÷ 45 [deg]
P8	β	Inclination angle of the inlet duct	0 ÷ 45 [deg]
P9	d	Distance between inlet and outlet ducts	4 ÷ 44 [mm]
P10	H_{GUN}	Distance between inlet gully and horizontal plane	0 ÷ 40 [mm]

Table 3 – Summary of the inlet parameters

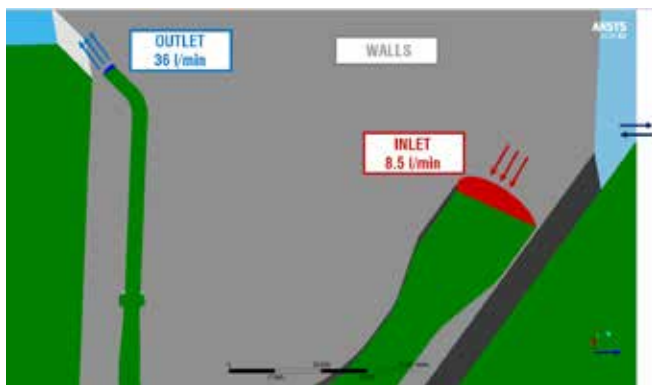


Fig. 6 - Summary of boundary conditions.

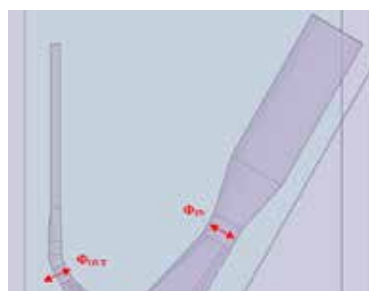


Fig. 7 - Representation of Φ_{IN} and Φ_{OUT} parameters for investigating gully shrinkage.

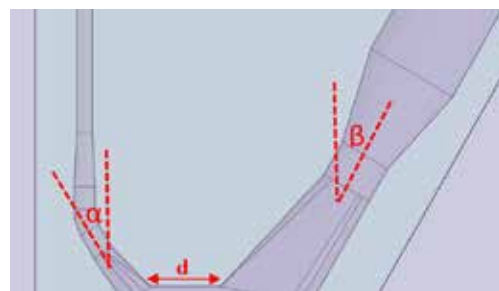


Fig. 8 - Representation of parameters α , β and d, to investigate the geometrical shape of the device.

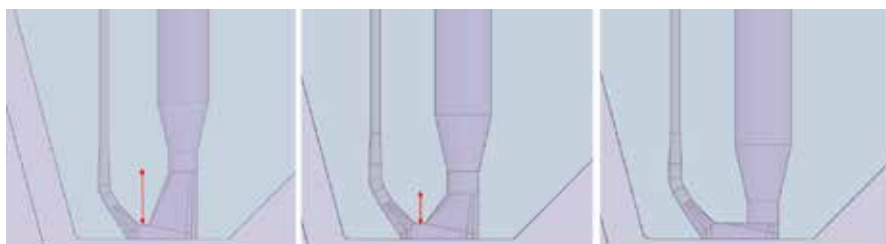


Fig. 9 - Representation of H_{gun} parameters, to investigate the geometrical shape of the device.

(Fig. 4) was composed of 8.7 million nodes and 1.8 million polyhedral cells.

Subsequently, the computational grid was imported into the Ansys Fluent solver, where the physical models, operating conditions, and numerical setup were defined. In particular, air was considered as an ideal gas to account for density variations. The suitcase was modelled as a polystyrene solid in conduction with the fluid. The physical properties of the materials are summarized in Table 1.

The flow considered is turbulent and the analyses were carried out in steady state, considering the physical phenomenon as fully developed.

The operating conditions, derived from the technical specification of the instruments and the EXA experimental data, are summarized in Table 2 and displayed in Fig. 5.

Exploring possible modifications of the aspiration system, several sets of parametric studies were performed, considering different input and output parameters. The input parameters represent both geometrical configurations and physical quantities. These are summarized in Table 3 and displayed in Figs. 7, 8, 9. The output parameters were set to investigate the objectives mentioned above, i.e. they are identified as follows:

- Average temperature at outlet
- Temperature distribution in the suitcase area
- Composition of the air sucked in by the pump
- Concentration of target molecules at the outlet

Results and discussion

The results made it possible to evaluate the actual performance of the system, to check parameters that had not been quantified experimentally and to improve layout performance by focusing on relevant quantities, i.e. it was possible to evaluate each flow path and determine the composition of the air sucked into the pump, passing through the measuring cell. The outlet flow is in fact a combination of ambient air and hot air from the heat gun. A correlation was found between input and output parameters, which guided the entire optimization procedure.

The following points list the main input and output considerations in order to summarize the relevant issues arising from each step of the simulation process:

- The inlet temperature (T_{gun}) is related to the temperature of the suitcase.
- The conveyor belt velocity (V_{belt}) has a limited impact on the temperature, pressure, and velocity profiles.
- The inlet diameter (Φ_{IN}) has a strong influence on the sample temperature. For smaller diameters, there is less collection of molecules because

there is more dispersion of the heated air to the environment. In fact, for smaller diameter configurations, the impact with the surface is greater as the velocity increases, preventing air from being collected in the outlet duct.

- The outlet diameter (Φ_{OUT}) has a negligible impact on the output parameters considered, so it can be excluded from further considerations.
- The mass flow inlet (Q_{IN}) has a medium sensitivity, with direct correlation to temperature and suitcase coverage.
- The mass flow outlet (Q_{OUT}) is a high sensitivity parameter, with inverse correlation to temperature and suitcase coverage.
- The angle of inclination of the outlet duct, α , has a low influence, showing that the mass flow is relevant for the aspiration duct, while the diameter and inclination are not.
- The angle of inclination of the inlet duct, β , has a strong impact on the suitcase coverage and the outlet concentration.
- The distance between the ducts, d , has a strong influence on all outputs.

A greater distance between the two ducts leads to overheating of the sample and, consequently, to a higher suction and suitcase temperature, and suitcase coverage.

- The distance between the inlet gully and the horizontal plane (H_{GUN}) does not have a major impact on the suitcase coverage, which remains unchanged when the distance between the heat-gun and the horizontal plane varies.

The simulation campaigns made it possible to conduct a product development study to identify new prototypes. In particular, the device evolved in two phases which are shown in Figs. 10, 11, 12, 13. During this procedure, the choice of new layouts was guided by the following aspects, which were selected as high priority and experimentally validated on the test bench:

- miniaturization of the device
- reduction of sample coverage
- increase of detected molecules

The reduction in area, referred to in the second point, is due to the fact that if the target molecules were restricted to a

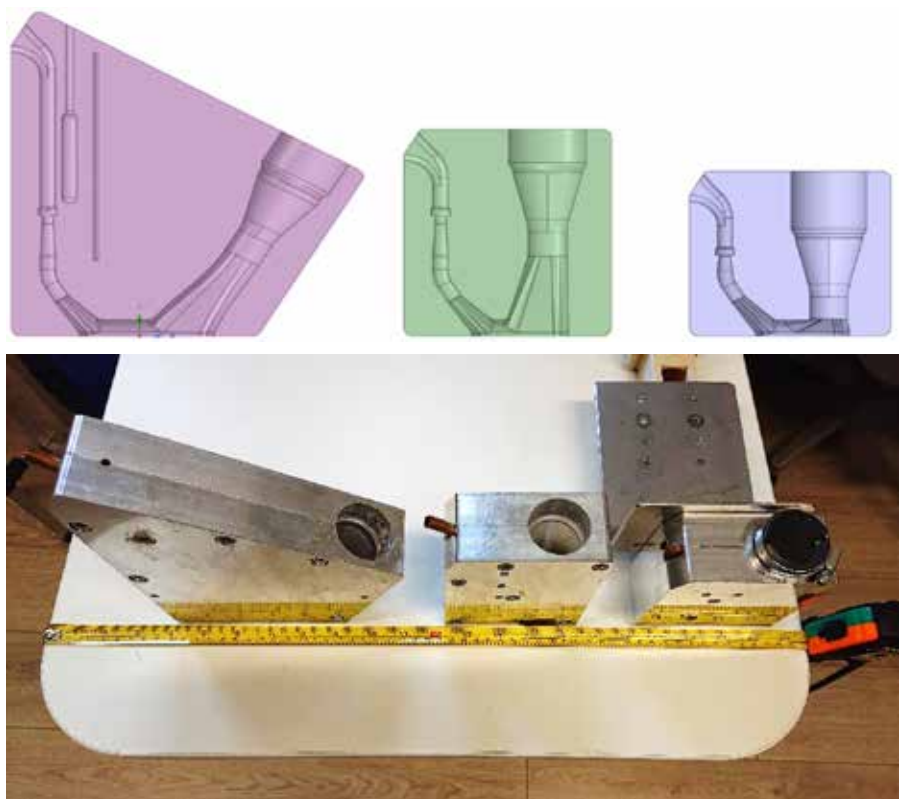


Fig. 10 - Evolution of the layout: CAD model (top), manufactured product (bottom).

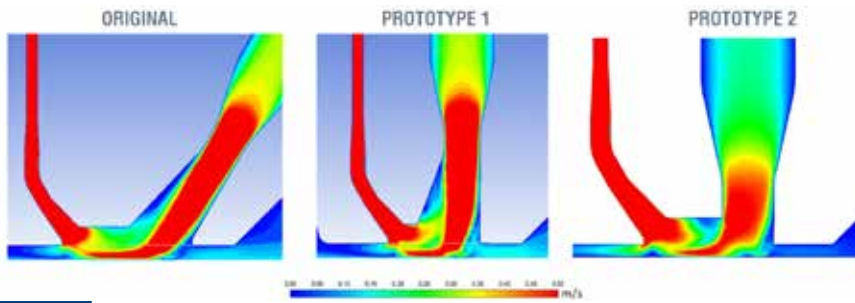


Fig. 11 - Velocity profile in three cases.

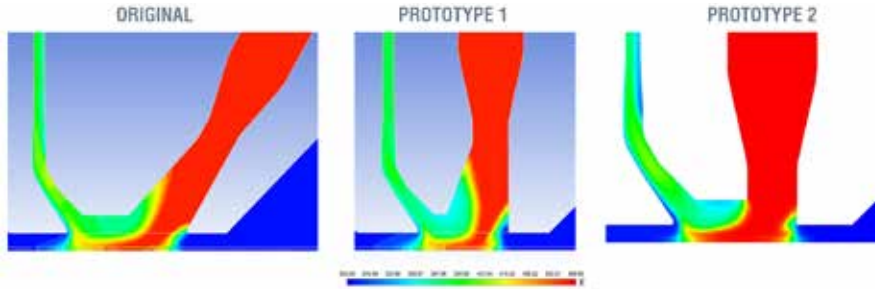


Fig. 12 - Temperature profile in three cases.

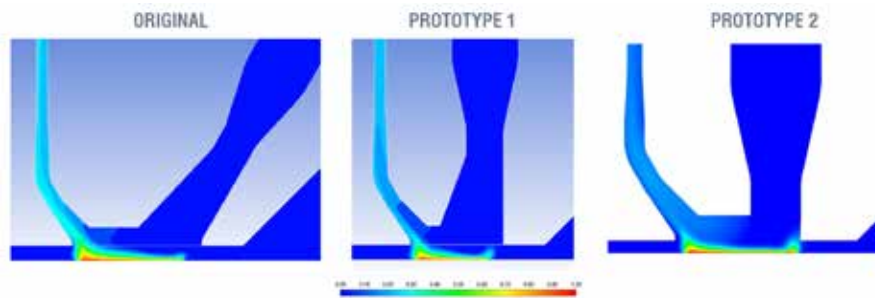


Fig. 13 - Distribution of target molecule in three cases.

limited region of high concentration, high coverage could result in excessive dilution of the air sample.

The selection of the best design minimizes the distance between the ducts (d), places the inlet duct in a vertical position, and minimizes the distance between the inlet gully and the horizontal plane (HGUN).

Conclusions and future work

CFD simulation was successfully applied to design and optimize all components of the system for the contactless detection of hazardous substances in hand luggage.

The final optimal design met the objectives and was experimentally validated on the test bench with the following KPIs:

- miniaturization of the device through the optimization of the air system in terms of the fraction of air intake compared to the luggage area analysed;

- reduction of sample coverage with optimization of sampling, thanks to a fully automated system that varies the position of the detection system according to the height of the luggage;
- an increase in the number of molecules detected by parallel detection of several molecules, through the development of a multi-spot sensor and a suitable

optical system including a massive reduction of false positive results due to specific control spots incorporated into the optoelectronic sensor.

A final prototype was produced and validated in a bench test.

EXA's next main objective is to apply this technology to other sectors where security is paramount, e.g. civil security and food processing chains. This will be achieved thanks to the great versatility EXA technology, which can be applied in any situation that requires careful and reliable real-time analysis, especially on moving samples.



The VOLPE project is funded by the Veneto region of Italy in the program "POR FESR 2014/2020 Asse 1 Azione 1.1.4"

For more information:

Diana Magnabosco - EnginSoft
d.magnabosco@enginsoft.com

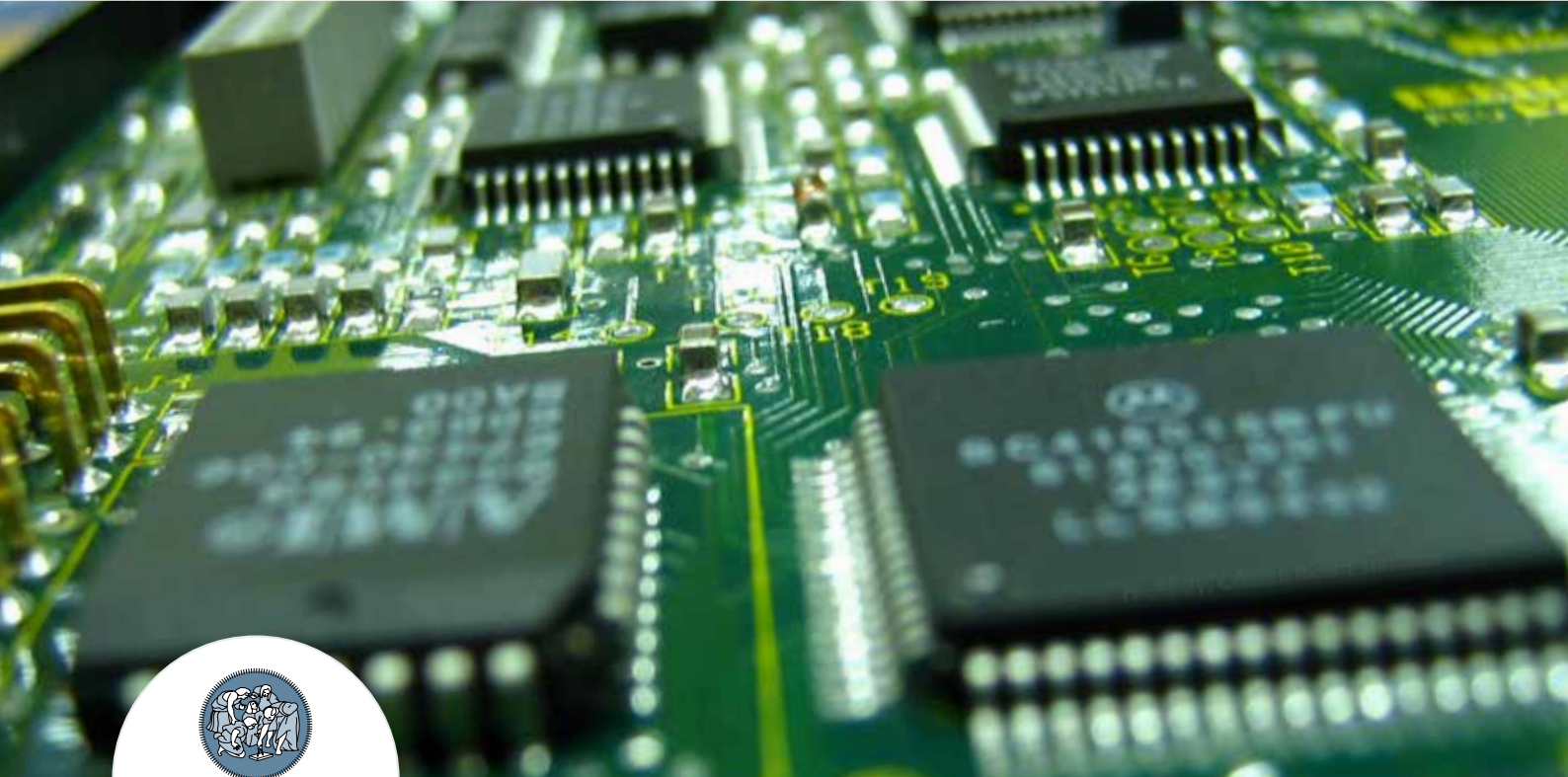
About EXA

EXA is an Innovative SME established in 2016 for developing a detection system of dangerous molecules, e.g., explosives and drugs, in gas samples. This activity was based on a technology transfer process from university research results to the safety equipment market.

Based on an analysis of the characteristics and requirements of the security sector, the company developed a prototype driven by critical technology drivers: real-time analysis, operational autonomy, continuous and contactless analysis, high sensitivity and high throughput. This first prototype was installed in Venice airport for testing on hand luggage boarding checkpoints.



Deep learning-based reduced order models: the new frontier in numerical simulation for microsystems



POLITECNICO
MILANO 1863

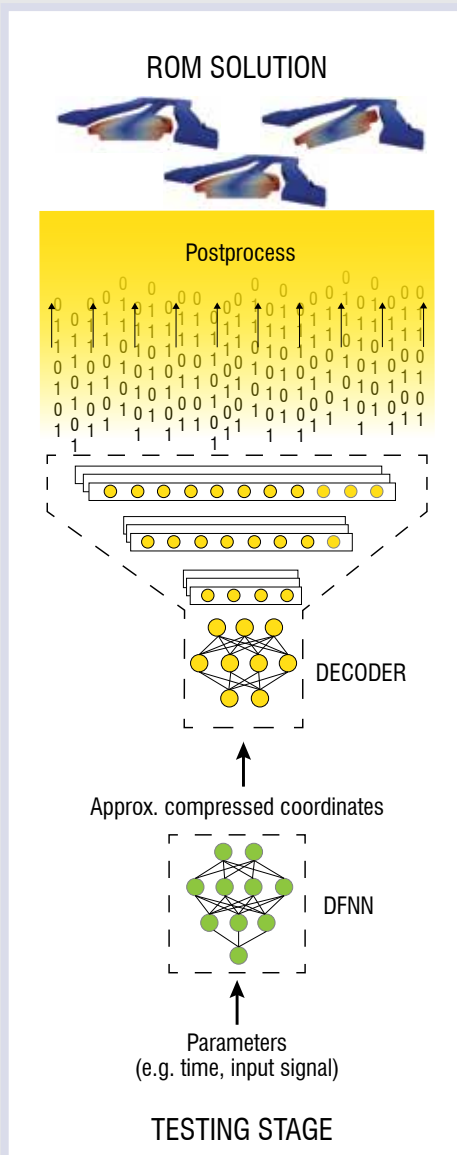
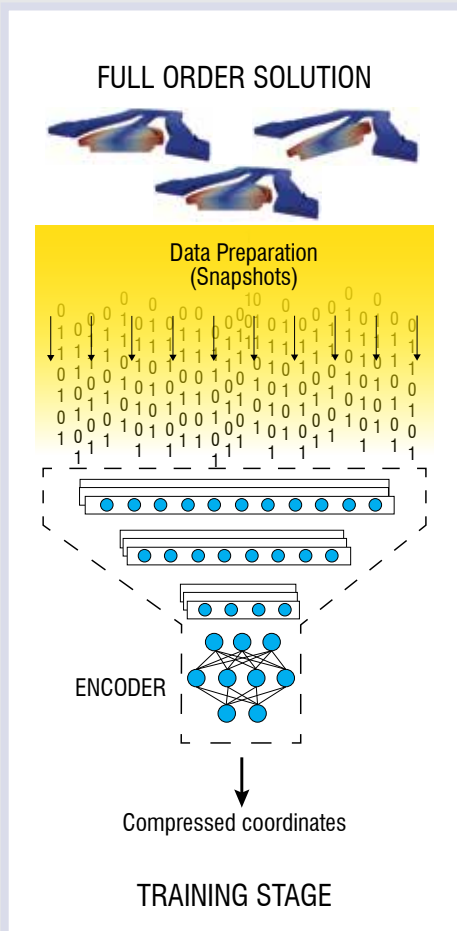
by **Stefania Fresca, Giorgio Gobat, Attilio Frangi and Andrea Manzoni**
Politecnico di Milano

Nonlinear modelling in solid and structural mechanics has received an impressive boost in recent years thanks to the increasing availability of computational resources, particularly in the field of micro-electro-mechanical-systems (MEMS) dynamics.

While numerical methods offer a general solution for tackling MEMS simulation, the computational cost of high-fidelity approaches remains a major issue, and even a true bottleneck. Among the different options, reduced order models (ROMs) represent a key numerical tool to generate efficient, reliable approximations in solving parametrized differential problems.

Exploiting deep learning (DL) algorithms to construct surrogates of dynamic systems has recently become an area of increasing interest to the system dynamics community. Fresca et al. [1,2] have proposed a non-intrusive DL-based ROM technique, which we refer to as DL-ROM.

In this contribution, we explore the efficient simulation of MEMS devices by exploiting the DL-ROM method [3].



Overview of the DL-ROM method

If we consider a MEMS device operating in different conditions/configurations, the DL-ROM method can be explained according to its two stages: training and testing (Fig. 1).

Training stage

A few numerical simulations are performed on a limited number of operating conditions of interest. These solutions, called snapshots, provide instantaneous representations of the state of the MEMS device at a given time and for given conditions e.g. the input electronic signals. The snapshots represent a set of high dimensional, i.e. many degrees of freedom, input data sources.

The data is compressed by the encoder that finds the pattern (i.e. the hidden relationships) between the data points and then removes the unnecessary components resulting in a low dimensional version of the input data. The compressed data represents the ground truth underlying the system and can be generated by relating it to the system input parameters, e.g. time, input signal, operating conditions.

The relationship between the parameters and the compressed input is learnt by a deep feedforward neural network (DFNN). The compressed coordinates approximated by the DFNN cannot be interpreted directly since they are coded, i.e. the .zip file cannot be read directly as a .txt file. Thus, a decompression function is required. This task is performed by the decoder from the compressed coordinates that supply an approximation of the initial high dimensional input data as an output.

Testing stage

Once the DFNN and the decoder have learnt the rules that govern the system from the data, they can be used separately. The DFNN provides a compressed coordinate for a given set of parameters. This is passed to the decoder which reconstructs the high dimensional data so that it can be easily interpreted and used. This stage is almost instantaneous since no equations are solved.

Fig. 1 - Schematic representation of the DL-ROM method.

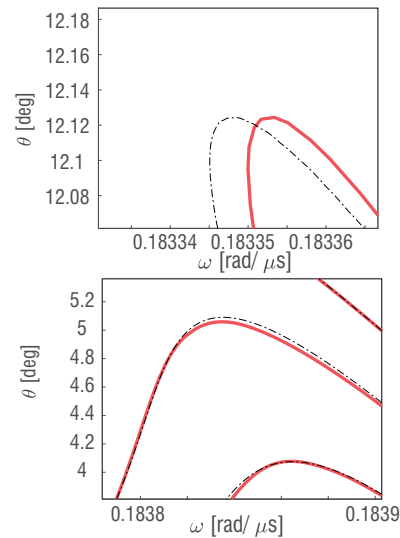
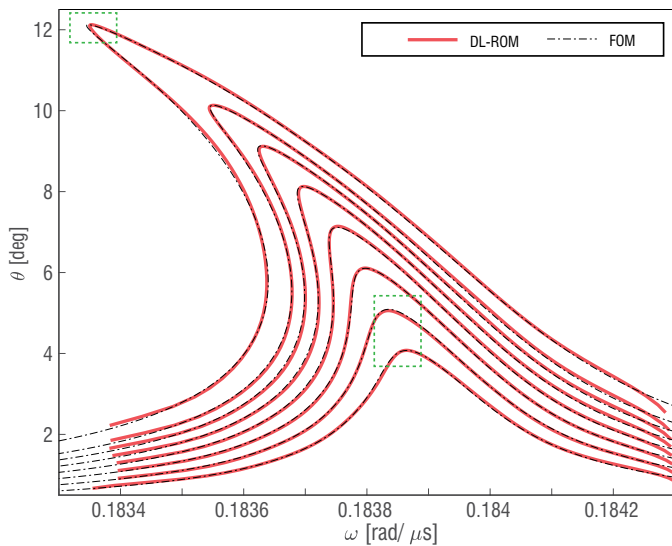


Fig. 2 - Frequency response functions of the MEMS micromirrors under increasing input levels. The DL-ROM solution is compared with a finite element solution.

DL-ROM application and performance

Considering the MEMS micromirror (see the image on the right), we obtained the results in Fig. 2 by following the procedure explained in the previous section.

The dynamic's frequency response function is reproduced with sufficient accuracy and the acceleration compared to a finite element model ranges from 10^3 to 10^5 depending on the number of queries.

Furthermore, as shown in Fig. 3, the data generated with a DL-ROM neural network can also be used for post-processing purposes to recover e.g. the Von Mises stress field of the device.

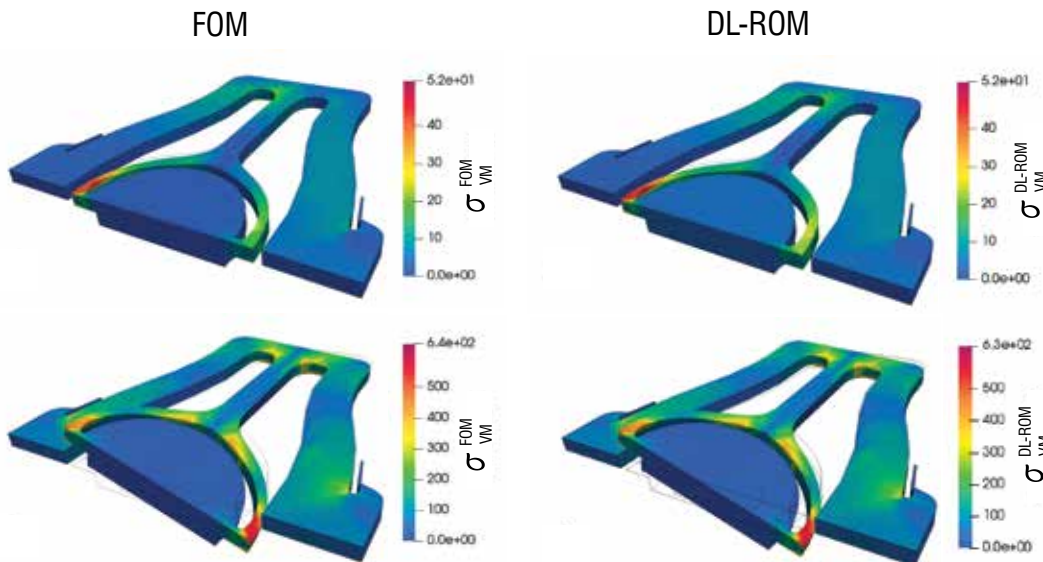
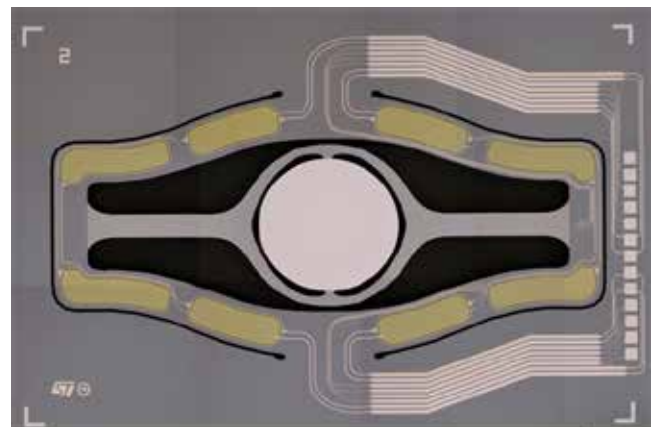


Fig. 3 - Von Mises stress field in the micromirror: comparison between the DL-ROM solution post process and the Finite Element Solution. Two different rotation levels are considered.

This paper formed the basis for one of the five winning posters in the Poster Award at the 2021 International CAE Conference and Exhibition.

For more information:

Stefania Fresca, stefania.fresca@polimi.it

Giorgio Gobat, giorgio.gobat@polimi.it

References

- [1] Fresca et al., "A comprehensive deep learning-based approach to reduced order modelling of nonlinear time-dependent parametrized PDEs." *Journal of Scientific Computing* 87.2 (2021): 1-36.
- [2] Fresca et al., "POD-DL-ROM: enhancing deep learning-based reduced order models for nonlinear parametrized PDEs by proper orthogonal decomposition." *Computer Methods in Applied Mechanics and Engineering* 388 (2022): 114181.
- [3] Fresca et al., "Deep learning-based reduced order models for the real-time simulation of the nonlinear dynamics of microstructures." *arXiv preprint arXiv:2111.12511* (2021).

Overview of the latest developments in Multiscale.Sim, a virtual material testing tool to accelerate materials design

by Koji Yamamoto
CYBERNET SYSTEMS CO., LTD.



Multiscale.Sim from CYBERNET SYSTEMS is a versatile, easy-to-use Ansys add-on tool for multiscale analysis. Using an analytical approach based on the homogenization method, it can perform virtual material tests and identify anisotropic material constants from macroscopic material responses in different deformation modes. A particularly unique feature is the support for many types of non-linear and non-structural problems. As a stand-alone tool, it is very powerful for facilitating material design, offers maximum advantage when used in combination with a variety of Ansys solutions. This article introduces the latest developments with analysis examples, focusing on the integration with Ansys products.

Overview of Multiscale.Sim

The first version of Multiscale.Sim [1] was released in 2007. Initially, many customers had problems preparing material properties, despite the high anisotropy of the material. This is particularly noticeable with fibre-reinforced plastic (FRP) and other fibre-based composites. Adding additional fillers results in a very large number of possible material combinations, so an approach based on testing of actual materials is not suitable for material design. We proposed to solve these problems with virtual material testing.

Fig. 1 summarises the main differences between real and virtual material testing procedures to illustrate the advantages of analysis-based material testing. Testing of actual materials is very costly from preparation to execution of test specimens and processing of test results. Special jigs may be required to obtain the anisotropic properties. If the material property to be evaluated is creep or fatigue resistance, the time requirement is often in the range of days or months. Above all, the same running costs are incurred for every material studied. This is very incompatible with composites which have a myriad of combinations. Virtual material testing techniques can be used to significantly address these problems.

With this approach, all steps are carried out virtually with the whole process being enabled by our solution. It consists of several steps and all the Ansys products or additional Ansys tools work together seamlessly in an integrated GUI environment, which is one of the unique features of our solution. The functions of each work step are summarized in Fig. 2. We provide virtual material testing technology based on the homogenization method. In this method, firstly, an analytical model (hereafter referred to as a micromodel) is created to represent the microstructural heterogeneity of the specimen. This model is created as a rectangle with periodic symmetry in all directions. Micromodels are the most important information characterizing the accuracy of virtual material tests and should be prepared with care. On the other hand, since so many case studies are required for material design, it is also important for them to be easy to create. Due to the complexity of



Fig. 1 - Comparison of virtual and numerical material testing with a focus on cost.

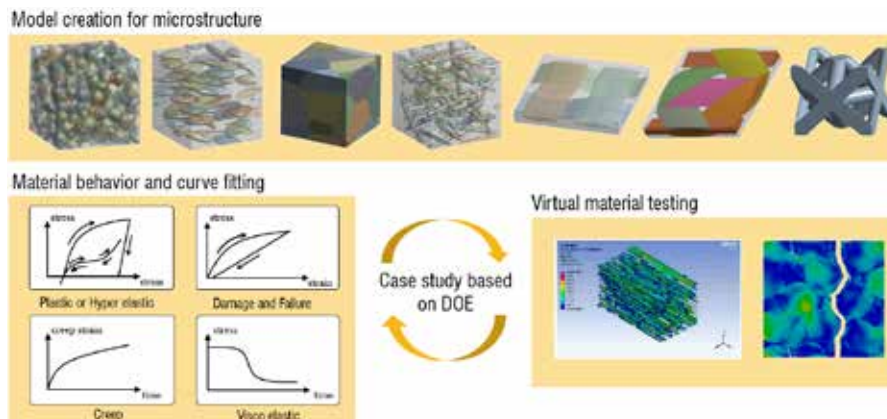


Fig. 2 - Overview of Multiscale.Sim.

the material microstructure, manual modelling is not feasible. This can be solved using the template function we provide. For randomness, statistical information can be used. For short fibre dispersion materials, the fibre orientation ratio; for filler dispersion materials, the probability distribution of the existing dimensions or the degree of cohesion, etc. It is also not practical to model this information manually in a standard CAD system; script-based approaches are more effective. The virtual material test is achieved by defining strict boundary conditions that reflect the ideal deformation modes of the actual material tests. This feature is extremely versatile and can easily reproduce any deformation mode, not just general uniaxial testing, making it a very important feature for understanding the behaviour of anisotropic materials. Needless to say, observing the behaviour of a material over a long period of time in a simulated environment is not a problem.

The output is a macroscopic material response and corresponds to various results obtained by averaging the volume of the results within the microstructure using a microscopic model. In addition to the elastic response, it is possible to evaluate the behaviour of various non-linear materials such as elastoplasticity, fracture damage, viscoelasticity and creep. When performing large structural analyses that reflect the behaviour of macroscopic materials, it is also necessary to prepare macroscopic material constants to describe the material behaviour. We provide macroscopic material constitutive laws for this purpose as well as curve-fitting functions to identify the constants. The combination of these functions allows multiscale analysis for sequential coupling of micro and macro models.

Multiscale.Sim development trends

This section describes the latest developments in Multiscale.Sim. All features are designed to make virtual material testing technology more convenient and accurate.

SpaceClaim migration of the micro modelling function

Due to the wide variety of microstructures in composites, expanding modelling capabilities has always been a top priority. Therefore, we

listen to our customers' needs and actively incorporate them into our development plans. So far, this functionality has mainly been implemented in Ansys DesignModeler, but we are actively migrating it to SpaceClaim. This is also an effort to keep pace with Ansys' development strategy. This allows users of Ansys Mechanical Enterprise to create models without additional licenses. Our goal is to migrate all the modelling functionality currently implemented in DesignModeler to SpaceClaim by the end of this year.

Granta MI interface for managing and using the material database

The response obtained from the virtual material test is converted into material constants by curve fitting and recorded in the engineering data, which is a standard function of Ansys Workbench. However, aggregating the material data locally is not sufficient to achieve maximum benefit. The high-end materials database system Ansys Granta solves all these problems. Multiscale.Sim has developed an interface that works with Granta MI. It allows bi-directional data association between Multiscale.Sim and Granta MI. Granta MI allows users to record not only the material constants used in the analysis, but also various other information about the material. This means that both input and output information can be managed for homogenization analysis, which not only improves data traceability,

but also enables the use of AI in materials informatics [2].

Let's take a look at a simple example of how to use it. The material to be analysed is a lattice structure created by 3D printing consisting of columns of various cross-sectional shapes and angles. By changing the thickness and angle of the columns, not only the density but also the material properties such as modulus of elasticity, change significantly. This feature can be used to create the optimal material behaviour for the product. The lattice structure is controlled by several shape parameters such as topology, column thickness (assuming a circular cross-section), and the aspect ratio. The raw material used to construct the lattice is fixed to titanium.

Fig. 3 shows a visualization of an aggregated dataset in Granta MI. The modulus of elasticity and Poisson's ratio are placed on the axes, respectively. The microstructure of four typical conditions is also shown in the same figure. With Granta MI users can not only see the general trend of the data, but also refine their search to find the optimal lattice structure for their product.

Composites also facilitate the creation of materials with unsampled area properties. Finally, we use AI to try to predict a lattice structure that matches the desired material

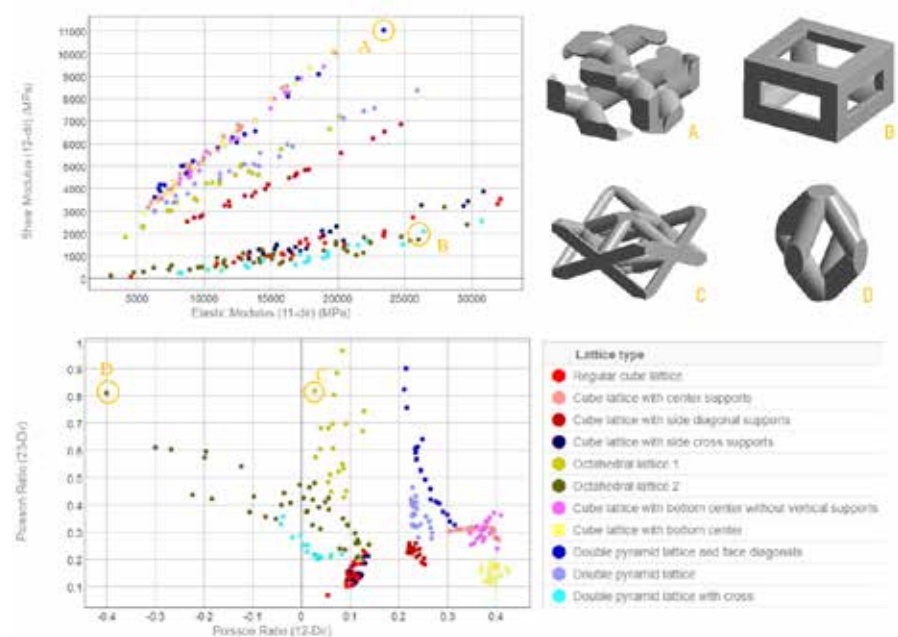
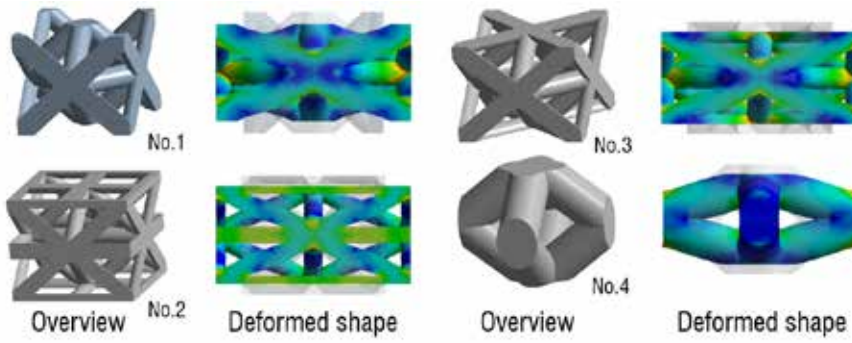


Fig. 3 - An example of the materials database displayed by Granta MI



Elastic constants obtained by virtual material testing

Properties	Direction	Candidate ID No.			
		1	2	3	4
Young Modulus [GPa]	X	10.001	9.9885	9.9890	9.9704
	Y and Z	7.1713	3.9354	4.7810	8.0266
Poisson's Ratio [-]	XY	0.0079	0.0071	0.2516	-0.1280
	YZ and XZ	0.4982	0.5035	0.4999	0.5019
Shear Modulus [GPa]	XY	4.0840	0.4391	5.4378	0.6039
	YZ and XZ	5.8174	2.6447	4.5385	5.3495

Fig. 4 - Example of inverse lattice structure identification by AI trained on a materials database.

behaviour (which does not exist in the materials database). This problem can be solved by response surface optimization analysis. Suppose we need a lattice structure with a longitudinal modulus of 10 [GPa] in the x-direction and a Poisson's ratio of 0.50 [-] in the yz-direction. Fig. 4 shows four candidates for the lattice structure predicted by AI. Virtual material tests were performed on these lattice structures to validate the results, which are also summarized in Fig. 4. It can be seen that the modulus and Poisson's ratio given as target values are reproduced with very high accuracy for all lattice structures. Of course, the properties of other components vary from lattice structure to lattice structure.

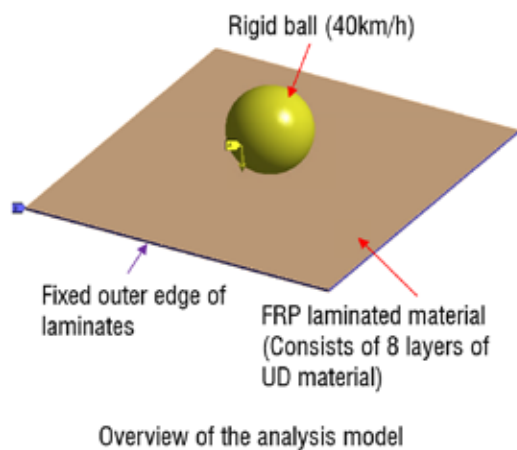
LS-DYNA interface supporting strong non-linearity such as impact fracture problems

In composites, which are a mixture of materials with very different stiffnesses, high stresses are concentrated at the material interface, which is the starting point for failure. Such problems are highly non-linear and implicit analysis approaches have limited applicability. We are also developing an explicit virtual material testing technique which can be carried out by coupling with LS-DYNA. This allows multi-scale analysis, mainly for composite fracture problems. A simple analysis example is shown in Fig. 5. A rigid ball is dropped onto a composite material made of unidirectional

reinforcing fibres (referred to as UD material). Three different lamination patterns were prepared. Each of them has a very different tendency to anisotropy and therefore shows very different fracture behaviour on impact. This analysis is possible by accurately observing the anisotropic fracture behaviour of the UD material through virtual material testing. Fig. 6 shows the actual results of this analysis. The material behaviour can be observed, considering various failure modes such as de-bonding at the material interface and transverse cracking and propagation. The obtained anisotropic fracture strength can be used to perform the fracture analysis of any macrostructure made of the UD material.

Resin flow analysis tools to incorporate moulding history

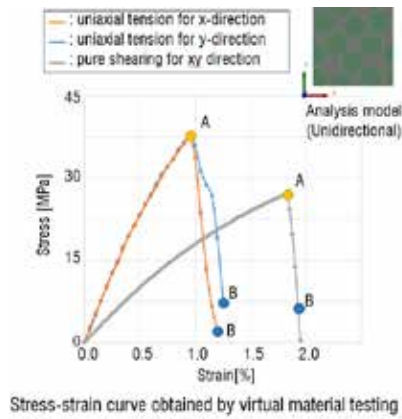
It is important to consider the moulding history when analysing material behaviour as injection moulded products contain discontinuous fibres and their orientation is not uniform throughout the product. Multiscale.Sim can map the distribution of fibre orientations based on the moulding history and the corresponding material constants. The microstructure of injection-moulded parts varies from region to region. Of course, it is not possible to carry out virtual material tests of every region. Therefore, independent of the moulding analysis, the equivalent material constants for the microstructure of a typical fibre orientation pattern are evaluated. By converting these results into response surfaces as material constants equivalent to directional pairs, it is possible to interpolate material constants other than the sampling points. It is then possible to



Fracture behavior for different lamination patterns (equivalent stress distribution)

Timing	Lamination Pattern		
	[0/0/0] _{sym.}	[0/90/0/90] _{sym.}	[0/90/45/-45] _{sym.}
Immediately after impact			
After impact			

Fig. 5 - Fracture analysis of a laminated unidirectional reinforcement



Equivalent stress distribution inside a microstructure

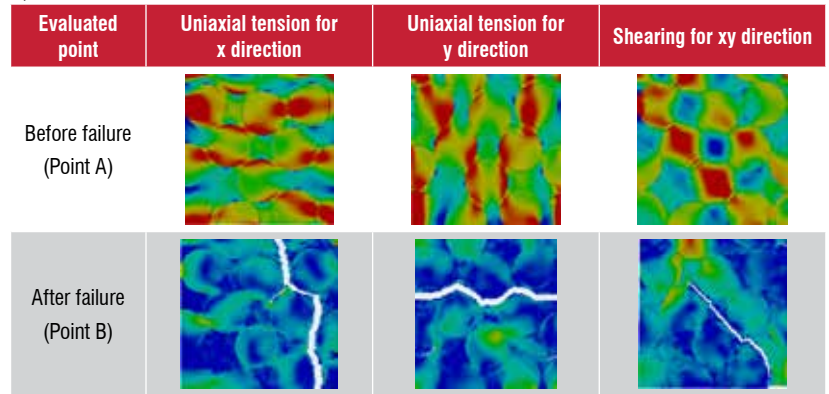


Fig. 6 - Example of observed fracture behaviour of unidirectionally reinforced material using virtual material testing

use this response surface to map the material constants onto the fibre distribution obtained from the resin flow analysis. The advantage of using this method is that it can be used to map any constitutive law. This includes not only problems related to elasticity, but also any material non-linearities.

Link to Rocky for the creation of microstructures based on physical phenomena

For some composites such as porous materials and powders, it is not always possible to achieve sufficient analytical accuracy without preparing microstructures based on physical phenomena. To overcome this problem, you can use a modelling approach in combination with particle simulation software Rocky. The forming process of the material is analysed in Rocky and the results are used as a micromodel in Multiscale.Sim.

To outline the function, we will use a powder made of spherical particles as an example. Fig. 7 shows the results of a powder material with a particle size distribution that has been used to fill a container by free falling and tapping. Smaller particles fall through the spaces created between the large particles.

As a result, the microstructure of the filling material shows features of segregation. Towards the bottom surface, the proportion of smaller particles increases. An interface currently under development can be used to extract the microstructure of a particular region from the results of this analysis. Since the material behaviour of powders cannot be represented by elasto-plastic material models such as those used for metallic materials, it is necessary to use the Drucker Prager model which is specialized for powder materials. We are also developing a curve-fitting function for this purpose. An example of a real analysis of powdered materials was introduced in a previous issue of this magazine [3]. For segregated materials, as in the case of injection moulding described in the previous section, the material properties are not uniform. This can also be overcome with a mapping technique based on the response surface.

Conclusion

This paper provided an overview of the functionality of Multiscale.Sim, an Ansys add-in tool for performing multiscale analysis, as well as the latest development trends. We are constantly developing this product to help you in your material design process. While

focusing on the integration of Multiscale.Sim and Ansys products, we are also actively working with our customers to develop specific functional requirements.

A special thanks to EnginSoft S.p.A. for their collaboration. EnginSoft is a Multiscale.Sim Channel Partner in Italy, France, Germany, the Nordic region, Turkey, the UK and other countries in Europe.

For more information:

Alessandro Mellone - EnginSoft
a.mellone@enginsoft.com

References

- [1] About CYBERNET Multiscale.Sim: Multi-physics analysis program for Ansys. [online] Available at: www.cybernet.co.jp/ansys/product/lineup/multiscale/en/multiscale/
- [2] Honda cuts the number of prototype materials and tests during model-based development in half. [online] Available at: www.ansys.com/resource-center/case-study/honda-motors-materials
- [3] EnginSoft Newsletter, 2020. Filling and compression analysis of metallic powders composed of spherical particles. [online] (Autumn 2020), pp.12-15. Available at: www.enginsoft.com/assets/pdf/newsletter/newsletter2020_3.pdf.

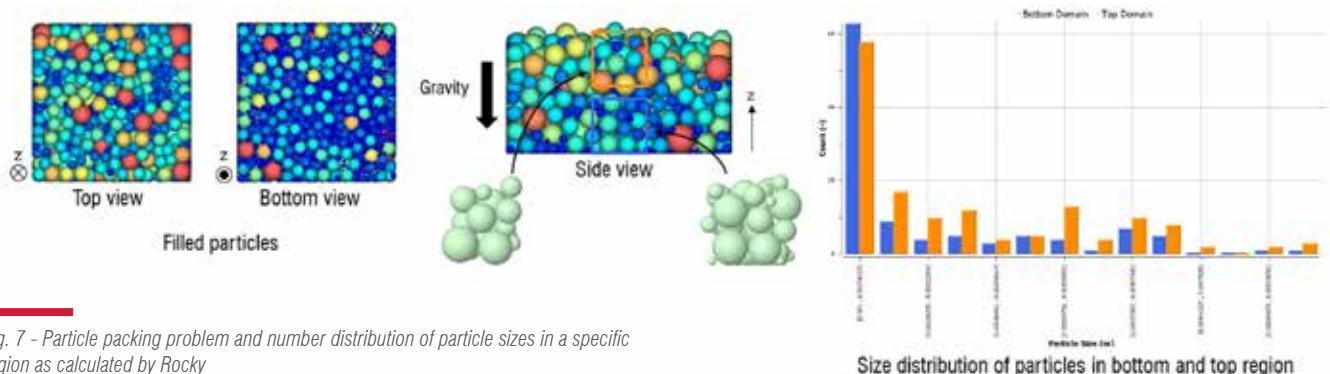


Fig. 7 - Particle packing problem and number distribution of particle sizes in a specific region as calculated by Rocky



Ansys 2022 R1: CFD release highlights

Delivers scalable solutions that leverage new algorithms, advanced workflows and more comprehensive physics

by Alessandro Arcidiacono, Diana Magnabosco and Fabio Villa
EnginSoft

In Ansys 2022 R1, the fluids product line continues to make major advancements to improve productivity, streamline workflows, and accelerate simulation time.

This release allows engineers to innovate at new levels in applications involving turbomachinery, aerospace, acoustics and more, with new transformative features, as will be described in this article.

Ansys Discovery

Ansys 3D product design tools offer real-time physics simulations (Explore mode) and accurate high-fidelity simulations (Refine mode) together in one easy-to-use interface, allowing engineers to easily evaluate feedback on design changes.

Ansys 2022 R1 expands Discovery's real-time physics into the critical area of thermal management through the addition of **coupled fluid-solid simulation** (Fig. 1). This approach allows rapid prediction of heat dissipation and heat transfer in many fluid flow scenarios, without any geometry preparation, as fluid-solid and solid-solid interfaces are created automatically.

In this new version, it is now possible to specify the **ideal gas** as part of the material definition, so that the compressible flow can be studied in both Explore and Refine modes. Therefore, gas density and Mach number can be post-processed in high-speed gas flows or flows with large temperature variations. In addition, **temperature-dependent material properties** can be defined to improve accuracy for solid thermal simulation.

New **post-processing capabilities** have been introduced to accelerate the simulation procedure from setup to results. Greater flexibility can be exploited for monitoring positions, which can be defined on 2D regions, lines or points. The legend shows the contour value at the cursor position using interactive probes. Streamlets can be visualized to better understand the flow field through curved vectors. In addition, a heat flux vector can be created in a solid region for conjugate heat transfer.

History Tracking has been expanded: modelling and physics operations can be recorded and played back when connecting

via CAD interfaces. Parameters can be promoted and passed to Workbench for design optimizations, while sketches can now also be updated through History Tracking.

Scripting is also part of this major release, which enables powerful automation and covers modelling and simulation within Discovery.

Finally, the **Reverse Engineering** tab and the **Facet Tools** are now exposed with different functionalities such as Autoskin, Skin surface, Fit spline, Split, Scale and Shell.

Ansys Fluent meshing

Ansys Fluent Meshing guides the user through a simplified workflow to generate high-quality unstructured meshes in a single-window approach. Two wizards are available: the Watertight Geometry Workflow (WTM) and the Fault-Tolerant Meshing Workflow (FTM). The first general improvement regards the colour scheme, which can now be chosen as pastel instead of classic (Fig. 2). This option is similar to the visualization in SpaceClaim and allows better representation of mesh edges.

File management has changed slightly: a **Temporary files folder** is now created inside the current working directory but can be changed if necessary via the preferences panel. Intermediate files with .pmdb and .fmd extensions are automatically saved in the working directory to enable the files to be ported to a different machine.

A **Workflow Template Folder** can be defined to store .wft files. These workflow templates can be collected in a unique folder so that they are available in the drop-down list in the Select Workflow Type menu.

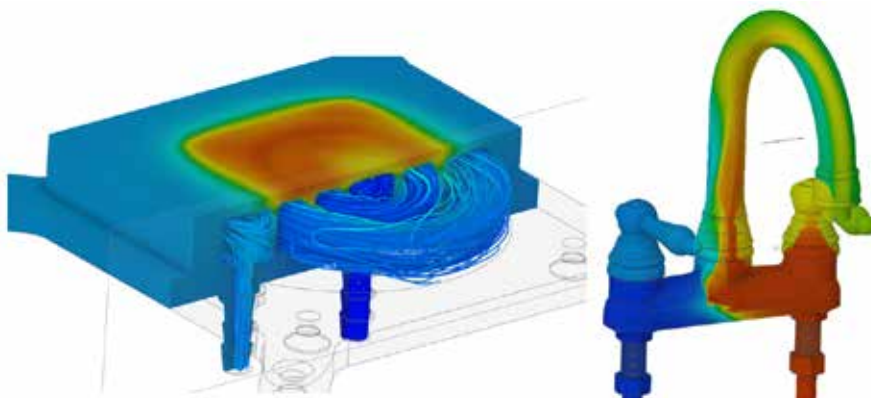


Fig. 1 - Rapid fluid-solid thermal management.

More information about the **unit** is available directly in the Graphical User Interface (GUI), i.e. all dimension inputs show the unit and measurements in the graphics window and console. Once the user has chosen the units in the Import/Part Management Task, all subsequent panels are synchronized, except for parameters without units, which are dimensionless (such as growth rate, cell per gap, etc.).

To simplify automation in label selection, **multiple wildcards** are now supported, which can be combined with operators (NOT, OR, AND functions). This option works for Filter Text and Use Wildcard and reduces the need to create multiple subtasks.

With regard to the WTM workflow, the possibility of removing fine geometry details is added (**Remove Steps** Option). This is particularly useful for step-like imperfections, CAD artefacts and skewed triangles, which can be removed via the Surface Mesh task or the Surface Mesh Improve task.

An alternative method (called **Interface Connect**) of handling Share Topology properties is added, allowing a conformal mesh. Instead of using the Join/Intersect approach, this method first connects the edges and then removes one of the overlapping faces, gaining robustness and speed.

The Add Local Sizing task now includes an additional **Refine Thin Regions (Ignore Orientation)** option (when considering the face or face/edge proximity). This option allows you to apply better refinement to thin areas, for example between plates.

The Create Surface Mesh task now includes an additional **Ignore Proximity Across Objects** option to ignore any small artificial spaces that may exist between two objects/bodies; this is particularly applicable to assemblies that typically have duplicate faces and edges between each body.

Moving on to the FTM workflow, there are a number of improvements to the **Import CAD**

and Part Management task, including multiple import, visualization, transformation and re-faceting.

The Add Boundary Layers task now includes greater flexibility for refining the volume mesh along the flow boundary, providing the ability to add split prisms to boundary layer definitions (Fig. 3).

In the Generate Surface Mesh task, the **Merge Interior Pockets** field can now be used to extend the surface meshing into interior cavities. This is particularly useful for meshing objects that contain various internal pockets such as automobile interiors.

The **Identify Construction Surface** task allows a construction surface to be created using an existing object or zone, a bounding box, or an offset surface.

You can now examine the effects of replacing parts in your imported CAD model by adding the **Choose Part Replacement Options** task after generating the volume mesh. This task allows you to add additional CAD part files, remove parts, or replace parts (e.g. remove or replace mirrors, bumpers, or spoilers on cars), to see the effects in the meshing and solution, if needed.

Ansys Fluent

The new functions and enhancements to Ansys Fluent are outlined below for User Experience, Workflows, GPU-Solver, Gap Models, Combustion instability and the GEKO-model.

User experience and post processing

The post-processing tools are even better in the latest version. Firstly, users can simultaneously create several views from a consistent point of view and synchronize all sub-windows (Fig. 4). User-defined surfaces can be included in the Location for reduction functions (Average, Minimum, etc.). Many new solid materials available for rendering (brick, concrete, etc.) and Pulsed path animations can be saved in common video formats. Finally, Animation can be embedded in an existing window before the start of the simulation.

Attention is also paid to the aeroacoustics field. From 2022 R1, Discrete Fourier Transformation Tonal Analysis can be performed during the

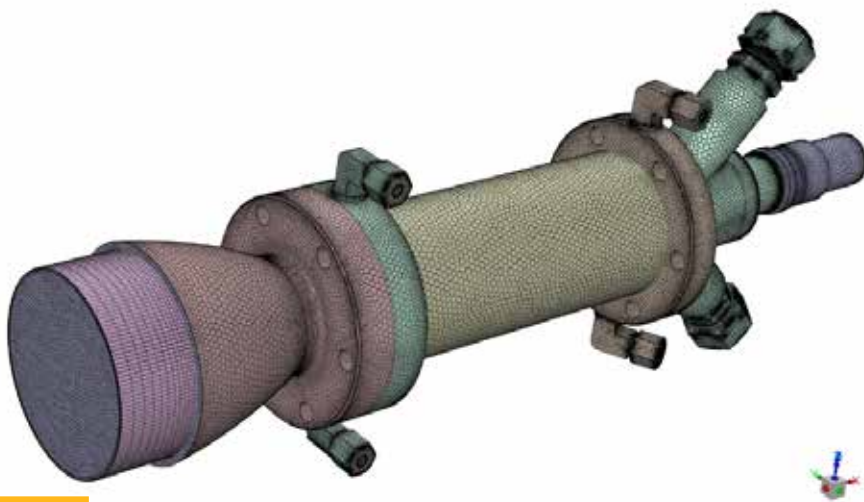


Fig. 2 - Pastel colour scheme.

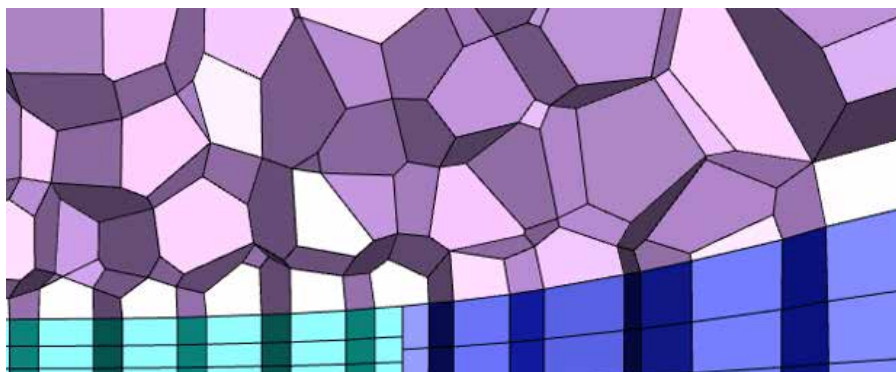


Fig. 3 - Split prisms.

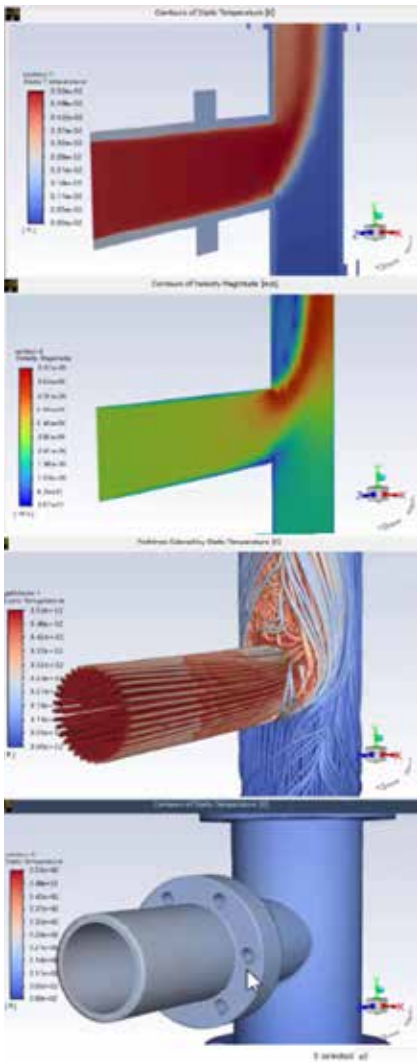


Fig. 4 - Synchronize all sub-windows.

solution. It calculates the magnitude and phase information of the selected frequencies for subsequent post-processing.

Aero and Turbo WorkFlow

Specific workflows easily guide the user in setting up the case. Two new workflows are present in this release:

Turbo-workflow (Fig. 5) allows a turbo-machinery flow problem to be set up quickly. It eliminates repeated user input and minimizes user error during setup. Configuration is available for Axial/Radial Compressors and Turbines. Specific post-processing (performance parameters) is also automatically generated.

Fluent Aero Workspace (Fig. 6) is a dedicated Fluent Workspace for aerospace external aerodynamics simulations.

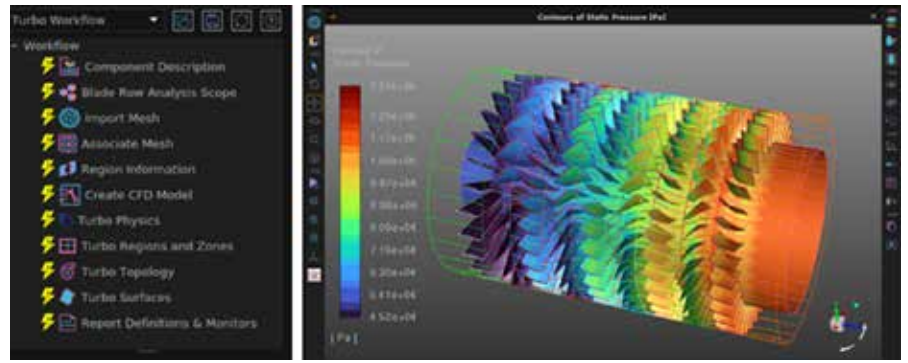


Fig. 5 - Turbo workflow.

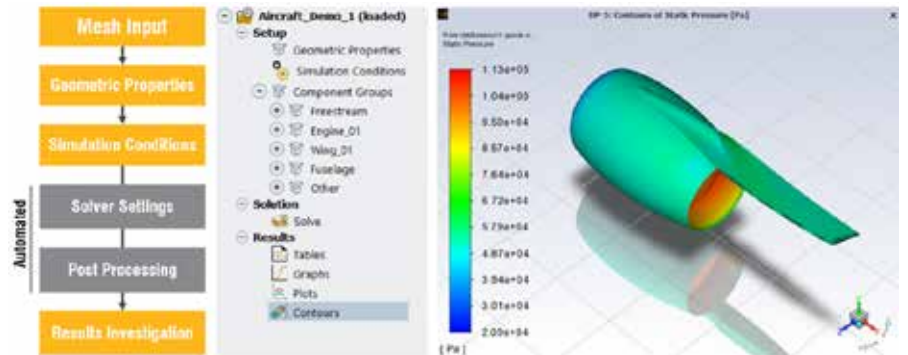


Fig. 6 - Aero-workflow.

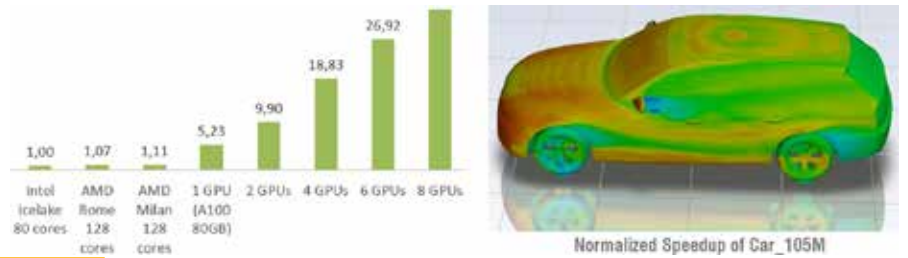


Fig. 7 - GPU/CPU solver case benchmark.

A simplified configuration and analysis tool for the aerospace workspace includes built-in best practices to minimize the need for the user to adjust models and settings.

The user can automate solver settings, post-processing output parameters, tables and chart plots.

GPU-solver

A new multi-GPU solver is available as a beta feature in 2022 R1. The advantage of GPUs in accelerating simulations (compared to the classical CPU solver) includes acceleration (1 GPU ≈ 200 CPU cores), lower hardware acquisition cost (1/7), and lower power consumption (1/4). Target applications so far are external/internal flow simulation and heat transfer.

The scalability on the multi-GPU configuration is remarkable, as shown in Fig. 7.

Gap models

Several models are implemented and improved in this release. A modelling solution for flow through narrow gaps in mobile mesh solutions is provided. A sponge-layer method artificially increases the viscosity according to the Reynolds number provided by the user in the gap region. If the gaps are smaller than a user-defined threshold value, the flow blocking option will be triggered.

Combustion instability

The improved non-adiabatic strained FGM combustion model offers the ability to account for heat loss and the effect of strain on flame speed. Accounting for high strain is important to accurately predict the blow-off equivalence ratio. Fluent validation for hydrogen combustion provides a reasonable prediction of flashback, another important instability phenomenon of combustion (Fig. 8).

GEKO-model

The GEKO (generalized k-omega) turbulence model can now be trained to produce results more similar to a high fidelity, high-cost scale resolution simulation. First, a Neural Network (NN) is trained on experimental or simulation data in order to generalize the correlation between the optimized GEKO coefficients and flow characteristics. Thereafter, the GEKO with the trained coefficient from the NN can almost match the LES (Large Eddy Simulation)/Experiment (as shown in Fig. 9).

Ansys CFX

Ansyes is constantly developing new functionality to help customers perform accurate turbomachinery simulations.

Ansyes BladeModeler is integrated with Ansyes DesignModeler to provide full 3D geometry modelling capabilities and allow any number of geometric features to be added, such as hub metal, blade fillets, and cut-offs and trims.

BladeModeler has released additional support for the BladeGen to BladeEditor workflow via NDF updates, which apply incremental changes to an existing model rather than creating the model from scratch with each update. This avoids the need to create scripts for all BladeEditor steps for a parametric workflow by applying parametric changes via iterative NDF updates. The Ellipse Location with Tangent option is now available in BladeEditor and supports NDF updates.

Ansyes TurboGrid software includes new technology that aims for full automation combined with an unprecedented level of mesh quality for even the most complex blade shape. The hybrid meshing can be used to create a conformal mesh for blade tips to account for movement due to flutter and for secondary flow paths and axisymmetric cavities.

In 2022 R1 the hybrid meshing supports partial tip/hub gaps including buttons or other features

on rounded blades. This is achieved through a fully automated, repeatable meshing process to mesh low and high-fidelity blade geometry, with 1:1 mesh connectivity between pure hex and hybrid mesh parts. The hybrid meshing retains mostly block-structured hexahedral elements and still operates on a single Global Mesh Size parameter. The hexahedral mesh topology is retained during mesh refinement studies to minimize solution differences.

Ansyes CFX is a high-performance computational fluid dynamics (CFD) software tool that provides reliable and accurate solutions quickly and robustly across a wide range of CFD and multiphysics applications. CFX is recognized for its exceptional accuracy, robustness and speed when simulating turbomachinery, such as pumps, fans, compressors and gas and hydraulic turbines.

Harmonic Analysis speeds up solutions to transient and multistage blade row problems by calculating only one blade per row and reducing computational time. In 2022 R1, thanks to multifrequency HA, turbocharger turbine durability analysis can be reduced by a factor of 100 times. Turbocharger turbines are subject to exhaust gas pulses that have a much lower frequency than the turbine's rotational speed. The calculation of the variation of the transient force on the blades is important for the analysis of structural durability. Due to the different time scales, transient simulations are extremely expensive: Harmonic Analysis now compresses the simulation time to a few hundred iterations of the solver, over 100 times faster than a transient simulation.

For the Blade Film Cooling model, the visualization of injection positions, injection shape, and injection angles has been improved.

The CFF mesh can now be imported to CFX Pre and the performance of loading CFF files into CFD Post has also been improved.

For more information:

Diana Magnabosco - EnginSoft
d.magnabosco@enginsoft.com

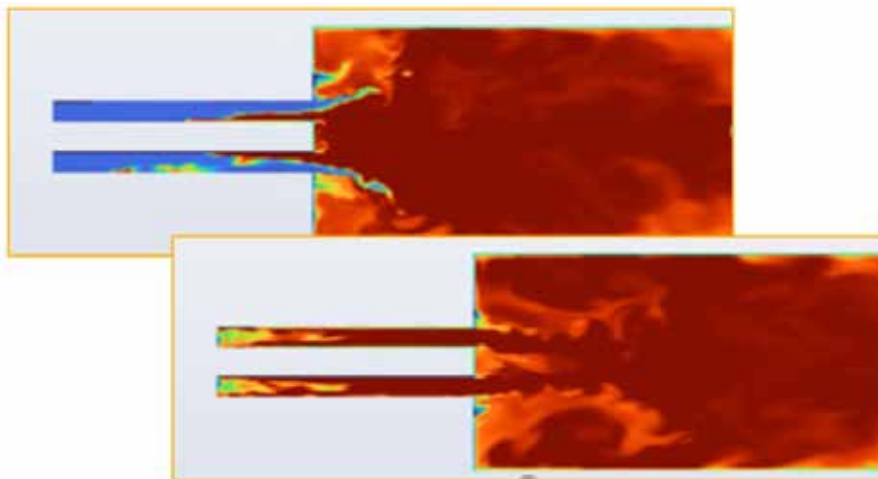


Fig. 8 - Flame flash back with H2. This also uses the non-adiabatic strained FGM model, which takes into account the cooling of the flame in the nozzle and its impact on flame speed.

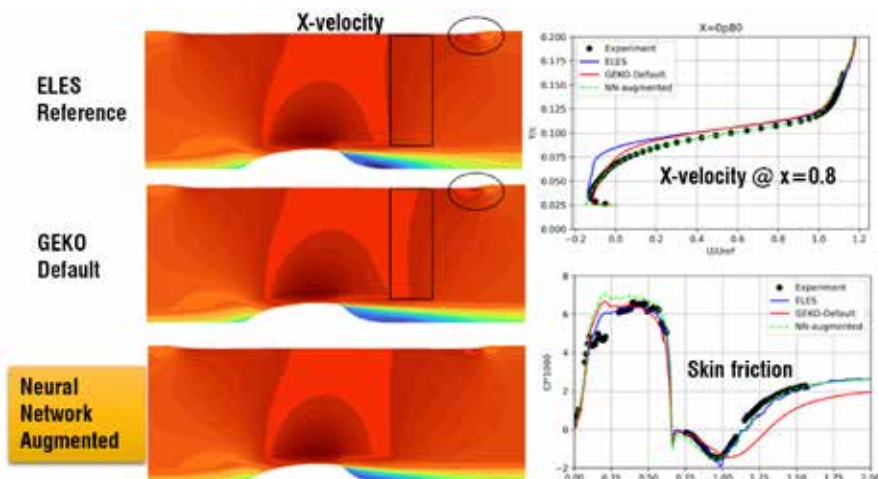


Fig. 9 - NN augmented GEKO speed almost corresponds to ELES/Exp.

Your feedback matters

Take a few minutes
to answer our survey:
with your input and suggestions
we can make our magazine
even more interesting



www.enginsoft.com/futurities-survey